KAUNAS UNIVERSITY OF TECHNOLOGY

MARTYNAS TICHONOVAS

# APPLICATION OF THE ADVANCED OXIDATION PROCESSES FOR THE DECOMPOSITION OF THE EMERGING WATER POLLUTANTS

Doctoral dissertation

Technological Sciences, Environmental Engineering (04T)

2018, Kaunas

KAUNO TECHNOLOGIJOS UNIVERSITETAS

MARTYNAS TICHONOVAS

# PAŽANGIOSIOS OKSIDACIJOS PROCESŲ TAIKYMAS PROBLEMINIAMS VANDENS TERŠALAMS SKAIDYTI

Daktaro disertacija

Technologijos mokslai, aplinkos inžinerija (04T)

2018, Kaunas

**ACKNOWLEDGEMENTS**

# LIST OF TABLES

# LIST OF FIGURES

# CONTENT

# LIST OF ABBREVIATIONS

AC – alternating current

AO – advanced oxidation

AOP – advanced oxidation processes

BOD – biological oxygen demand

CAS – chemical abstracts service

COD – chemical oxygen demand

DBD – dielectric barrier discharge

DC – direct current

FTIR – Fourier-transform infrared spectroscopy

GC-MS – gas chromatography–mass spectrometry

HPLC-UV – high-performance liquid chromatography–mass spectrometry

MW – molecular weight

SDBD – surface dielectric barrier discharge

SEM – scanning electron microscopy

TOC – total organic carbon

TRL – technology readiness level

UPLC-MS – ultra performance liquid chromatography–mass spectrometry

UV – ultraviolet

VUV – vacuum ultraviolet

XRD – X-ray diffraction

# INTRODUCTION

Advanced oxidation (AO) technology undergoes an intensive scientific exploration for its ability to decompose persistent organic compounds in water, which are hardly degradable by using conventional technologies (Tijani et al., 2014; Fernández-Castro et al., 2015). The use of conventional wastewater technologies is usually limited due to their insufficient oxidative capabilities, the formation of secondary waste, or sensitivity to hazardous substances. The AO processes are not selective, and theoretically, all organic substances can be fully mineralized. The ozone based AO processes are among the most promising as they only require electrical energy for ozone generation but avoid additional chemical materials. The adaptation of ozone based AO technology towards industrial applications faces several challenges, such as energy consumption, operation costs, formation of toxic intermediates, or upscaling. For this purpose, the technology must be optimized for each industrial setting. The energy requirements can be decreased by selecting the optimal combination of advanced oxidation processes (AOPs).

AO process is often amended by supporting the processes to increase its effectiveness. Photocatalysis was suggested as the most effective one with the $TiO_2$ as a superior material for such designs due to its chemical stability and activation by the ultraviolet (UV) radiation. Most of these studies were conducted under small laboratory-scale experiments with reactor volumes up to 1 L, aiming to explore the reaction mechanisms, possible degradation products, and kinetics (Dai et al., 2014; Solís et al., 2016). The decomposition of the broad range of organic pollutants, including various dyes, pharmaceuticals, phenolic compounds, organic acids, etc., was tested by Xia et al. (2015). Several attempts to treat the real wastewater have been reported as well. These studies confirmed the effectiveness of ozone based AO processes for the degradation of pollutants: almost full mineralization can be achieved after the sufficient time of treatment. However, the lack of investigations devoted to the upscaling of such AO systems to the industrial level have been emphasized in recent reviews (Nawrocki, 2013; Xiao et al., 2015).

This dissertation presents attempts in the development of the AO wastewater treatment reactor based on the bench scale ozone and applied for the treatment of the wastewater polluted with various hardly degradable compounds. The design includes the option of immobilized catalyst use, UV radiation source and is easily up-scalable. The highly efficient dielectric barrier discharge (DBD) plasma reactor and resonant high voltage power supply was used for the ozone generation. A combination of plasma/$O_3$ with UV/visible light photocatalysis was found to be very promising to increase the effectiveness of these processes as compared to the same methods used alone. In most cases, the full degradation of pollutants as determined by the total organic carbon (TOC) value and the complete loss in the toxicity have been reached. It was proved that the AO method of plasma-UV-catalyst can be successfully applied for the treatment of wastewater containing hardly degradable organic compounds. The

results provide background for the further investigations of this AO system to the industrial applications, confirming the versatility of such reactor design and the selected AO method.

**Aim of the thesis:**

To research the parameters of the advanced oxidation processes based on the ozone-UV-catalysis for the pollutant decomposition in the wastewater.

**Hypothesis**

The breakdown of waterborne pollutants by the photocatalytic ozonation leads to the highest efficiency, lowest energy consumption, and highest toxicity reduction among the advanced oxidation processes based on ozone.

**Objectives of the dissertation:**

1. To investigate the plasma based process for the generation of ozone and other oxidizing species followed by the application in the advanced oxidation reactor for the degradation of pollutants in the water.
2. To investigate the synergetic effects of various factors while performing the treatment of model wastewater polluted with target compounds in an up-scaled AOP system.
3. To examine the possibility to apply the optimized AOP system for the treatment of the real industrial wastewater.

**Scientific novelty**

1. The effects of the operational parameters on the yield of ozone and degradation of various organic pollutants as well as the treatment efficiency of real wastewater in the original newly developed AO reactor have been presented.
2. New synergetic associations between process variables, including treatment duration, ozone supply, UV radiation and catalysis, have been provided for the efficient decomposition and toxicity reduction to zero values for the most organic pollutants.

**Structure and outline of the dissertation**

This dissertation consists of the following parts: introduction, literature review, methods and measurements, results and discussion, recommendations and discussion for the future research, conclusions, list of 88 references, and list of publications on

the dissertation topic. The literature review, methodology, and results of the research are presented in 97 pages, including 10 tables and 31 figures.

**Publication of the research results**

The results are presented in 4 publications in journals listed in the Clarivate Analytics Web of Science database and reported at 3 international conferences.

**Practical value of the work**

1. The investigation brings the advanced oxidation process of the photocatalytic ozonation closer to the industry-scale application. The new legislation in wastewater treatment requiring zero emissions of the micro pollutants will give this technology a boost in the applications in the near future.
2. The methods section describes the methodology for the full investigation of ozone – UV – catalysis based AO wastewater treatment system, which can be used in the future experiments with higher technology readiness level (TRL) equipment.
3. The experimental data is presented including the energy requirements for each pollutant degradation, toxicity reduction, and the efficiencies of different AO methods. This data lays a background for the creation of industrial scale system.
4. An example of effective and durable immobilized $TiO_2$ catalyst installation is presented providing possible pattern for the further development.

**Author's contribution**

Author participated in the experiments and data analysis as well as manuscript preparation process of the results presented in the chapter **3.2. The results of the full factorial experiment of 2-naphthol polluted water treatment by using DBD plasma reactor**. This passage is quoted from the article entitled "Decomposition of 2-naphthol in water using a non-thermal plasma reactor" (10.1016/j.cej.2014.08.098) with permission of Elsevier.

The author participated in the experiments and manuscript preparation process of the results presented in the chapter **3.3 Pharmaceuticals removal from water using photocatalytic ozonation**. This passage is quoted from the article entitled "Removal of diclofenac, ketoprofen, and carbamazepine from simulated drinking water by advanced oxidation in a model reactor" (10.1007/s11270-017-3517-z) with permission of Springer Nature.

14

Author conducted the experiments presented in the chapter **3.4. The treatment of various organic compounds polluted water by using photocatalytic ozonation**, analyzed the data, and prepared the manuscript. This passage is quoted from the article entitled "Ozone-UV-catalysis based advanced oxidation process for wastewater treatment" (10.1007/s11356-017-9381-y) with permission of Springer Nature.

Author conducted the experiments presented in the chapter **3.5. The treatment of industry wastewater by using photocatalytic ozonation**, analyzed the data, and prepared the manuscript. This passage is quoted from the article entitled "Advanced oxidation-based treatment of furniture industry wastewater" (10.1007/s11356-017-9381-y) with permission of Taylor & Francis Group.

# 1.  LITERATURE REVIEW

## 1.1.  The current status of the wastewater treatment

Wastewater treatment methods involve various physical, chemical, and biological processes. They can be categorized in different ways based on the aim of treatment, utilized processes, etc. One of the possible classifications of wastewater treatment methods is presented in the **Figure 1.1**
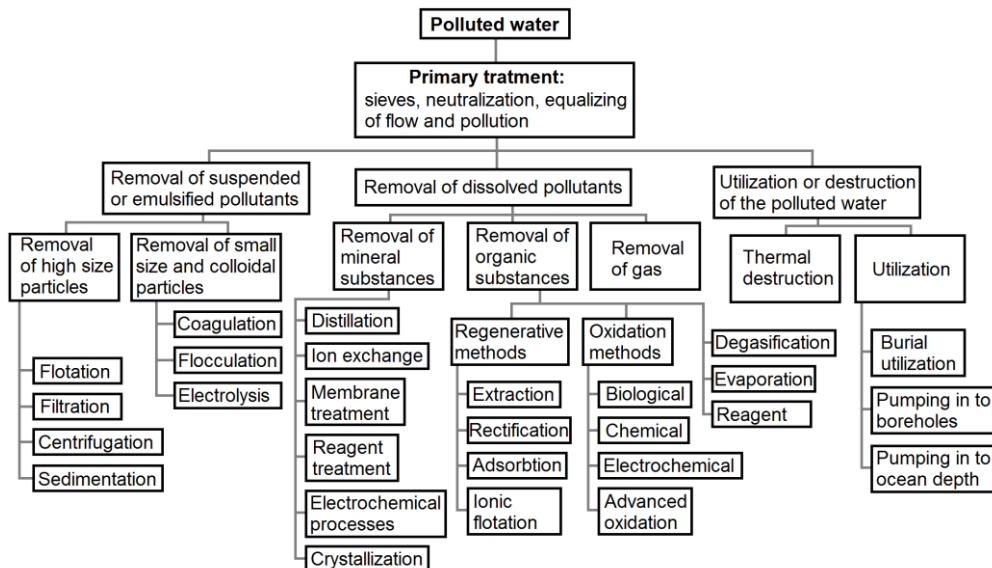


**Figure 1.1.** Classification of water and wastewater treatment technologies.

The challenges of wastewater treatment are diverse and differ depending on the technological issues, legislative requirements for the effluent control, etc. Nowadays, there is a growing concern towards the minimization of discharge of emergency pollutants into the environment. As a result, new wastewater treatment technologies started to be developed in order to overcome the limits of the wastewater treatment efficiency attained by the conventional treatment methods. The demand for new technologies is even higher for the treatment of industrial wastewater, as complex molecules of the anthropogenic pollutants are hardly biodegradable. Recently, looking for the novel technologies, the attention was directed towards the advanced oxidation processes. One of the main advantages of AOP compared to the conventional technologies is that they can effectively degrade recalcitrant pollutants by producing simpler organic compounds, or in a case of full mineralization, carbon dioxide, water, and inorganic salts (Moreira et al., 2016; Tijani et al., 2014; Yen and Kang, 2016).

## 1.2.  AO technologies

Generally, AO processes utilize the in situ formation of reactive hydroxyl and oxygen radicals, which serve as oxidative agents. Such highly reactive environments are achieved primarily by two techniques differing by reaction phases: homogeneous

processes, based on the salvation of plasma ionized gas (including $O_3$) or $H_2O_2$ and $Fe^{2+}$ ions together with the ultraviolet radiation (UV), or heterogeneous processes, based on the application of the (photo)catalyst (Tijani et al., 2014).

The advanced oxidation technologies can be classified as presented in **Figure 1.2** (Tijani et al., 2014; Fernández-Castro et al., 2015). This classification is based on dividing technologies into homogeneous and heterogeneous processes. In case of homogeneous processes, the additional material must be introduced into the wastewater, whether it is a liquid or gaseous element. Additionally, in the homogeneous processes, this additional oxidative material can be produced in the wastewater under the effect of energy source, for example, under the impact of ultrasound or electrical energy, as at the electrohydraulic discharge treatment.

The heterogeneous processes utilize the introduction of solid-state material with catalytic activity. In this case, the homogeneous material can be used (catalytic ozonation, etc.) or not (photocatalysis). The most important AO processes are presented in the following sections **1.2.1. – 1.2.5.**
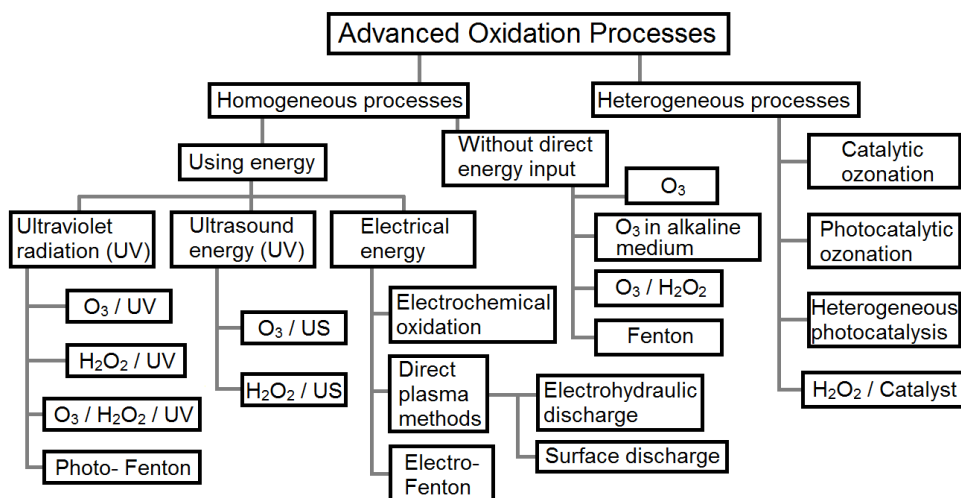
**Figure 1.2.** Classification of the AO technologies for the wastewater treatment (Tijani et al., 2014; Fernández-Castro et al., 2015)

### 1.2.1. Ozone based methods

Looking through the classification above, the ozone component can be found in the most cases of advanced oxidation technologies. As the use of ozone alone is not comparatively efficient (Tijani et al., 2014), the joint use with other AO components is recommended to decrease the energy and material requirements as well as increase the efficiency. It has been found that the common use with UV radiation (Chang et al., 2015), ultrasound (Tijani et al., 2014), chemical-homogeneous process (Tijani et al., 2014), and heterogeneous catalysis (Mano et al., 2015) can increase the total efficiency several times. The efficiency increase is caused by the changes of the hydroxyl radical formation mechanisms, leading increased yield of this radical. The

principles of ozone utilization enhancement are discussed more broadly in the section (**1.4.**).

### 1.2.2. Fenton method

The Fenton method is one of the most frequently used AOP (Wang et al., 2016) due its high efficiency on removal of many hazardous organic pollutants from the water (Neyens and Baeyens, 2003). The method is based on *in situ* generation of hydroxyl radical by using hydrogen peroxide as oxidant and ferrous ion ($Fe^{2+}$). The most important reactions are presented as follows (Neyens and Baeyens, 2003):

$$Fe^{2+} + H_2O_2 \rightarrow Fe^{3+} + HO\bullet + OH^-; \qquad (1)$$

$$Fe^{3+} + H_2O_2 \leftrightarrow Fe\text{-}OOH^{2+} + H^+; \qquad (2)$$

$$Fe\text{-}OOH^{2+} \rightarrow HO_2\bullet + Fe^{2+}. \qquad (3)$$
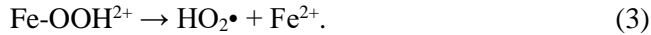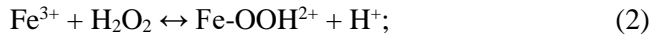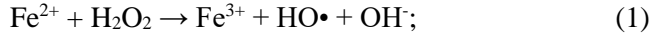
As seen from the reactions above, the iron ions are not consumed in opposite as hydrogen peroxide, which is consumable material in this AO process. Likewise, as ozone, the Fenton method can be combined with other AO processes to develop wastewater treatment technology, thus reducing the consumption of energy and material resources.

### 1.2.3. Ultrasound

The effect of ultrasound is based on its physical and chemical effects through cavitation (Li et al., 2013). Under the effect of the ultrasound, the micro cavitation bubbles are formed, and their collapse creates energetic micro-environment of extremely high local temperature and pressure (temperature up to 5000 K and pressure up to 500 bar). Under these conditions, various radicals are created from water molecules (Li et al., 2013):

$$H_2O \text{ (ultrasound waves)} \rightarrow H\bullet + HO\bullet; \qquad (4)$$

$$HO\bullet + HO\bullet \rightarrow H_2 + O_2; \qquad (5)$$

$$H\bullet + O_2 \rightarrow H_2O\bullet. \qquad (6)$$
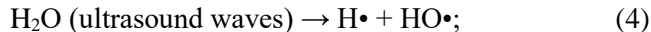
The oxygen molecule can be split into radicals as well (Tijani et al., 2014):

$$O_2 \rightarrow 2O\bullet. \qquad (7)$$

As the advantage of the ultrasonic water treatment, it does not require to use additional chemical substances (Tijani et al., 2014), however, due to high energy consumption, the technology should be combined with other methods as ozone, hydrogen peroxide, Fenton, and others (Li et al., 2013).

### 1.2.4. Electro-methods

There are two main technologies utilizing electric current for the wastewater treatment: one is electrical discharge based plasma methods, and the other one is electrochemical oxidation.

**Direct plasma methods.** The plasma methods utilize the direct formation of plasma discharge by using high voltage in the wastewater or/and above it. The method of discharge formation in water is called electrohydraulic discharge. During this process, the water layer between two electrodes is broken by high voltage potential, and the formed high current arc acts as the energy source for the radical formation mechanisms. The hydroxyl radical forms in the reaction of water molecule dissociation and ionization (Jiang et al., 2014):

$$\text{dissociation:} \quad H_2O + e \rightarrow HO\bullet + H\bullet + e; \tag{8}$$

$$\text{ionization:} \quad H_2O + e \rightarrow 2e + 2H_2O^+; \tag{9}$$

$$2H_2O^+ + H_2O \rightarrow HO\bullet + H_3O^+. \tag{10}$$
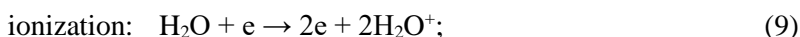
During the electrohydraulic discharge, the side effects as UV radiation and shock waves are formed; both of them can lead to the degradation of water pollutants. The other wide area of direct plasma application is the so-called surface plasma method when the plasma discharge is formed above the water. In this case, various configurations of reactors can be used, including gliding arc discharge, dielectric barrier discharge over thin liquid layer or others. The discharge in the gaseous phase produces mainly ozone (if oxygen is present in the gas) nitrogen oxides (if air is used) and hydroxyl radicals over the water surface. As the discharge occurs on the surface of the water, the short living radicals that are formed in the plasma (the same $HO\bullet$) can participate in the pollutant degradation process. Mass transfer of the pollutant to the surface layer of the wastewater mainly limits the efficiency of the surface plasma methods. For this reason, the large-scale applications are mainly related to the surface treatment.

**Electrochemical oxidation.** Generally, during the electrochemical oxidation, the hydroxyl radicals are formed on the metal electrode surface (anodic oxidation); the other oxidative agents can be formed through various pathways as well (Moreira et al., 2017):

$$M + H_2O \rightarrow M(HO\bullet) + H^+ + e^-; \tag{11}$$

$$2M(HO\bullet) \rightarrow 2MO + H_2O_2; \tag{12}$$

$$3H_2O \rightarrow O_3 + 6H^+ + 6e^-; \tag{13}$$
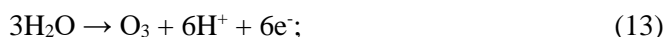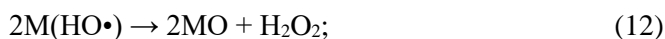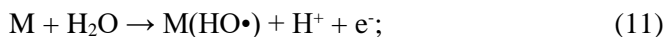
where M is anode surface.

The efficiency of the method depends on the mass transfer of pollutants from the total volume of the wastewater to the anode surface, anode material, presence of

inorganic ions in the wastewater. Other types of electrochemical oxidation are known, i.e., electro-Fenton and photoelectro-Fenton.

### 1.2.5. Photocatalysis

Photocatalysis is classified as the heterogeneous AO process, as the solid-state catalysts are used in most cases. The semiconductor materials (as $TiO_2$) are used as heterogeneous catalyst most frequently. In heterogeneous photocatalysis, the photocatalyst is present as a solid with the reactions taking place at the interface between phases, i.e., solid-liquid or solid-gas. The oxidation or reduction reactions involves the hole and electron transfer from the photo-excited semiconductor. The semiconductor is excited by the absorption of electromagnetic radiation with energy equal to or greater than the band gap energy. This results in the promotion of the electron from the valence band to the conduction band, leaving positive hole in the valence band. The electron/hole pairs may recombine with the energy that is being re-emitted as heat or light, or the charge carriers can migrate to the particle surface. The conduction band electron can be passed on to the electron acceptor with a more positive electrochemical reduction potential than the conduction band edge potential. The valence band hole may accept electrons from the donor species with a less positive electrochemical reduction potential than the valence band edge potential. Overall, these processes result in the reduction of the acceptor species and the oxidation of donor species (Byrne et al., 2015). The principle described above can be visualized as presented in **Figure 1.3**.
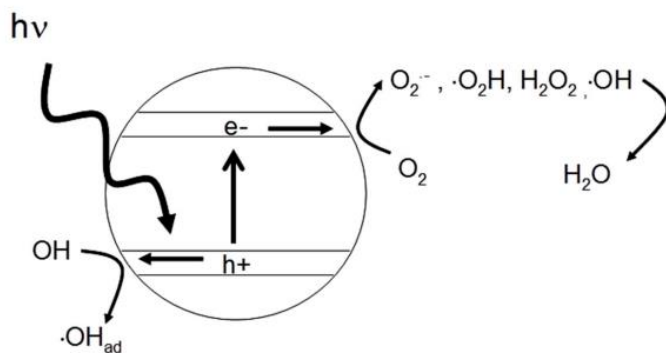


**Figure 1.3.** Schematic view of the photocatalytic mechanism on the titanium dioxide particle leading to the production of reactive oxygen and hydroxyl species (Byrne et al., 2015).

The photocatalysis process has been extensively investigated in recent years, and many successful examples of application for the decontamination of hazardous water pollutants were reported. Although, the growing interest on the photocatalysis supplementation with ozone indicates the advantage of the combined technology against the single photocatalysis.

### 1.3. Methods of ozone generation

Nowadays, the main technique for ozone generation is plasma based. The electrochemical method (Christensen et al., 2013) or photochemical method (Hashem et al., 1997) can be mentioned as minor technologies in the ozone production. From the view of plasma based methods, there are several types of techniques for ozone generation that are classified according to type of used electric current.

### 1.3.1. Electrochemical ozone generation

The ozone can be generated electrochemically by performing electrolysis by using special solution and suitable anode. The electrochemical generation of ozone has many advantages, including (Wei et al., 2016; Christensen et al., 2013) low voltage operation, no need of gas feed, simple system design, generating high concentrations of ozone, in particular, reduced loss of ozone by the thermal decomposition during the handling. The mechanism of ozone generation has been proposed to consist of water split and oxygen atom transfer reactions (Wei et al., 2016); the additional oxygen molecule is dissolved as follows:

$$3H_2O \rightarrow O_3 + 6H^+ + 6e^-; \tag{14}$$

$$H_2O \rightarrow HO\bullet + H^+ + e^-; \tag{15}$$

$$O_2 + HO\bullet \rightarrow HO_3\bullet; \tag{16}$$

$$HO_3\bullet \rightarrow HO_3^+ + e^-; \tag{17}$$

$$HO_3^+ \rightarrow O_3 + H^+. \tag{18}$$

The generation of ozone depends on the electrolysis current density, electrolyte composition, anode material, temperature, and physical construction of the generator cell. The electrode material is usually platinum, lead oxide ($PbO_2$), and other metal oxides as well as boron-doped diamond. The investigation of cheap and highly efficient anode material is still going on, and it is possible that the method will be industrially available in the future.

### 1.3.2. Photochemical ozone generation

The photochemical reactions occurring in the presence of electromagnetic radiation are potentially capable of exciting molecular oxygen in the gas, producing oxygen atom, and resulting in the formation of ozone molecule. Mechanistic studies indicated that UV irradiation favors the excitation of singlet or triplet oxygen atom from the ground state oxygen molecule (Wei et al., 2016), depending on the radiation wavelength:

$$O_2 + h\nu \rightarrow O(^3P) + O(^1D), \lambda < 175 \text{ nm}; \tag{19}$$

$$O_2 + h\nu \rightarrow 2O(^3P), 200 \text{ nm} < \lambda < 242 \text{ nm}. \tag{20}$$
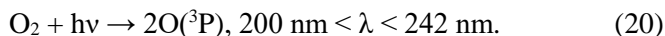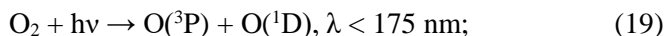
Only the very short wavelength UV radiation can produce ozone (<242 nm); therefore, the standard UV-C mercury vapor lamp is not suitable (254 nm). For this purpose, the vacuum ultraviolet lamp (VUV) is used (Hashem et al., 1997); the most common are special "ozone producing" 185 nm mercury vapor lamps.

### 1.3.3. Gaseous discharge ozone generation

Electrical discharge in the gas media (plasma) is the main technique for the ozone generation. There are two main ways, i.e., DBD discharge and corona discharge. Both of them are classified as non-thermal plasma, while other type of discharge – arc discharge – is classified as thermal plasma and is not efficient for the ozone generation. The main equations of ozone formation in plasma are presented (Wei et al., 2016):

$$e + O_2 \rightarrow O + O^-; \tag{21}$$

$$O^- + O_2 \rightarrow O_3 + e. \tag{22}$$
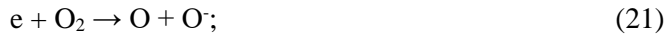
**DBD discharge.** This type of discharge can be generated in the reactors where the configurations of dielectric layers are either covered on the surface of the electrodes inside the discharge gap or suspended between them (Wei et al., 2016). The main reactor configurations are presented in **Figure 1.4**. Those configurations, consisting of the plate or cylindrical electrodes with a dielectric layer between them, generate "volume" discharge (Pekárek, 2013).
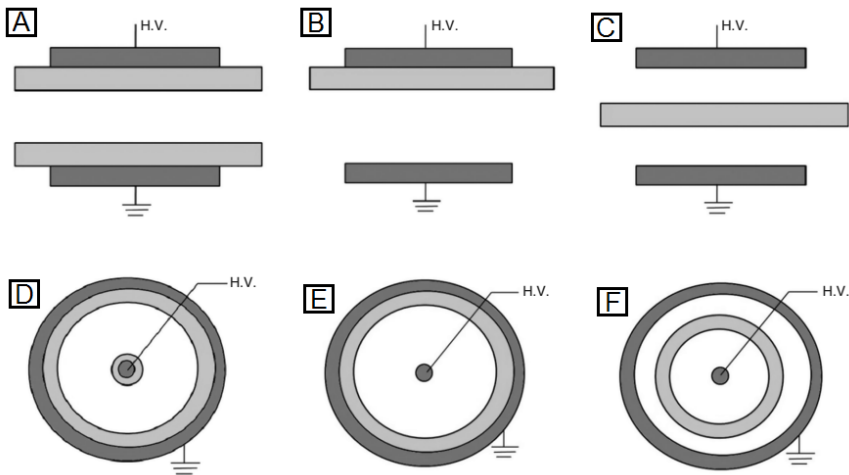


**Figure 1.4.** The main configurations of DBD discharge reactors for the ozone generation (Wei et al., 2016). A, B, C – planar configuration with plate electrodes, D, E, F – coaxial type with tube and rod electrodes, dark gray – conducting electrodes, light gray – dielectric material, H.V. – high voltage.

Nowadays, the novel types of the DBD reactors, i.e., surface DBD (SDBD) and packed bed DBD, raise the interest in the ozone generation. In the surface type of DBD reactor, the plasma is generated at the configuration with the surface electrode on one side of the dielectric plate/cylinder and the second electrode on the reverse side of the plate/cylinder. In the case of the coplanar discharge, the pair/pairs of electrodes are embedded at the fixed distance in the dielectric, and the discharge develops in channels on the dielectric surface between the positions of the electrodes (Pekárek, 2013). The principal layout is presented in **Figure 1.5**.
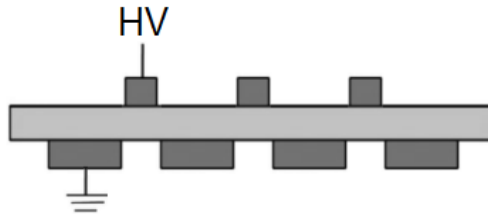


**Figure 1.5.** The principal layout of the SDBD plasma reactor. Dark gray – conducting electrodes, light gray – dielectric material, H.V. – high voltage.

The other type of the DBD reactor – packed bed – utilizes the placing dielectric pellets within the discharge volume inside the plasma reactor. The dielectric materials used to include glass, quartz, aluminum oxides, ceramic, and ferroelectrics. The physical properties of packing pellets would significantly influence the plasma characteristics as well as the performance. The pellets could be either noncatalytic or catalytic; the second ones can be used for the pollutant removal from air (Chen et al., 2008). The geometry of the packed-bed reactor, as shown in **Figure 1.6,** could be either parallel-plate or cylindrical (or so-called "coaxial"). Packed-bed reactors can be constructed without the dielectric layer between the packing pellets and electrode as well (Chen et al., 2008).
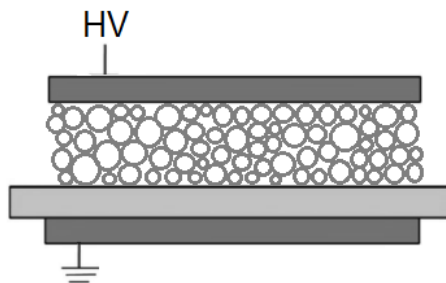


**Figure 1.6.** The principal layout of the packed-bed plasma reactor. Dark gray – conducting electrodes, light gray – dielectric material, white – packing pellets.

In the DBD reactor types that were described above, the discharge in the DBD gap occurs when the high voltage alternating current (AC) is supplied to the high voltage electrode. The dielectric material is non-conductive for the electric current; however, at the frequencies of several kHz (or less, depending on the configuration and materials), the current can pass the dielectric layer. The efficiency of processes in the DBD reactors is in general proportional to the amount of charge flowing through the reactor, which is associated with the discharge current (Pekárek, 2013). In this case, the DBD reactor works as a capacitor, an electronic component, which is electrically conductive for alternating current and resistive to the direct current. Various materials can be used for the dielectric layer: mica, glass, ceramics, layer thickness of 0.5 – 3 mm (Wei et al., 2016).

**Corona discharge.** Unlike the DBD discharge, the corona discharge is characterized by the lower energy density, higher volume of plasma zone, and lesser production of ozone (Moon and Jung, 2007). The main configurations of the corona discharge reactors are presented in **Figure 1.7**.
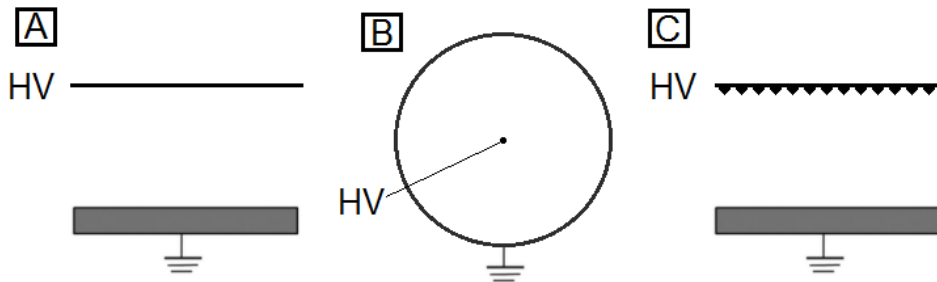


**Figure 1.7.** The principal layout of the corona discharge reactors. A – wire to plate, B – wire to the cylinder, C –high voltage electrode with "saw" type.

The high voltage direct current (DC) or pulsed current is used to feed the corona discharge reactors. As the DC voltage is used, the high voltage electrode can be charged positively or negatively, thus generating positive or negative corona discharge. The type of the discharge depends on the required task.

## 1.4. Improvement of ozone based water and wastewater treatment methods

The utilization of ozone can be increased, and the total efficiency of the wastewater treatment process can be elevated by the usage of additional advanced oxidation elements. Mostly, this option includes common use of UV radiation, catalysis, photocatalysis, additional oxidative material as $H_2O_2$, and other techniques (**Figure 1.2**). These additional elements affect the radical formation mechanisms and may increase the yield of formed hydroxyl radical through various pathways. Nowadays, the most promising results are obtained by using catalysis or/and electromagnetic radiation.

**Ozone and photo-catalysts.** Various photo and ozone heterogeneous catalysts have been recently researched for their application in the photocatalysis in the plasma based advanced oxidation wastewater treatment processes. Transition metal oxides or their mixtures, such as $TiO_2$, $MnO_2$, $Fe_2O_3$, $WO_3$ (Bloh et al., 2012; Mano et al., 2015; Xiao et al., 2015; Huang et al., 2016), elemental metal powders (Wen et al., 2014), or metal fibers (Zhu et al., 2014) were tested. UV-activated $TiO_2$ catalyst was proved the most feasible catalyst for the wastewater treatment, as the most stable and efficient (Mano et al., 2015; Xiao et al., 2015). Mostly, $TiO_2$ was introduced to the wastewater in a powder form, making it difficult to remove after the treatment. $TiO_2$ immobilization on supports was used less frequently by usually utilizing micro-sized support particles (Choi et al., 2016), while experiments utilizing $TiO_2$ coatings on the fixed support surfaces are rare. The use of immobilized heterogeneous catalyst for the wastewater treatment has been suggested as technologically superior (Mehrjouei et al., 2015) due to the avoided necessity of the separation of the catalyst from the treated water, such as in the case of the powdered form of the catalyst.

**UV radiation.** The UV radiation effect on the ozone based water treatment method was reported (Mano et al., 2015; Mehrjouei et al., 2015). The effect is explained by the UV effect on water and ozone molecules (Chang et al., 2015; Mehrjouei et al., 2015):

$$O_3 + H_2O + h\nu \rightarrow O_2 + H_2O_2; \tag{23}$$

$$H_2O_2 + h\nu \rightarrow 2HO\bullet; \tag{24}$$

$$O_3 + h\nu \rightarrow O\bullet + O_2; \tag{25}$$

$$O\bullet + H_2O \rightarrow HO\bullet. \tag{26}$$
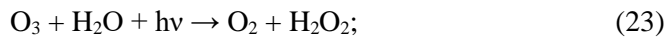
**Photocatalytic ozonation.** The presence of photocatalysts (in addition to ozone) in the oxidation medium and the adsorption of ozone and pollutants on its surface can essentially change the oxidation mechanisms, which indicates that photocatalytic ozonation is a different process from the ozonation in the absence of the photocatalyst. Principally, photocatalytic reactions commence by photoexciting the surface of photocatalyst with UV radiation, which can provide the appropriate band gap energy to generate photoactivated electron–hole pairs. In parallel, ozone molecules can adsorb on the surface of the photocatalyst via three different interactions: physical adsorption, formation of weak hydrogen bonds with surface hydroxyl groups, and molecular or dissociative adsorption into Lewis acid sites, each interaction resulting in the production of active oxygen radicals. These active oxygen radicals react with water molecules to produce hydroxyl radicals, which play a key role in the photocatalytic ozonation processes (Mehrjouei et al., 2015). Photocatalytic ozonation is still considered as a more expensive treatment technology, and its use for the removal of biodegradable pollutants from water is not economically justifiable. The particular importance of this oxidation process applies to destroying poorly-biodegradable organic compounds or improving the biological degradability of wastewater samples containing these compounds (Mehrjouei et al., 2015).

## 1.5.   AO applications in the wastewater treatment

Currently, the available conventional treatment technologies have inherent challenges and shortcomings with respect to the applications, design, effectiveness, and economics. Biological treatment, for instance, does not produce satisfactory result, especially when treating industrial wastewater. This is due to the presence of biologically recalcitrant, inhibitory, and toxic pollutants that are resistant to the biological degradation. Other treatment methods, such as air stripping, coagulation, flocculation, reverse osmosis, ultrafiltration, chlorination, etc., can produce toxic by-products that are genotoxic, mutagenic, and carcinogenic to human health. Adsorption produces toxic sludge, and pollutants are transformed from one phase to another without necessarily being decomposed (Tijani et al., 2014).

Due to the increasing global concern for the environment protection, the concept of AO technologies for water and wastewater treatment was conceived. Up to date, studies still uphold advanced oxidation technologies (AOTs) as the most promising and highly competitive, innovative water and wastewater treatment methods for the removal of biorecalcitrant compounds. AOPs stands as one of the viable technologies capable of decomposing biologically recalcitrant, persistent organic pollutants (Tijani et al., 2014). For this reason, the AO can be a perfect solution for the treatment of wastewater polluted with hardly degradable or toxic organic compounds.

For this time, the most investigated AO processes are $H_2O_2$ based, single ozone/UV, or joint use of ozone/UV technologies. While the ozonation or UV-photolysis technologies are increasingly used in industry, the technology of photocatalytic ozonation is still in the research stage. Most of the reported data from the AO systems based on the plasma-catalysis-UV simultaneous process has been reported from the small laboratory-scale experiments with reactor volumes up to 1 L. There is a lack of research devoted to the upscaling of such AO systems to the industrial level, which has been emphasized in recent reviews (Nawrocki, 2013; Xiao et al., 2015). Recent attempts to convert fundamental processes to the technological upscaling include removal of contaminants of the emerging concern (diclofenac, carbamazepine, etc.) from water by using photocatalytic ozonation reactor packed with $TiO_2$-coated glass rings (Moreira et al., 2016); decomposition of emerging pollutants (antipyrine, bisphenol A, etc.) in municipal wastewater in a solar photocatalytic reactor, working with powdered $TiO_2$ as catalyst (Quiñones et al., 2015); the degradation of methyl orange, amoxicillin, and 3-chlorophenol by using $TiO_2$-coated silica gel beads in the photocatalysis reactor (Li et al., 2015). The further research, focused on the photocatalytic ozonation process upscaling up to the real industrial use, is necessary, bringing this highly effective AO process to the practical use.

### 1.6. Summary of the implications of the earlier research to those presented in the PhD thesis

The ozone based AOPs are discussed as one of the most promising group of methods for future applications due to their high efficiency. The achievements on reduction of one of the major obstacles, namely, the high operational costs, were overviewed. Nowadays, non-thermal plasma based ozone generation technologies are much more energy efficient. As a result, the yield of ozone reaching up to few hundreds g/kWh can be achieved.

The reduced operational costs as well as costs of installation have led to the rising interest in the application of ozone based technologies in the field of wastewater treatment. However, the use of ozone alone for the wastewater treatment can be comparatively inefficient. As a result, currently, scientific investigations are focused towards the enhancement of ozone utilization during the treatment process. Some studies revealed that due to the synergistic effects, the addition of photocatalysis process has a strong influence on the utilization of ozone for the degradation of pollutants in water.

Many studies were carried out aiming to develop effective catalysts with suitable UV source. The $TiO_2$ catalyst was identified as one of the most efficient for the application in photocatalysis and photocatalytic ozonation. The inertness of this catalytic material is highly favorable for the wastewater treatment, as it may contain chemically aggressive pollutants. Unfortunately, due to the poor adhesion to the surface of catalyst holder, the inertness of $TiO_2$, can cause problems during the process of catalyst preparation. In the analyzed studies, usually a powdered form of $TiO_2$ was used during the wastewater treatment experiments. The problem of separation of catalyst from the treated water has not been observed. Thinking of industrial application, the investigations on the development of the special construction of catalyst are important.

The review has revealed that most of the studies were performed with small-scale laboratory equipment by using simulated wastewater and focusing mainly on the investigation of process of chemistry and kinetics. Only in a few cases, the results, obtained from a pilot-scale or by using real industrial wastewater for the experiments, were reported. Obviously, this academic research has proved the applicability of AOPs for the wastewater treatment. What is really missing is the research on the up-scaling of photocatalytic ozonation technology bringing it closer to the industrial application.

Thus, this dissertation addresses several issues associated with the ozone based advanced oxidation water treatment technology that need to be clarified before the application of this process to the industrial usage.

One of them is the confirmation of the possibility to decompose all the organic compounds in water, whether they are alone or in matrix with other substances. The information about various organic compounds' behavior under the action of the advanced oxidation processes is necessary; however, usually, this information is only available from the studies with various reactor designs. In this dissertation, the same reactor was used in the experiments of various organic pollutant degradations by using various advanced oxidation processes. The use of the identical operational conditions is expected to allow comparing the persistency of model pollutants on each AO process and obtain an overall view on the pollutant degradation kinetics. The wastewater treatment experiment should be conducted with simulated wastewater, followed by the treatment of the real industrial wastewater, though diluted. The obtained results should focus on the efficiency tendencies of various ozone based AO processes and allow to estimate the operational parameters and preliminary final values, e.g., the energy consumption at the large-scale reactors in the future uses.

## 2. METHODS AND MEASUREMENTS

### 2.1. Experimental setup

*The primary setup.* Two experimental water treatment setups were used during this research. The first setup was a semi-continuously operated reactor utilizing the in situ DBD plasma reactor for ionized air production and simultaneous by-produced gas distribution in the water. This apparatus can be called as water-cooled DBD reactor with liquid electrodes. Such design is popular among the other researchers in the early versions of DBD reactors used for the investigations of DBD plasma applications for the water treatment (Mok et al., 2008). The reactor was hand-manufactured from glass and quartz (Simax, Kavalierglass Co. Ltd., Praha, the Czech Republic) at a glassblowing workshop of Kaunas University of Technology. The reactor volume was 2 L with 1 L utilized as a working volume during the experiments. The principal layout of this setup is presented in **Figure 2.1** (Tichonovas et al., 2013):
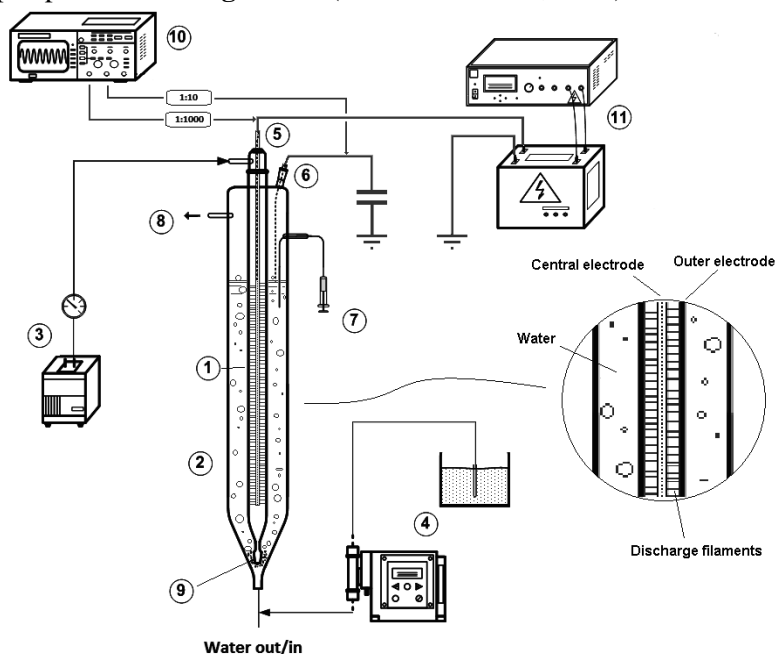


**Figure 2.1.** Experimental DBD reactor for the textile dyes degradation in the water. 1 - DBD plasma reactor, 2 - Reaction vessel, 3 - Air supply pump, 4 – Dye supply pump, 5 - Discharge electrode, 6 - Grounded electrode, 7 - Sampling syringe with a hose, 8 - Excess gas outlet hose, 9 - Gas diffusers, 10 – Oscilloscope, 11 – HVAC power supply (driver and transformer).

DBD plasma was generated in the 4 mm air gap between the walls of two quartz and glass cylinders (1). The first cylinder was a high voltage central glass electrode (5) of 10 mm diameter that was filled with NaCl solution (concentration 100 g/L). The other cylinder was a UV-transparent quartz tube of 16 mm inner diameter, which was surrounded by the model wastewater. A grounded copper rod (6) was immersed into

29

the wastewater. Wastewater acted as a cooling medium for the DBD reactor. Reaction vessel (2) was fabricated of the glass tube, measuring 80 mm in inner diameter and 600 mm in height with the wall thickness of 2 mm. DBD plasma was generated by using AC high voltage power supply (peak-to-peak voltage from 30 kV to 50 kV) (11). Power supply consisted of the transformer and its driver. The AC frequency was set to 8000 Hz as the resonant frequency of the high voltage transformer. The air supply pump (3) was used to supply air into the reactor at the flow rate of 14.5 L/min. Such flow rate was determined by preliminary tests as the optimal one for assuring sufficient cooling of electrodes and producing high quality plasma. Higher flow rates increased the bubbling of the wastewater and the size of bubbles, reducing the solubility of gases. The air flowed into the gap between electrodes; plasma (ozone and highly reactive species) was generated in the DBD discharge zone. $O_3$ and other highly reactive species enriched in air were dispersed into the model wastewater by five 10 x 30 mm ceramic diffusers (9). The outlet gasses were directed to the exhaust (8). The discharge as well produced UV radiation that was able to reach the wastewater through the quartz cylinder walls. Liquid dosing pump (DME2, Grundfos Holding A/S, France) (4) was used for the accurate dosage of dye solution. The samples were taken by using 10 and 50 mL syringes (7). The treatment of wastewater was carried out for 10 min. During that time, the solution of most dyes became completely decolorized. An oscilloscope (Rigol DS1052E, Rigol Technologies, Inc., PRC) (10) was connected to the system through a 1:1000 voltage divider for the measurements of the electrical parameters. Discharge power in the DBD reactor was measured by using the Lissajous figure method (Cai et al., 2010). For this purpose, 27 nF capacitor was connected in series to the reactor. This apparatus allows investigating the treatment of various chemicals polluted water by using ionized gas (mainly ozone) that was generated in the DBD plasma. As well as the polluted water treatment experiments, this setup was suitable for the DBD plasma reactor investigations, including the determination of ozone generation issues, the impact of power and other parameters. This is possible due to the variable settings of the air supply rate, variable power and frequency of the high voltage supply.

*The up-scaled setup.* In the next stage of experiments, the research on ozone usage enhancement (including the utilization of catalysis and photolysis) was planned; thus, the up-scaled experimental setup was designed and manufactured. The bench scale advanced oxidation system based on the plasma-UV-catalysis processes was designed and assembled in the Department of Environmental Technology at Kaunas University of Technology. The design of the DBD reactor for plasma production was similar as in the previous experiment in the small-scale system. The current setup was designed for the bench scale experiments for various combinations of plasma (ozonation) and photocatalysis processes to degrade pollutants in the water. The principal scheme of the setup is presented in **Figure 2.2**.
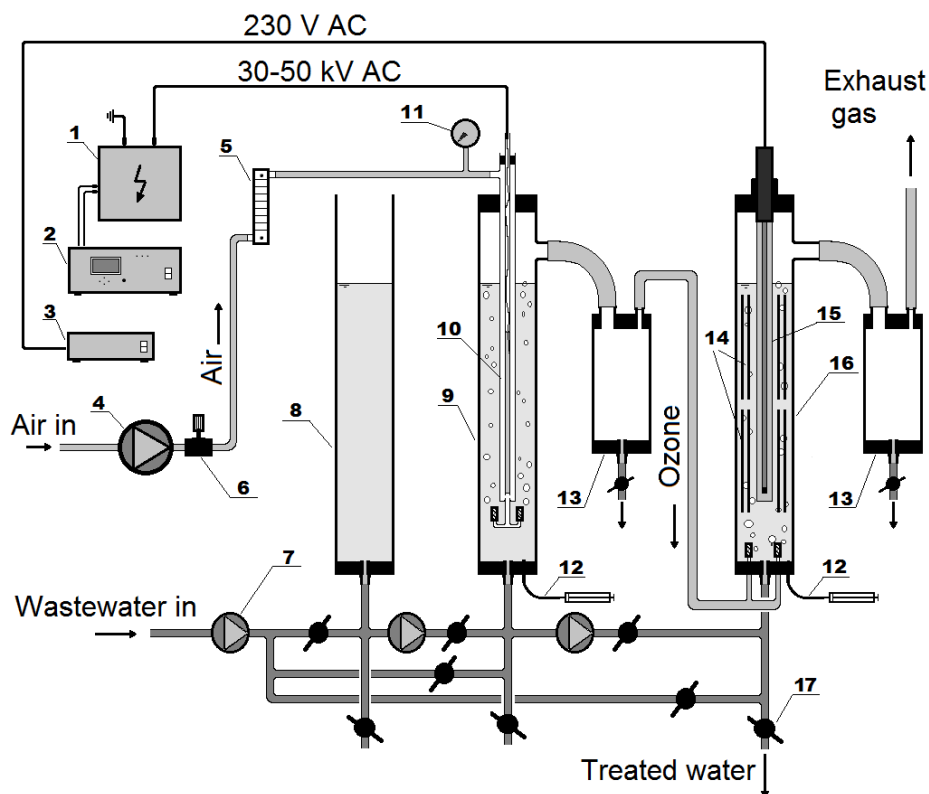
**Figure 2.2.** The principal layout of the bench scale advanced oxidation system for the decomposition of the wastewater pollutants. 1 – high voltage transformer, 2 – high voltage controller, 3 – UV controller, 4 – air supply pump, 5 – rotameter, 6 – air flow valve, 7 – liquid pumps, 8 – buffer vessel, 9 – DBD reactor vessel, 10 – DBD reactor, 11 – pressure measurement, 12 – sampling syringes, 13 – foam damper, 14 – frames of the rod-like catalyst, 15 – UV lamp with quartz cover, 16 – UV-photocatalysis reactor, 17 – valves.

This setup is based on the batch operation and employs a system of three vessels, each of 2 L volume. Initially, the wastewater is pumped into the buffer vessel (8), which has volume markers, to measure the amount needed for the experiments (1.6 L). Afterwards, the water is supplied either to the second vessel (9) (DBD plasma reactor vessel) or the third vessel (16) (photocatalysis reactor). The DBD plasma reactor (10) consists of a double wall quartz tube installed in the center of the vessel and containing a high voltage central electrode based on the salt solution and a gap between two quartz walls. The outer quartz wall surface is surrounded by the water when the device is under operation; the water in this vessel is electrically grounded and at the same time acts as a cooling medium for the reactor. The air is supplied to the gap of the DBD reactor, where the plasma forms when the high voltage generation is activated. Then, the formed plasma is bubbled to the wastewater trough ceramic diffusers in the same reactor. The third reactor has a UVC lamp (15) (40 W model

F980078BU, LightTech, Hungary) installed in the middle of this vessel, and a frame for the mounting of rod-like catalyst (14) as well as diffusers for bubbling the remaining ozone from the DBD reactor. Thus, the third reactor employs all three factors: ozone, UV radiation, and catalyst. In addition to the reaction vessels, two foam dampers, air flow and UV controllers, power measurement unit, and high voltage generator are employed. The latter had the power control and adjustment of frequency in the range of 1 – 10 kHz. Such versatile system can be used to study separate or simultaneous effects of plasma, UV, and catalyst to the pollutant decomposition. In the further experiments, the DBD plasma reactor was used as the ozone generator, and all the decomposition processes with model wastewater were performed in the third vessel, i.e., UV reactor. For ozone generation purposes, the DBD reactor vessel was filled with clean synthetic tap water in each experiment; this water can be changed before every run. During the experiment described in section 2.4.2., the rod-like catalyst was changed to the radially positioned plate-like catalyst frames, as shown in the simplified layout of the experimental equipment (**Figure 2.3**):
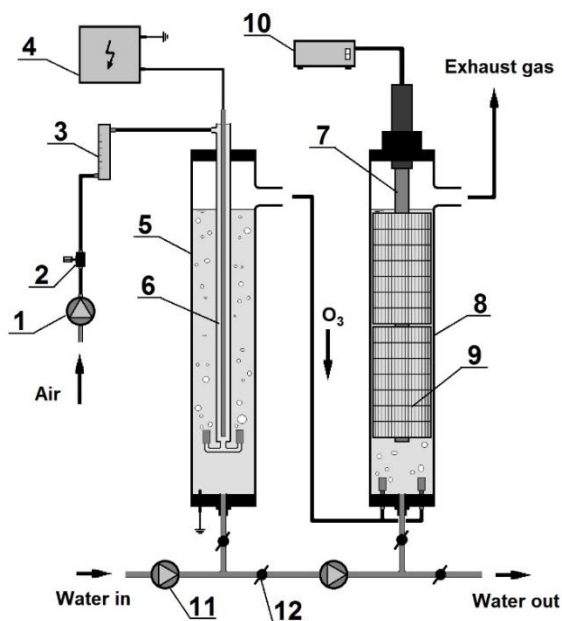


**Figure 2.3.** The simplified principal layout of the equipment with plate-like catalysts inserted in the UV-photocatalysis reactor. 1 - air supply pump, 2 - air flow regulating valve, 3 – rotameter, 4 - high-voltage supply, 5 - DBD reactor vessel, 6 - DBD reactor, 7 - UV lamp with quartz cover, 8 - UV-photocatalysis reactor, 9 – catalyst, 10 - UV lamp power supply, 11 - water pump, 12 - water-regulating valve.

## 2.2. Measurement and analysis methods

**DBD power measurements.** Power measurements of DBD reactor were made following the standard Lissajous power measurement method (Cai et al., 2010). The oscilloscope Rigol DS1052E (Rigol technologies, P.R.C.) and 1000x high voltage

probe (Tektronix, P.R.C.) were used for the measurements. The capacitor of 6.8×10−8 F was connected to the DBD reactor and ground during the measurements. The results of the electrical measurements were analyzed by using Matlab 7 software.

**COD analysis.** The COD analyses were performed following the LST ISO 6060:2003 (ISO 6060:1989) standard procedures. All samples were analyzed on the same day avoiding the possible reduction of pollution over time.

**BOD analysis.** The BOD analyses were performed following the ISO 5815-1:2003 standard procedures. All samples were analyzed on the same day (and prepared for 7-day incubation) avoiding the possible reduction of pollution over time.

**TOC analysis.** All TOC analyses were performed by using TOC analyzer (TOC-L, Shimadzu, Japan) following the LST EN 1484:2002 (EN 1484:1997) standard. The samples were analyzed immediately after sampling, ensuring high reliability of the results.

**Ozone measurements.** Ozone concentration in the gas phase was determined by using the standard iodometric analysis method (Standardized Procedure 001/96, International Ozone Association). The gas containing ozone was sampled from the DBD reactor outlet by using a vacuum pump at 1 L/min flow rate. The ozone absorption solution was analyzed immediately after the sampling.

**Toxicity testing.** Two different methods were used to test water sample toxicity testing. First of them utilizes the adapted *Daphnia magna* toxicity testing procedure (Daphtoxkit F™), (MicroBioTests Inc., Belgium). In this case, the toxicity of untreated and treated model wastewater samples was diluted from 2 to 8 times before testing; three repetitions of each test were made. The daphnia mortality was checked after 24–72 hours.

The second method was performed through applying the adapted method of acute toxicity test proposed by Weltje et al. (2007). The testing method was based on the toxicity measurements with Chironomus sp. larvae obtained from the same culture and grown in the laboratory. The tests were performed in triplicate petri dishes, containing 30 mL of sample and 10 Chironomus sp. larvae. All samples were tested without dilution. Test dishes were kept at room temperature. Mortality of larvae was measured for 24 h every 3 h with 15 h night break. Toxicity results are presented as 24 h cumulative larvae mortality rate.

**XRD and SEM analyses.** The X-ray diffractometer D8 Advance (Bruker, the USA) was used for the XRD analysis, while SEM images were obtained by EVOMA15 (Zeiss, Germany) electron microscope. Both analysis methods were used for the characterization of the catalyst.

**UPLC-MS analysis.** UPLC-MS analysis was performed by using Acquity UPLC (Waters, the USA) system equipped with the mass spectrometer Maixis 4G (Bruker, the USA). The Acquity UPLC BEH C18 column was used for separation; 0.1% formic acid (v/v) in the ultrapure water and methanol were used as mobile phases. The MS operated at the capillary voltage of 4500 V, a nebulizer pressure of

2.5 bars, and dry gas (nitrogen) flow of 10 L/min at the temperature of 200 °C. Ion polarity was set to negative with scan range of 80–1200 m/z. The analysis method was used for the identification of degradation by-products formed during the water treatment process.

**FTIR analysis.** FTIR analysis was performed by using Spectrum 65 (PerkinElmer Inc., the US) FTIR spectrometer. The spectra were collected from 400 to 4000 cm$^{-1}$ with the resolution of 1 cm$^{-1}$. The analysis method was used for the identification of degradation by-products formed during the water treatment process.

**HPLC-UV analysis.** The HPLC-UV system consisted of two pumps (HPLC Pumps 501, Waters Corporation, the USA), an injector (7725i Reodyne, IDEX Health & Science, the USA) equipped with 20 μL sampling loop, and a UV detector (Lambda-Max 481, Waters Corporation, the US). Data analysis was performed by using Unichrom V (New Analytical Systems Ltd., Belarus) chromatographic data system. A Supelcosil L-1 (Supelco Analytical, the US) column (250 mm × 4.6 mm, 5 μm) was used for the separation. The mobile phase was composed of 40% acetonitrile (HPLC grade) and 60% deionized (<3 μS) water. The flow rate was 0.7 mL/min, and UV detection was at 290 nm. The samples were injected into the HPLC system by using a micro-syringe. The injection volume was 100 μL. The analysis method was used for the determination of pollutant concentration in the water.

**GC-MS analysis.** For the GC-MS analysis, the GCMS-QP2010 Ultra analytical system (Shimadzu Corporation, Japan) was used. Split injection was set at a split ratio of 1:5 and carried out at 290 ºC. The injection volume was 1 μL. Helium was employed as a carrier gas at a flow rate of 1.2 mL/min. The oven temperature was set to 40 ºC for 1 min and then raised to 300 ºC at a rate of 20 ºC/min. The mass spectrometer was scanned in the m/z range from 30 to 400, and the scan rate was 0.30 s per scan. The ionization source and interface temperature were 300 ºC. The mass spectrometer was operated by using electron-impact (EI) mode (70 eV). The analysis method was used for the identification of degradation by-products formed during the water treatment process.

**Calculations of the energy requirements.** The energy requirements for the decomposition of pollutant (as pollutant mass or TOC mass) were calculated by using the following formula:

$$E(kJ/g) = \frac{t(s) \times P(W)}{m(mg)};$$
(27)

where t is treatment duration (s); P is total power of treatment equipment used at the current experiment (W); m is the mass of the pollutant, initial compound, or TOC (mg).

## 2.3. Procedures of the catalyst preparation

**Preparation of the plate-like catalyst.** Fourteen corrugated 316L stainless steel plates with dimensions of 19.5 × 2.5 cm$^2$ and 0.5 mm in thickness were used as the catalyst support material. The catalyst coating on stainless steel was prepared by

using commercially available $TiO_2$ nanopowder Aeroxide P25; primary particle size was 21 nm (Evonik Degussa GmbH, Germany). First, stainless steel plates were placed for 1 h in 1 M $H_2SO_4$ solution for surface acidic corrosion assisted with ultrasound. This was followed by washing plates with distilled water and drying for 2 h at 150 °C. Then, plates were rinsed with hexane for 10 min; the air was dried to remove excess solvent and heated at 500 °C for 30 min in the muffle furnace. The $TiO_2$ powder was dispersed into methanol at the concentration of 20 g/L and ultrasonicated for 30 min. $TiO_2$ coatings were obtained from $TiO_2$ suspension by the electrophoretic deposition. Two stainless steel plates were immersed into $TiO_2$ suspension. A standard spacing of 1.5 cm was used between the cathode and anode. Electrophoretic deposition was performed at constant voltage (30 V) and controlled by using the DC power supply unit. Deposition time was 30 s. Coatings were calcinated at 500 °C for 5 h. The catalyst specific surface area in the reactor was approximately 92 $m^2/m^3$.

**Preparation of the rod-like catalyst.** The catalyst coating on glass was prepared using commercially available $TiO_2$ nanopowder Aeroxide P25; primary particle size was 21 nm (Evonik Degussa GmbH, Germany). Glass rods (Simax) of 5 mm in diameter and 20 cm in length were used as the catalyst support. The $TiO_2$ powder was dispersed into methanol at the concentration of 10 g/L and ultrasonicated for 30 min. The glass rods were positioned on the heating plate and sprayed with $TiO_2$-methanol suspension using atomizer nozzle. The procedure was repeated several times to form a uniform layer of the catalyst. The glass rods with $TiO_2$ coating were placed in the muffle furnace and heated at 450 °C for 3 h. The prepared rods were fastened in polytetrafluoroethylene (PTFE) and stainless steel frames. This frame consisted of two PTFE rings, which have been fastened in parallel position to each other with two stainless steel bolts. The rings had holes for the mounting of glass rod ends. Thirty rods were positioned in a radial arrangement around the center of the cylindrical construction with an orifice for UV lamp positioned in the center. Two frames of the prepared catalyst were installed in the reactor. The catalyst specific surface area in the reactor, calculated as glass substrate surface area divided by the wastewater volume, was approximately 111.8 $m^2/m^3$.

## 2.4. Experimental design

All experiments presented in this doctoral thesis were made according to the plan, which was adjusted taking into account the observations during the research. The whole research can be separated into two main parts:

- The investigation of application of DBD plasma for ozone (ionized gas) generation and polluted water treatment;
- Improving and upscaling of the previously described method using additional AO elements and testing.

The first part includes designing and manufacturing of the DBD reactor and its power supply, constructing the primary setup for application of the DBD plasma method for the polluted water treatment. The layout of this equipment was presented before (**Figure 2.1**).

After this, the equipment was redesigned taking into account the observations from the performed experiments as well as the additional review of scientific literature. The review was mainly focused on the application of additional AO components for the ozone based (or DBD plasma based) water treatment methods. The decision was made to install the UV radiation source and immobilized catalyst frames. The layout of the up-scaled setup was presented before (**Figure 2.2**). As the experiments in the first part were made in the vessel, in which the DBD reactor was installed, in the case of the following experiments, the secondary photocatalysis reactor was used. The experiments for the investigation of application of UV-photocatalysis for the ozone based water treatment method was planned to measure the effect of various experimental conditions, including the single component effect (e.g., UV radiation) or combination of various AO components (e.g., joint ozone and UV). The whole experimental work can be represented graphically (**Figure 2.4**):
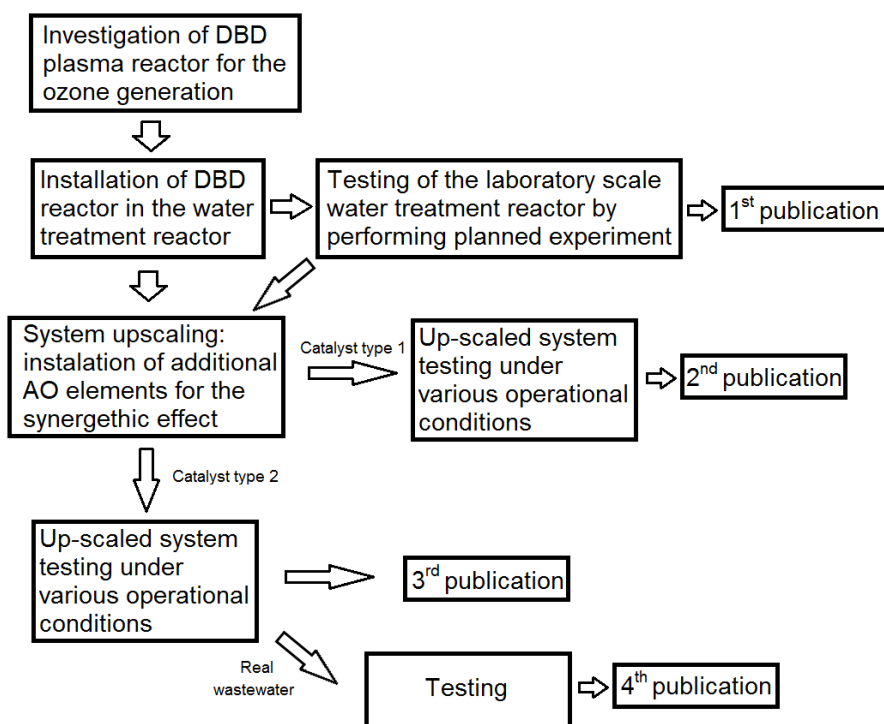


**Figure 2.4.** The summarized activities of the doctoral research.

The results were published in four scientific publications; for each of them, the separate experimental planning was made. This information is presented in the following sections (2.4.1. – 2.4.4.).

## 2.4.1. Factors affecting the treatment efficiency of DBD plasma wastewater treatment method by performing full factorial experiment

**Objective.** The efficiency of the DBD plasma water treatment method based on the salvation of the ionized gas in the water was investigated in the treatment of

simulated wastewater. The 2-naphthol was selected as the model pollutant in this group of experiments. A full factorial screening experiment was carried out in order to identify the key factors affecting the degradation process for 2-naphthol. The primary experimental setup was used in this investigation (**Figure 2.1**).

**Model wastewater.** For this purpose, the stock solution (concentration of 100 mg/L) was prepared by dissolving 2-naphthol (Sigma–Aldrich) crystals in 200 mL fresh tap water (pH ~7.5, conductivity ~500 µS, room temperature). Due to the poor 2-naphthol solubility, an ultrasonic bath was used for 30 min. The working solution was prepared by diluting the stock solution with fresh tap water to the required concentration.

**Screening experiment.** Modeling software Modde 7 (Umetrics Inc., Sweden) was used for the experiment planning and the identification of optimum process conditions according to the results of experiments (**Table 2.1**). The used software allows the statistical analysis of the results as well as the process modeling. During the screening experiment, initial variables that were provided to the software were DBD power (from 5 to 20W), reactor air flow (7–14.5 L/min), air humidity (ambient of 50–100%), and the initial pollutant concentration (5–30 mg/L). These parameters were determined heuristically during the preliminary instrumental runs. Full factorial experiment with three middle points was selected for the theoretical screening experiment. The constant parameter was the working reactor volume of 1 L. Then, nineteen experiments were provided by the software, and they were performed experimentally to obtain the response parameters, namely decomposition efficiency as well as the ozone concentration in air and water. Samples were taken for the analysis after 6 min. The modeling data was fitted to the partial least squares regression model using software. The response curves that were shown in Figs. 3.4.–3.5. were obtained and will be discussed further in the text.

**Main experiment.** Decomposition kinetics and intermediate product identification were explored in the experiments using four different power values of 5, 10, 20 W, the same as in the screening experiment, as well as one additional of 33 W. The air flow rate was set to a constant value of 7 L/min, and the 2-naphthol concentration was 10 mg/L. The concentration of 2-naphthol was measured using HPLC-UV, while the intermediate products were determined using GC-MS analysis. Samples were taken after 0, 0.5, 1, 3, 6, and 12 min. A blank experiment was performed as well. The treated wastewater after the plasma exposure at 33W was analyzed for the TOC content and toxicity. Finally, possible degradation products were determined using FTIR analysis. In this case, the initial concentration of 2-naphthol was increased to 100 mg/L due to the relatively low method sensitivity. Treatment time was increased with samples taken at 0, 3, 6, 15, and 30 min as well.

**Table 2.1.** Design of the full factorial screening experiment, including the results of ozone determination.
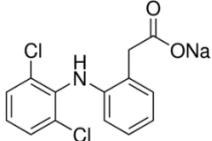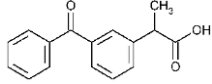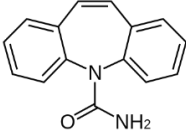
| Experiment No. | Run order | DBD power, W | Aeration, L/min | Initial concentration, mg/L | Air (dry/humid) | Decomposition efficiency, % | Ozone concentration in air, mg/L | Energy for ozone formation, kJ/g | Energy for ozone formation, Wh/g |
|---|---|---|---|---|---|---|---|---|---|
| 1 | 9 | 5 | 7 | 5 | Humid | 88 | 0.66 | 64.94 | 18.04 |
| 2 | 14 | 20 | 7 | 5 | Humid | 94 | 1.52 | 112.78 | 31.33 |
| 3 | 6 | 5 | 14.5 | 5 | Humid | 90 | 0.58 | 35.67 | 9.91 |
| 4 | 17 | 20 | 14.5 | 5 | Humid | 94 | 1.12 | 73.89 | 20.53 |
| 5 | 18 | 5 | 7 | 30 | Humid | 78 | 0.61 | 70.26 | 19.52 |
| 6 | 15 | 20 | 7 | 30 | Humid | 85 | 1.43 | 119.88 | 33.30 |
| 7 | 11 | 5 | 14.5 | 30 | Humid | 83 | 0.55 | 37.62 | 10.45 |
| 8 | 5 | 20 | 14.5 | 30 | Humid | 84 | 1.08 | 76.63 | 21.29 |
| 9 | 1 | 5 | 7 | 5 | Dry | 90 | 0.42 | 102.04 | 28.34 |
| 10 | 2 | 20 | 7 | 5 | Dry | 95 | 1.44 | 119.05 | 33.07 |
| 11 | 13 | 5 | 14.5 | 5 | Dry | 90 | 0.64 | 32.33 | 8.98 |
| 12 | 12 | 20 | 14.5 | 5 | Dry | 95 | 1.2 | 68.97 | 19.16 |
| 13 | 7 | 5 | 7 | 30 | Dry | 79 | 0.39 | 109.89 | 30.53 |
| 14 | 16 | 20 | 7 | 30 | Dry | 86 | 1.38 | 124.22 | 34.51 |
| 15 | 8 | 5 | 14.5 | 30 | Dry | 82 | 0.62 | 33.37 | 9.27 |
| 16 | 4 | 20 | 14.5 | 30 | Dry | 87 | 1.11 | 74.56 | 20.71 |
| 17 | 19 | 10 | 10.75 | 17.5 | Humid | 88 | 1.04 | 53.67 | 14.91 |
| 18 | 3 | 10 | 10.75 | 17.5 | Humid | 90 | 1.11 | 50.28 | 13.97 |
| 19 | 10 | 10 | 10.75 | 17.5 | Humid | 88 | 1.01 | 55.26 | 15.35 |

## 2.4.2. Application of photocatalytic ozonation for the pharmaceuticals degradation in water

**Objective.** The efficiency of the DBD plasma water treatment method based on the salvation of ionized gas in water was improved using UV radiation source. The catalyst is made from $TiO_2$ that is electrochemically deposited on the stainless steel plates. A screening experiment was carried out in order to identify the key factors affecting the pharmaceutical decomposition process and select the optimal parameters of DBD reactor. The up-scaled experimental setup with plate-like catalysts inserted in the UV-photocatalysis reactor (**Figure 2.3**) was used in this group of experiments.

**Model water.** The model water was prepared by dissolving target pharmaceutical compounds in the synthetic tap water obtaining solutions with initial concentration of compounds being 10 mg/L. Diclofenac sodium salt (purity ≥ 98.5%), ketoprofen (purity ≥ 98%), and carbamazepine (purity ≥ 99%) were purchased from Sigma–Aldrich Chemical Co. The characteristics of target compounds are presented in **Table 2.2**. Synthetic tap water was prepared by dissolving the analytical grade inorganic salts in distilled water (TOC value <0.1 mg/L, conductivity <15 μS/cm) according to the methodology described by Morrow et al. (2008). The pH and conductivity of synthetic tap water was 7.3 and 300 μS/cm, respectively. The model water was employed in the experiments immediately after the preparation to avoid possible degradation and other reactions over time.

**Table 2.2.** Main information about the target pollutants.

| Model water No. | Substance name; CAS No. | Structure | Molecular formula; Molecular weight | Acute toxicity: LD50 (rat, oral), mg/kg | Ozone degradation[a] |
|---|---|---|---|---|---|
| 1 | Diclofenac; CAS 15307-79-6 | | $C_{14}H_{10}Cl_2NNaO_2$; 318.13 | 53 | Easily degradable |
| 2 | Ketoprofen; CAS 22071-15-4 | | $C_{16}H_{14}O_3$; 254.28 | 62.4 | Easily degradable |
| 3 | Carbamazepine; CAS 298-46-4 | | $C_{15}H_{12}N_2O$; 236.27 | 1957 | Recalcitrant towards ozone degradation |

a – Antoniou et al., 2013.

**Screening experiment for the determination of optimal operational parameters of the DBD reactor.** Modeling software Modde 10 (Umetrics Inc., Sweden) was used for the experiment planning and determination of the optimal parameters: air flow rate, DBD power, and treatment duration (**Table 2.3**). During the screening experiment, initial variables provided to the software were DBD power (from 13.6 to 81.6 W), reactor air flow (from 3 to 11 L/min), and duration of treatment (from 0.25 to 12 min). Full factorial experiment type with three middle points was selected for the theoretical screening experiment. The constant parameters were the working volume of the reactor, which is 1.6 L, and the concentration of diclofenac in model water of 10 mg/L. Thirty experiments were provided by the software, and they were performed experimentally in order to obtain the response parameters, namely the residual concentration of diclofenac in treated water (mg/L), decomposition efficiency (%), ozone concentration in air (mg/L), and the amount of energy required for the ozone formation (kJ/g). Then, the modeling data were fitted to the partial least squares regression model using the software.

**Table 2.3.** Design of the full factorial screening experiment.

| Experiment No | Air flow, L/min | DBD power, W | Duration of decomposition, min | Residual conc. of diclofenac | Calculated energy for ozone |
|---|---|---|---|---|---|

|  |  |  |  |  | formation, kJ/g* |
|---|---|---|---|---|---|
| 1 | 3 | 13.6 | 0.25 | 8.9 | 196 |
| 2 | 3 | 13.6 | 6.125 | 0.3 | 213 |
| 3 | 3 | 13.6 | 12 | 0.5 | 162 |
| 4 | 7 | 13.6 | 0.25 | 6.9 | 153 |
| 5 | 7 | 13.6 | 6.125 | 0.3 | 130 |
| 6 | 7 | 13.6 | 12 | 0.3 | 151 |
| 7 | 11 | 13.6 | 0.25 | 8.0 | 181 |
| 8 | 11 | 13.6 | 6.125 | 0.3 | 132 |
| 9 | 11 | 13.6 | 12 | 0.3 | 148 |
| 10 | 3 | 39.2 | 0.25 | 5.9 | 231 |
| 11 | 3 | 39.2 | 6.125 | 0.1 | 225 |
| 12 | 3 | 39.2 | 12 | 0.1 | 245 |
| 13 | 7 | 39.2 | 0.25 | 4.1 | 177 |
| 14 | 7 | 39.2 | 6.125 | 0.1 | 182 |
| 15 | 7 | 39.2 | 12 | 0.1 | 184 |
| 16 | 11 | 39.2 | 0.25 | 3.8 | 152 |
| 17 | 11 | 39.2 | 6.125 | 0.1 | 127 |
| 18 | 11 | 39.2 | 12 | 0.1 | 155 |
| 19 | 3 | 81.6 | 0.25 | 3.7 | 373 |
| 20 | 3 | 81.6 | 6.125 | 0.1 | 390 |
| 21 | 3 | 81.6 | 12 | 0.1 | 363 |
| 22 | 7 | 81.6 | 0.25 | 1.1 | 222 |
| 23 | 7 | 81.6 | 6.125 | 0.2 | 243 |
| 24 | 7 | 81.6 | 12 | 0.2 | 235 |
| 25 | 11 | 81.6 | 0.25 | 0.7 | 204 |
| 26 | 11 | 81.6 | 6.125 | 0.3 | 189 |
| 27 | 11 | 81.6 | 12 | 0.3 | 173 |
| 28 | 7 | 39.2 | 6.125 | 0.1 | 200 |
| 29 | 7 | 39.2 | 6.125 | 0.1 | 167 |
| 30 | 7 | 39.2 | 6.125 | 0.0 | 178 |

* - decomposition efficiency and energy required for the ozone formation were calculated.

**Comparative assessment of various AOPs.** After the screening experiment, a comparative assessment of four ozone based advanced oxidation processes was performed under the optimal DBD reactor operation conditions determined during the screening experiment:

- $O_3$ only (ozonation);
- $O_3$ + UV (photolytic ozonation);
- $O_3$ + Catalyst (catalytic ozonation);
- $O_3$ + UV + Catalyst (photocatalytic ozonation).

Single ozonation was taken as a "zero point". For these experiments, 1.6 L of modelwater, containing 10 mg/L of diclofenac, ketoprofen, or carbamazepine, respectively, was first pretreated for 2 min in the DBD reactor and then transferred into the UV-photocatalysis reactor for further pollutant decomposition. Assessing the performance of various advanced oxidation processes, the samples from the UV-photocatalysis reactor were taken after 0, 0.5, 1, 2, 3, 4.5, 6, 8, and 10 min. Then, the treatment efficiency was evaluated by measuring the concentration of tested pharmaceutical compounds applying HPLC-UV and the remaining TOC content in

40
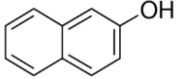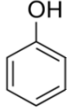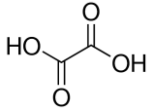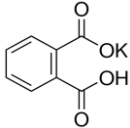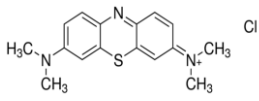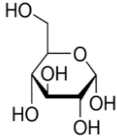
the treated water. The selected advanced oxidation processes were tested for the toxicity changes during the treatment process under the same process conditions as described earlier. The samples from the UV-photocatalysis reactor for toxicity tests were taken after 2.5 and 5 min of treatment.

## 2.4.3. Application of the photocatalytic ozonation for various organic compounds' degradation in water

**Objective.** The efficiency of the DBD plasma water treatment method based on the salvation of the ionized gas in the water was improved using UV radiation source and the catalyst made from the $TiO_2$ deposited on the glass rods. The construction of the glass rod-type catalysts was selected as more technologically useful for the up-scaling as well the easier construction and higher surface to volume ratio (as presented in section 2.3.), and practically inert behavior as it is made from the glass and pure $TiO_2$.

**Model wastewater.** Model wastewater was prepared using six compounds (**Table 2.4**): 2-naphthol, phenol, oxalic acid, potassium hydrogen phthalate, methylene blue, and D-glucose, dissolving them in the synthetic tap water. Synthetic tap water was prepared according to the methodology described by Morrow et al. (2008), using the distilled water (TOC value <0.1 mg/L, conductivity <15 μS/cm) and analytical grade inorganic reagents. These representing pollutants could be discharged into the wastewater from various industrial processes. 2-naphtol, phenol, and phthalate were chosen due to their presence in the wastewaters of chemical industries (Contreras et al., 2011). Methylene blue was selected as an example of synthetic dye, which is common pollutant in the textile industry wastewater (Tichonovas et al., 2013). Oxalic acid was widely used as a chemical resistant to the ozonation (Orge et al., 2015). D-glucose was chosen as a potentially easy-to-degrade compound, which can compete with more persistent pollutants in the oxidation reactions. All the target chemicals and other chemicals were of analytical grade. Model wastewater was prepared by dissolving the target organic compounds in the synthetic tap water according to the concentrations presented in **Table 2.4**. In case of the mixture of six compounds, the concentration of every compound was calculated according to the desired TOC value of 50 mg/L, i.e., equal to 8.33 mg/L of TOC for each compound. Such concentrations of specific pollutants may be at a higher range for the real industrial wastewater, but they are suitable for the examination of decomposition technology. The efficient degradation at higher concentrations implies that the technology should be effective at the lower concentrations as well. The prepared model wastewater was employed in the experiments immediately after the preparation to avoid possible degradation and other reactions over time.

**Table 2.4.** Substances acting as pollutants in the model wastewater.

| Model waste-water No. | Substance name; CAS No. | Structure | Molecular formula; Molecular weight | Concentration, mg/L | TOC concentration, mg/L | Initial pH | Final pH |
|---|---|---|---|---|---|---|---|
| 1 | 2-naphthol; CAS 135-19-3 | | $C_{10}H_7OH$; 144.17 | 60.00 | 50 | 5.4 | 3.6— 5.9 |
| 2 | Phenol; CAS 108-95-2 | | $C_6H_5OH$; 94.11 | 65.35 | 50 | 5.4 | 3.7— 5.7 |
| 3 | Oxalic acid (dixydrate); CAS 144-62-7 | | $C_2H_2O_4$; 90.03 (126.03) | 262.64 | 50 | 2.7 | 3.2— 4.3 |
| 4 | Potassium hydrogen phthalate; CAS 877-24-7 | | $C_8H_5KO_4$; 204.22 | 106.36 | 50 | 4.3 | 3.5— 4.3 |
| 5 | Methylene blue (trihydrate); CAS 7220-79-3 | | $C_{16}H_{18}ClN_3S$; 319.85 (373.85) | 97.36 | 50 | 5.4 | 3.7— 5.2 |
| 6 | D-glucose; CAS 50-99-7 | | $C_6H_{12}O_6$; 180.16 | 137.61 | 50 | 5.7 | 3.6— 5.3 |
| 7 | Mixture of all 6 pollutants | - | - | 8.33 of each | 50 | 3.4 (3— 11) | 3.3— 8.7 |

**Determination of the optimal parameters of the DBD reactor and ozone production.** The DBD reactor system was adjusted to the resonant frequency with the aim to achieve the maximum power usage efficiency for the conversion of low voltage to high voltage.

**Efficiency of the AO system.** This experiment aimed to determine the effects of various combinations of ozonation, UV, and catalysis on the pollutant decomposition. These experiments were carried out in the third (UV) reactor. The following combinations of parameters were set:

- Air (no ozone) + UV (photolysis);
- Air (no ozone) + UV + Catalyst (photocatalysis);
- $O_3$ only (ozonation);
- $O_3$ + UV (photolytic ozonation);

- $O_3$ + Catalyst (catalytic ozonation);
- $O_3$ + UV + Catalyst (photocatalytic ozonation).

The treatment efficiency was evaluated by measuring TOC of the treated water. The amount of 1.6 L of the model wastewater was treated during every run. All the experiments lasted for 60 min with sampling intervals of 10 min (except for oxalic acid, where additional samples at 5, 15, and 25 min were taken). Three repeats of each test were made. The toxicity and UPLC-MS analyses were applied to the photocatalytic ozonation experiments to identify the possible products of the degradation and their toxicity.

**Determination of influence of the initial pH.** The model wastewater no. 7 (a mixture of all compounds) was used for testing the effects of the initial pH value to the decomposition efficiency of the photocatalytic ozonation process. pH values of 3, 7, and 11 were tested, making adjustments with 0.1 M $H_2SO_4$ or 0.1 M NaOH. The value of the pH was not controlled during the treatment.

**Determination of the catalyst durability.** The catalyst durability was measured by performing a series of photocatalytic ozonation experiments in a row, using fresh 2-naphthol model wastewater. Firstly, the experiments with freshly prepared catalyst were conducted as a series of 10 experiments in a row. After approx. 100 h of operation of the same catalyst with various pollutants, it was tested against 2-naphtol again by measuring its activity during a series of 5 experiments. All durability experiments lasted for 30 min. SEM and XRD analyses were performed for the characterization of new made and used catalyst as well as the commercial powder sample.

## 2.4.4. Testing of various ozone based AO methods on the treatment of real industry wastewater

**Objective.** The same equipment as described in 2.4.3. section was tested under the treatment of real industry wastewater. The furniture industry wastewater was used as a sample. The AOPs were studied by a series of experiments under various working conditions. The experimental design was separated into two main parts, i.e., uncontrolled pH experiment and controlled initial pH experiment.

**Model wastewater.** The wastewater used in this study was sampled from a furniture company operating in Lithuania. Three wastewater flows that originated during the manufacturing process include the polyvinyl acetate–containing wastewater flow from the furniture construction line, the formaldehyde-containing wastewater flow from the furniture decorating and finishing line, and mordant substances (including 1-methoxypropan-2-ol, methyl benzoylformate, phosphinates, acrylic acid, as declared in the material safety information sheet) containing wastewater flow from the wood preservation line. All three flows are combined together before the primary treatment, which is based on the coagulation process. After the primary treatment in a company, the effluent still contains a high concentration of recalcitrant dissolved organic pollutants and currently is being utilized as a hazardous waste. The application of secondary treatment addressing the decomposition of organic substances would allow direct discharge to the municipal

wastewater treatment plant. The procedure of sampling was designed to minimize the variations in the wastewater composition due to the storage as well as variations within the production process. Based on the recommendations of the technical staff of the company, the necessary amount of the wastewater was sampled from the reservoir where it was collected after the primary treatment. The composition of the wastewater was representative to the average pollution load. Then, the wastewater was brought to the laboratory and stored at temperature of 2°C. The properties of the initial industrial wastewater are listed in **Table 2.5**. High values of TOC and COD represent high concentrations of organic materials in the wastewater, including compounds such as polyvinyl acetate, formaldehyde, and others. The calculated COD/BOD ratio is 5.45, which indicates low biodegradability and high potential for the application of chemical or physical treatment processes. However, the direct application of AOPs for the treatment of such highly polluted wastewater may be inefficient. AOPs are known to work optimally at low concentrations of hardly degradable pollutants (Li et al., 2015). For this purpose, the initial wastewater brought from the company was diluted 124.4 times with synthetic tap water to achieve 50 mg/L concentration of TOC. The synthetic tap water was prepared as described in the previous sections. The characterization of the diluted wastewater used for the experiments is as well presented in **Table 2.5**.

**Table 2.5.** Parameters of the industrial wastewater and tested (diluted) wastewater.

| Parameter | Initial wastewater from the company | Diluted wastewater used in the AO experiments |
|---|---|---|
| TOC, mg/L | 6220 | 50 |
| COD, mgO$_2$/L | 16200 | 130 |
| BOD, mgO$_2$/L | 2970 | - |
| Conductivity, μs/cm | 4680 | 186 |
| pH | 8.4 | 6.7 |

**Uncontrolled pH experiment.** The wastewater without initial pH adjustment was used for testing various combinations of AOP components:

- Air (no ozone) + UV (photolysis);
- Air (no ozone) + UV + Catalyst (photocatalysis);
- O$_3$ only (ozonation);
- O$_3$ + UV (photolytic ozonation);
- O$_3$ + Catalyst (catalytic ozonation);
- O$_3$ + UV + Catalyst (photocatalytic ozonation).

This selection of AOPs includes combinations of the most important factors that may influence the treatment efficiency of organic pollutants in the industrial wastewater. pH of the diluted wastewater that was used for testing is 6.7. The samples for TOC analysis were drawn after 0, 20, 40, 60, 80, 100, 120, 140, 160, and 180 min of treatment, while those for toxicity testing were drawn after 0, 10, 20, 40, 60, 80, and 100 min of treatment and diluted two times before testing. The maximum time (180 min) was selected during the initial investigations which indicated that such duration is sufficient to achieve 100% mineralization during the most efficient conditions (O$_3$ + UV + catalyst). The sampling intervals of 20 min were selected to

44

be sufficient for the observation of process kinetics. All tests were repeated at least three times.

**Controlled initial pH experiment.** Three most effective AOPs were subsequently tested by using diluted wastewater with adjusted pH (3, 5, 9, and 11):

- Air (no ozone) + UV + Catalyst (photocatalysis);

- $O_3$ + UV (photolytic ozonation);

- $O_3$ + UV + Catalyst (photocatalytic ozonation).

The pH values of 3, 5, 9, and 11 were selected to represent the broad spectrum of possible pH values of real industrial effluents generated within various technological processes. The non-regulated initial pH experiment served as a midpoint experiment (pH = 6.7). The pH has a strong influence on the AO processes (Xiao et al., 2015; De Witte et al., 2010; Hansson et al., 2015; Martins and Quinta-Ferreira, 2014); thus, such testing allows determining the robustness of the system. Before the experiments, the pH of the diluted wastewater was adjusted by adding 1 M NaOH or $H_2SO_4$. The samples were taken at the same intervals as described in the uncontrolled pH experiments.

# 3. RESULTS AND DISCUSSION

## 3.1. Operational parameters

### 3.1.1. DBD reactor power measurements

The power measurements were performed in order to evaluate the optimal electric parameters of the DBD reactor, i.e., power supply system. The optimal use of energy in the DBD reactor can be reached by tuning resonant frequencies of high voltage transformer (a part of the power supply) and DBD reactor. The most important electrical parameter of the DBD reactor is capacitance, which depends on the width of the air gap, the active surface area of the central electrode, and the reactor construction materials. In this electrical system, the DBD reactor can be called a capacitive element of inductor – capacitor network (LC network). The second part – the secondary windings of power supply high voltage transformer – can be called an inductive element. Such LC system (DBD reactor – the transformer of the power supply) has its own resonant oscillation frequency, and the power controller must be adjusted to this frequency value for best energy conversion results.

***The DBD power measurements of the primary system.*** The measured power of the DBD reactor varied between 3 and 33W, which represents the power adjusted to the converter. In this case, the DBD powers of 3, 5.2, 9.8, 20.3, and 33W were achieved at 24, 27, 30, 33, and 36% of the converter power. Later, these DBD power values were used for the experiments of the ozone production. The DBD power was 0W at the converter powers less than 24% due to the absence of the DBD plasma at less voltage than required to break the dielectric layers. This indicates the shortcomings of the power converter, which was corrected in the up-scaled device.

***The DBD power measurements of the up-scaled system.*** Before power measurements, the DBD reactor vessel was filled with tap water (1.6L), and the aeration intensity was adjusted to 7 L/min. At the resonant frequency determination experiment, the power controller power was set to constant 15%. The peak-to peak voltage of the reactor high voltage electrode was measured while changing the controller frequency as well as DBD power value. The observed peaks of voltage and power identified the system resonant frequency value, which was used in all the succeeding experiments. The resonant frequency peak of the DBD reactor was determined at 5240 Hz. The power and voltage peak simultaneously in the frequency range of 5200 – 5380 Hz, clearly indicating the resonant value (**Figure 3.1A**). This setting was applied in all the next experiments.

After the procedure of resonant frequency determination, the DBD power values corresponding to the power of the controller were measured. Additionally, the power conversion efficiencies were calculated from the obtained measurement results. For this purpose, the controller power value was changed in the range of 5−30%, and the DBD power as well as the power consumed from the mains line was measured. Energy conversion efficiency was calculated by comparing the consumed electrical power with the produced DBD power. The relationships between the converter power vs. DBD power and conversion efficiency are presented in **Figure 3.1B**. The DBD power varied in the range of 1.8−133.6 W, while the conversion efficiency (for

conversion of low to high voltage) was found to reach 80−82% in the DBD power range of 28.8−133.6 W.
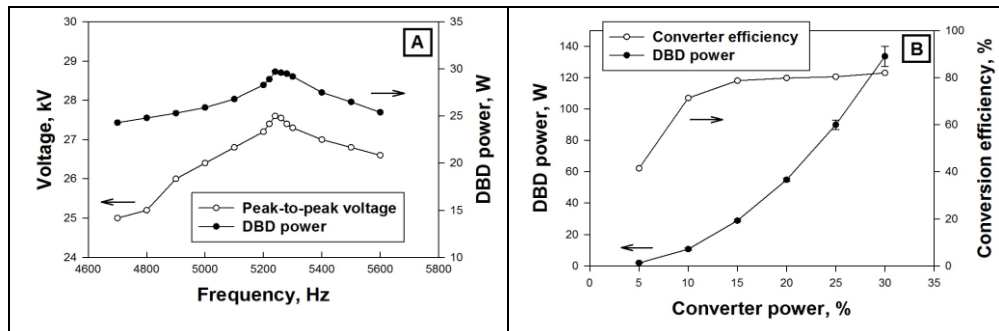


**Figure 3.1.** The up-scaled DBD reactor power parameters: A – the system resonant frequency, B - DBD power (W) vs. converter power (%), and conversion efficiency (%).

### 3.1.2. Ozone production

As the ozone production is the most important factor in the decomposition process of hardly degradable organic compounds using ozone based advanced oxidation technology, the ozone production using various DBD power values and various air flow rates were measured. DBD power values were changed accordingly as in the previous power measurement experiment. In both experimental setups (primary and up-scaled), the air flow rate varied between 3 – 15 L/min. Ozone was sampled from the DBD reactor vessel gas output, operating the reactor with 1.6L of the tap water. Before the measurements, this tap water was pretreated with ozone from the DBD reactor to avoid ozone concentration reduction due to the decomposition of trace organics in the used tap water. The water was changed before each experiment.

***The ozone production in the primary system.*** The relationship between the concentration of the ozone in the outlet gasses, ozone dissolved in water, and the applied discharge power in the reactor operating with blank water is depicted in **Figure 3.2**. The lowest ozone concentration (0.8 mg/L) in the outlet gasses was found in the case of the minimum power (3.0 W). The highest concentration of the ozone in the outlet gasses (1.92 mg/L) was achieved at the highest discharge power of 33.0 W.
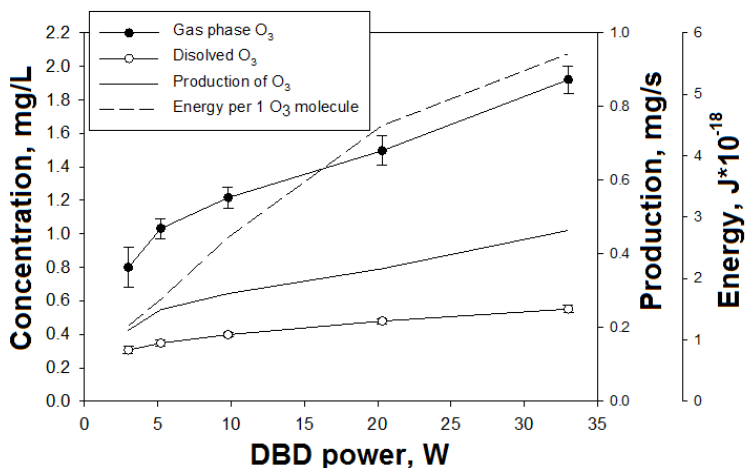
**Figure 3.2.** The relationship between the ozone production rate and discharge power. Error bars denote standard deviation of the replications. Ozone production and energy consumption to form one ozone molecule graphs are added.

***The ozone production in the up-scaled system.*** The concentration of ozone in the DBD output gases was measured at different air flow rates and DBD power values. The concentrations ranged from 0.34 to 5.47 mg/L, depending on the variable working parameters mentioned above. The lowest ozone concentration was registered at the highest feeding air flow rate (15 L/min) and the lowest DBD power (10.6 W), while the highest concentration of ozone was measured at the lowest air flow (3 L/min) and the highest power (133.7 W).

The direct non-linear (logarithmic) relationship between the concentration of produced $O_3$ in the air and the DBD power were observed (**Figure 3.3A**) at all feed air flowrates. Such findings agree with the results from the other studies using DBD reactors (Mok et al., 2008; Pekárek and Mikeš, 2014). The analysis of the ozone yield per consumed energy (**Figure 3.3B**) suggested two points of optimal parameters, namely at 11 L/min of air flow and 28.8 W of DBD power (this combination was used for the further experiments), as well as 15 L/min and 54.9 W, respectively. These findings suggest that the volumetric concentration of ozone can be increased by changing the DBD power and air flow rate; however, these parameters must be selected correctly to achieve the maximum ozone yield per energy amount.
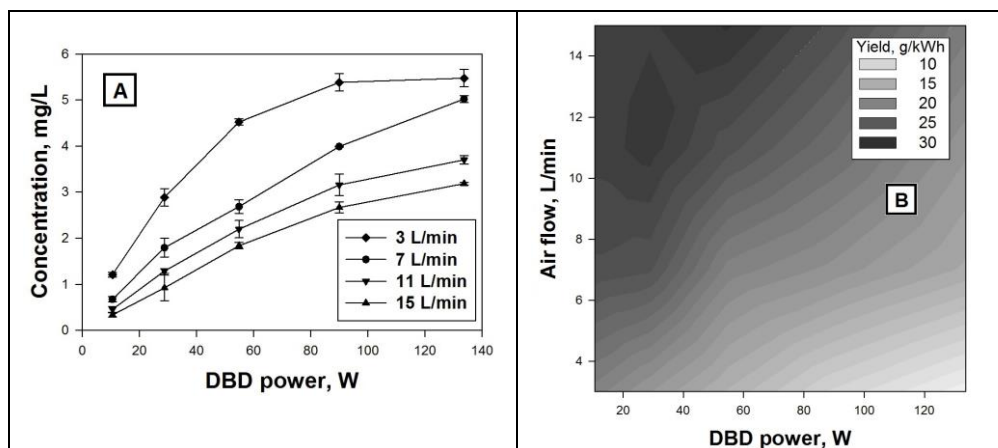
**Figure 3.3.** The generation of $O_3$ of the DBD reactor in the up-scaled device: A - Ozone concentration (mg/L) obtained at various air flow rates (L/min) and DBD power (W) settings, B - Ozone yield (g/kWh) at various air flow rates (L/min) and DBD power (W) settings.

## 3.2. The results of the full factorial experiment of 2-naphthol polluted water treatment by using DBD plasma reactor

This passage was quoted from the article entitled "Decomposition of 2-naphthol in water using a non-thermal plasma reactor" (10.1016/j.cej.2014.08.098) with permission of Elsevier.

### 3.2.1. 2-naphthol decomposition efficiency screening

The experiments of 2-naphthol decomposition were performed to define the initial variables for the regression modeling. Nineteen experiments were first defined by the software, and the laboratory experiments were further performed to obtain 2-naphthol decomposition efficiency as well as ozone concentration in the air. These data are compiled in **Table 2.1**. The experiments performed according to the full-factorial design yielded 2-naphthol decomposition efficiency ranging from 79% to 95% with ozone concentration in air ranging from 0.39 to 1.52 mg/L. These data were taken into account to obtain the final estimates of the regression model. The significance of the investigated experimental parameters is shown in **Figure 3.4A** and **3.4B** for 2-naphthol decomposition efficiency and ozone concentration in the air. It can be seen that the largest negative response was obtained in the initial concentration of 2-naphthol with the decomposition efficiency decreasing with the increasing 2-naphthol concentration. However, increasing power and, to a lesser extent, higher aeration intensity resulted in a positive response towards 2-naphthol decomposition efficiency. Other factors had very low significance and were very close to the standard error of modeling.
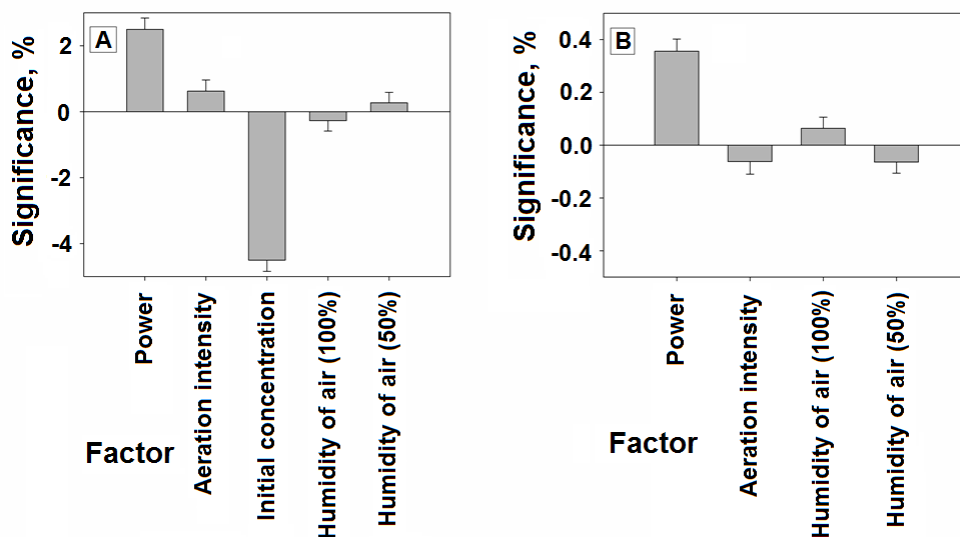
**Figure 3.4.** Process parameter effect coefficients for (A) 2-naphthol decomposition efficiency and (B) ozone concentration in air.

Next, the modelling of the dependence of 2-naphthol decomposition efficiency in various combinations of the experimental factors was performed as shown in **Figure 3.5**. In these surface plots, the effects of the simultaneous variation of two factors in the decomposition efficiency are presented. Specifically, power-aeration intensity plots for constant 2-naphthol concentration of 17.5 mg/L for dry and humid air as well as the power vs. initial 2-naphthol concentration at constant aeration intensity of 10.75 L/min for dry and humid air were determined and shown in **Figure 3.5A−D**. The highest decomposition efficiency was obtained by using the highest DBD power (**Figure 3.5A**) as well as the lowest initial concentration of 2-naphthol (**Figure 3.5C, D**) at the highest DBD power that was used.
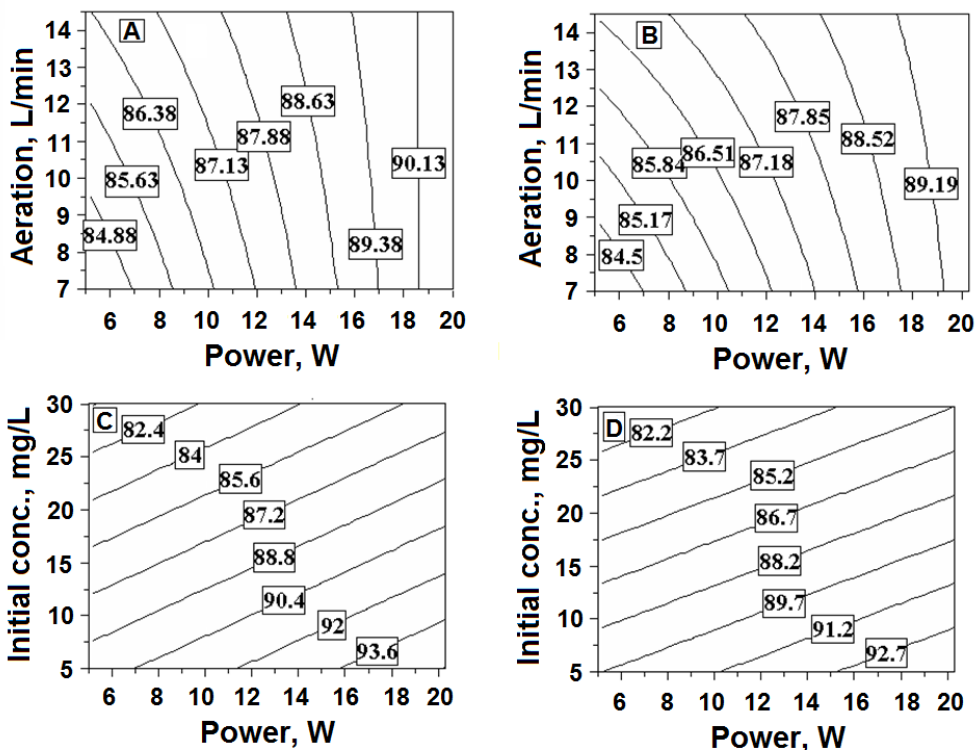
**Figure 3.5.** Process parameter effect on 2-naphthol decomposition efficiency: (A) power-aeration (dry, initial conc. 17.5 mg/L), (B) power-aeration (humid, initial conc. 17.5 mg/L), (C) power-initial concentration (dry, aeration 10.75 L/min), and (D) power-initial concentration (humid, aeration 10.75 L/min).

A slight improvement in 2-naphthol decomposition efficiency was obtained as well at the constant power using dry air. Additionally, aeration exhibited a significant effect on the 2-naphthol decomposition with higher aeration intensity increasing the decomposition efficiency at the constant power (**Figure 3.5A** and **B**). This is due to the increased aeration resulting in larger amounts of ozone production. For example, at 20W power and aeration of 7 L/min (humid air), the total amount of the produced ozone was 10.6 mg/min, while at the same, power and humidity with the aeration of 14.5 L/min ozone production increased to 16.2 mg/min.

### 3.2.2. 2-naphthol decomposition kinetics

Using optimal conditions described in the previous chapter, the 2-naphthol decomposition kinetics were investigated. The data were fitted with the exponential decay curve according to the equation:

$$C_i = C_o \times e^{-k \times t}; \tag{28}$$

where $C_0$ is initial 2-naphthol concentration (mg/L); $C_i$ is concentration at the time measured (mg/L); k is decay constant (min$^{-1}$); t is time (min) (Marotta et al.,

2011). The results of these measurements are shown in **Figure 3.6A**. The maximum reaction rate with the decay constant of 2.15 min$^{-1}$ was reached when the reactor power was at the maximum (33 W). The decay constant decreased at the lower power, namely k = 1.65 min$^{-1}$ at 20 W, k = 1.57 min$^{-1}$ at 10W, and k = 0.708 min$^{-1}$ at 5W.
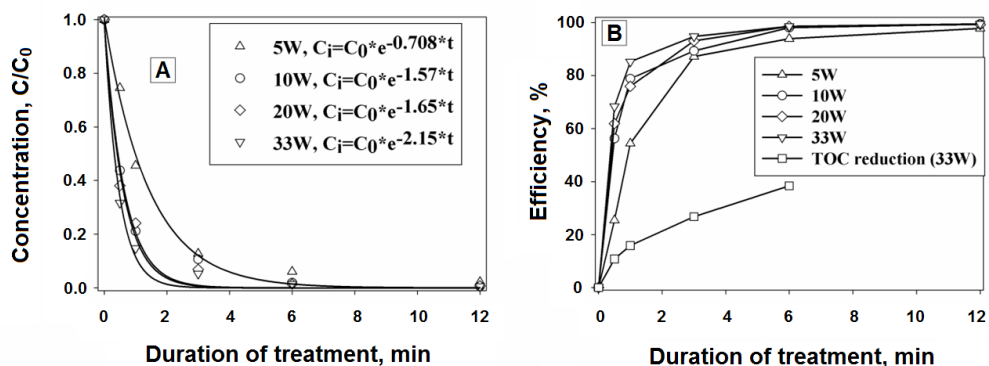


**Figure 3.6.** 2-Naphthol decomposition kinetics with varying DBD power for 12 min experiment: (A) decomposition kinetics and obtained exponential decay constants and (B) 2-naphthol decomposition efficiency using different DBD power (TOC reduction curve at 33W DBD power is shown as well).

The dependence of the 2-naphthol decomposition efficiency on the DBD power is shown in **Figure 3.6B**. The greatest decomposition efficiency was achieved using 20W and 33W power. For this power that was applied, 90% decomposition efficiency was reached after 2.6 and 1.95 min, respectively. The major amount of 2-naphthol (about 90%) was decomposed after the first 2 min. This value was taken as the optimal result based on the power consumption calculations (**Table 3.1**). These data are in a good agreement with the measured TOC values, where after 6 min at 33W DBD power, 38.4% mineralization degree was achieved. This mineralization degree can be explained by the formation of the intermediate non-volatile decomposition products listed in **Table 3.2**.

**Table 3.1.** Energy efficiency indicators of the DBD reactor.

| Parameter | DBD power value, W | | | |
|---|---|---|---|---|
| | 5 | 10 | 20 | 33 |
| Time to reach 90% efficiency, min | 4.15 | 3.2 | 2.6 | 1.95 |
| Used energy, J | 1245 | 1920 | 3120 | 3861 |
| Decomposed 2-naphthol, mg | 9 | 9 | 9 | 9 |
| Energy to decompose 1 g of 2-naphthol, kJ | 138 | 213 | 346 | 429 |

After the ~90% 2-naphthol decomposition, the decomposition efficiency increased very slowly. The energy requirement to decompose 1 g of 2-naphthol increased with the increasing DBD power and was 138 kJ/g at 5W, 213 kJ/g at 10 W, 346 kJ/g at 20W, and 429 kJ/g at 33 W. The increasing power resulted in the conversion of the electrical energy to heat, which is considered a wasteful process. These energy yields are of similar order of magnitude with other studies on difficult-

to-degrade pollutant decomposition (Tichonovas et al., 2013), where energy requirements to decompose various textile dyes was in the range from 18.7 to 866 kJ/g. Magureanu et al. (2010) found that the applied energy, required to decompose pharmaceutical pentoxifylline when using non-thermal plasma, was 225 kJ/g. Reddy et al. (2013) reported ~53.73 kJ/g energy consumption to decompose methylene blue in the non-thermal plasma reactor. The excess power can as well cause decomposition of the produced ozone. The non-linearity of the ozone production with the increasing DBD power was already pointed out and discussed previously (Chen et al., 2009; Mok et al., 2008). Lower DBD power values were favored in the case of non-restricted treatment duration. The data of this dissertation show that quick initial decomposition can be attained with a moderate energy consumption within a few minutes to decompose ~90% of the contaminant, followed by a proposed secondary reactor, based on the catalyst system (Bubnov et al., 2006), sorbents as activated carbon (Lu et al., 2012). As an example of such integral process, the study by Wei et al. (2013) included the coupling of the nonthermal plasma and biological processes to decompose dimethyl sulfide pollutant. Such combination applied to the wastewater treatment would lead to the creation of the integrated systems, utilizing excess electricity for the energy efficient, intensive initial decomposition of the contaminant, followed by the non-plasma based low contaminant concentration treatment.

### 3.2.3. Characterization of 2-naphthol decomposition intermediates and possible reactive pathways

The identification of the intermediary products and their toxicity analysis was performed. These collective data as well as the toxicity of DBD 2-naphthol decomposition intermediates, present in the reactive solution after 0.5, 1, 3, and 6 min, are shown in **Figure 3.7**. It can be seen that the initial 2-naphthol solution resulted in the mortality of 10% of specimens, while the DBD plasma treated solution (6 min of the DBD plasma treatment with >90% decomposition, as shown in **Figure 3.6**) had the resulting toxicity of approximately 15%. Very interesting results were achieved after 0.5 and 1 min of treatment, when the mortality of D. magna was 100% and 65%, respectively. This shows that some of the primary 2-naphthol decomposition products were highly toxic, but they were further decomposed to less harmful compounds.
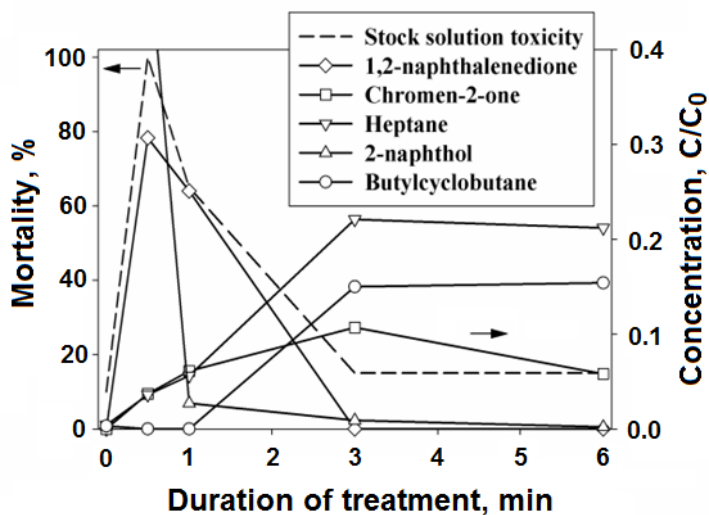
**Figure 3.7.** Intermediate reactive product, formed during the 2-naphthol decomposition by using DBD plasma, toxicity testing as well as their measured relative concentrations.

The reactive intermediates, formed during 2-naphthol decomposition using DBD plasma, were investigated using GC-MS analysis. The changes in their concentration were observed and, for the identified main intermediates, are reported in **Figure 3.7** with the corresponding values tabulated in **Table 3.2**. 2-naphthol rapidly decayed under the DBD treatment, and after 1 min, its concentration became negligible. The major intermediate, observed after 0.5 and 1 min, was 1,2-naphthalenedione. The formation of 1,2-naphtalenedione (1,2-naphthoquinone) has been previously reported in several studies (Zang et al., 2010; Qourzal et al., 2008; Vellaisamy et al., 2011; Panizza et al., 2001). Other observed intermediate decomposition products were heptane, chromen-2-one, (Z)-Octa-9- decenamide, bis(2-ethylhexyl) benzene-1,4-dicarboxylate. These were mostly prominent after 3 min of treatment. LD50 values that were compiled in **Table 3.2** show that 1,2-naphthalenedione, heptane, and chromen-2-one have the highest toxicity between the detected intermediates with the increase in 1,2-naphthalenedione concentration after 0.5 min correlating with the increased toxicity. The FTIR analysis was used to complement the GC-MS in identifying the functional groups of 2-naphthol decomposition intermediates and products. A large, broad peak observed in all the FTIR spectra between 3200 and 3650 $cm^{-1}$ is due to the –OH group stretching. There was a systematic shift of this spectra region towards the higher wavenumbers as the experiment proceeded due to the loss of the hydrogen bonds between the functional groups. The peak at 3051 $cm^{-1}$ in the blank sample occurred due to the C–H vibration of the aromatic compounds (Stuart and Ando, 1996). This peak decreased accordingly with the decomposition time and was not observed after 30 min decomposition, showing the degradation of the aromatic 2-naphthol rings during the decomposition. After 15 min of decomposition, the doublet at 2925 and 2854 $cm^{-1}$ became prominent

and was assigned to –CH$_2$– stretching vibrations. Additionally, the presence of the peak at 1465 cm$^{-1}$ showed –CH$_2$– deformational vibrations (Stuart and Ando, 1996). In the literature, C=O stretch of the carbonyl group has been shown around 1700 cm$^{-1}$, whereas that for the C=O stretch in ketones was observed at 1715 cm$^{-1}$ (Stuart and Ando, 1996; Pavia et al., 2000).

**Table 3.2.** Relative concentrations (C/C$_0$) of 2-naphthol and its decomposition products during the DBD treatment and their corresponding toxicity.

| Compound | Treatment time (min) | | | | | Specifications | |
|---|---|---|---|---|---|---|---|
| | 0 | 0.5 | 1 | 3 | 6 | CAS No. | LD50, mg/kg (rat) |
| 2-naphthol | 1.000 | 0.514 | 0.027 | 0.009 | 0.002 | 135-19-3 | 1960 |
| Heptane | 0.004 | 0.036 | 0.056 | 0.221 | 0.212 | 142-82-5 | >5000 |
| (Z)-octa-9-decenamide | 0.003 | 0.042 | 0.126 | 0.175 | 0.166 | 301-02-0 | >10000 |
| Butylcyclobutane | 0.003 | - | - | 0.150 | 0.154 | 13152-44-8 | - |
| Bis(2-ethylhexyl) benzene-1,4-dicarboxylate | 0.002 | 0.043 | 0.038 | 0.082 | 0.101 | 6422-86-2 | - |
| Diethyl phthalate | 0.002 | 0.009 | 0.015 | 0.037 | 0.045 | 84-66-2 | 8600 |
| 1,2-naphthalenedione | - | 0.307 | 0.251 | - | - | 524-42-5 | 250 |
| Chromen-2-one | - | 0.037 | 0.061 | 0.107 | 0.058 | 91-64-5 | 293 |
| Cyclohexane | - | 0.019 | 0.043 | - | - | 110-82-7 | 12705 |
| o-phthalaldehyde | - | - | 0.011 | 0.053 | - | 643-79-8 | 178 |
| Methylbenzene | - | - | 0.009 | 0.030 | 0.027 | 108-88-3 | 5580 |
| Pyridine | - | - | 0.019 | 0.055 | 0.096 | 110-86-1 | 897 |

The peak at 1698 cm$^{-1}$ appeared after 3 min of decomposition in **Figure 3.8** and increased in intensity by the decomposition time. This C=O shift to the higher wavenumber side with the decomposition time shows a decrease in the number of cyclic ketone groups (Stuart and Ando, 1996; Pavia et al., 2000). The peak at 1650 cm$^{-1}$ after 3 and 6 min of decomposition shows the presence of –CONH$_2$ functional group (Stuart and Ando, 1996) that is possibly occurring due to the breaking of N$_2$ molecular bond, followed by the resulting radical reaction with the residual organics (Liu et al., 2012). Alternatively, the bands at 1630 and 1600 cm$^{-1}$ were previously assigned to the aromatic C=C stretching vibrations (Pavia et al., 2000). The band at 1276 cm$^{-1}$ is attributed to the C–O stretching vibration (Pavia et al., 2000). During the decomposition process, this peak shifts towards the lower wavenumbers. This can be due to the formation of –COH functional group. The presence of the peak at 1100 cm$^{-1}$ after 3 min of the decomposition suggests C–O stretching in ethers, esters, alcohols, or phenolic compounds (Stuart and Ando, 1996; Pavia et al., 2000). This peak disappears after 30 min of treatment. FTIR data that is shown in **Figure 3.8** agrees well with the GC-MS results. FTIR analysis shows that many of the functional groups seen in the FTIR spectra after 3, 6, and 15 min of the decomposition disappear after 30 min of decomposition, especially in the range of 1500–400 cm$^{-1}$. This demonstrates the removal of organic compounds from the aqueous 2-naphthol solution during the DBD plasma decomposition.
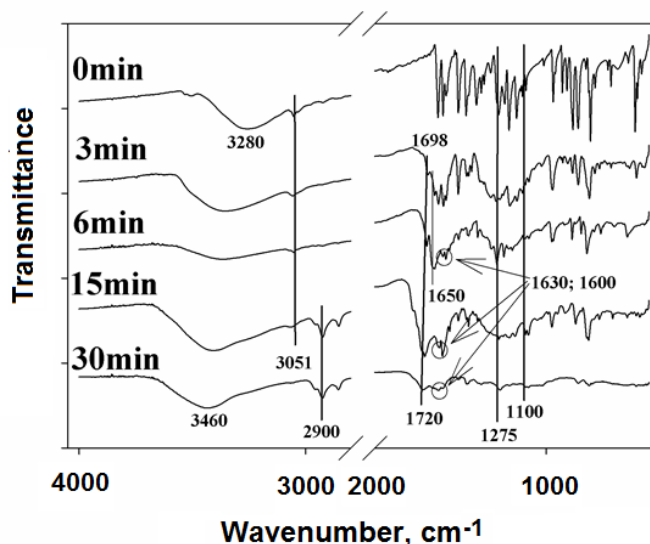
**Figure 3.8.** FTIR absorption spectra of the reactive intermediates that were formed during the 2-naphthol decomposition, using the DBD plasma.

Several studies have previously been reported on the 2-naphthol and 1-naphthol degradation with focus on the reaction kinetics, mechanisms, and the composition of the intermediary compounds. These are tabulated in **Table 3.3**, including the used initial concentrations, treatment method, and the detected intermediates. The used decomposition methods included electrochemical oxidation, photodegradation, chemical oxidation, plasma technology, and biodegradation (Zang et al., 2010; Qourzal et al., 2008; Vellaisamy et al., 2011; Panizza et al., 2001; Gao et al., 2001; Panizza and Cerisola, 2003; Panizza and Cerisola, 2004). Napthoxy radicals as well as 1,2-naphthoquinines were produced during the hydroxyl radical generating electrolytic oxidation based on the boron-doped diamond (Panizza et al., 2001). A two-step, one electron oxidation of 2-naphthol to the naphthyloxy radical and naphthyloxy cation, followed by its reaction with water in a two-step reaction, first producing 1,2-naphthalene-diol followed by the formation of 1,2-naphthoquinone, was proposed (Panizza et al., 2001). In another study, Panizza and Cerisola (2003) performed an electrochemical oxidation of 2-naphthol with an in situ electrogenerated active chlorine and determined that the main intermediate products were phthalic and maleic acids. Benzoic, malonic, formic, and oxalic acids were found in lower concentrations as well. Furthermore, a small amount of organochlorinated compounds was detected as well in the solution, which was further mineralized to $CO_2$ or oxidized to volatile chlorinated compounds (Panizza and Cerisola, 2003). Different anode materials, used by Panizza and Cerisola (2004), yielded similar formation of a large number of reaction intermediates, mainly phthalic and maleic acids. In addition to these compounds, at the very beginning of the electrolysis, unidentified oligomers were detected but rapidly disappeared. Qourzal et al. (2008) proposed photocatalytic degradation pathway of 2-naphthol in water with present titanium dioxide

photocatalyst. In particular, the attack of HO radicals may produce 1,2-naphthalene-diol and 1,2-naphthalene-dione. Later, 1,2-naphthalene-diol is converted to 1,2-naphthalene-dione by the same HO radicals. The decarboxylation of these via photo-Kolbe reaction would generate the formation of the 2-hydroxycinnamic acid.

**Table 3.3.** Tabulated literature data of 1- and 2-naphthol decomposition methods, used experimental conditions, and detected intermediates.

| Compound | Initial concentration, mg/L | Treatment method | Analytical method | Intermediates | Ref. |
|---|---|---|---|---|---|
| 2-naphthol | 288−1297 | Anodic oxidation of 2-naphthol at boron-doped diamond electrodes in acid media | Cyclic voltammetry, IR spectroscopy | 1,2- naphthoquinone, 1,2-dihydroxynaphthalene | (Panizza et al., 2001) |
| 2-naphthol | 720 | Electrochemical oxidation with in situ electrogenerated active chlorine | HPLC | Main: phthalic and maleic acid, other: benzoic, malonic, formic, and oxalic acids | (Panizza and Cerisola, 2003) |
| 2-naphthol | 720 | Electrochemical oxidation | HPLC, TOC | Mainly phthalic and maleic acids | (Panizza and Cerisola, 2004) |
| 2-naphthol | 28.8−144 | Photodegradation by artificial light illumination using TiO2 photocatalyst | HPLC–MS | 1,2-naphthalenediol, 1,2-naphthalene-dione, muconic acid, 2-hydroxycinamic acid | (Qourzal et al., 2008) |
| 2-naphthol | 4325−7208 | Oxidation by nicotiniumdichromate | IR spectroscopy | 1,2 naphthoquinone | (Vellaisamy et al., 2011) |
| 1-naphthol | 20−80 | Plasma (contact glow-discharge electrolysis) | HPLC, UV absorption | o-phthalic acid and dicarboxylic acid, such as oxalic, tartaric, and malic acid as well as formic and acetic acid, naphthalene-l,4-diol, o-hydroxylbenzoic acid | (Gao et al., 2001) |
| 2-naphthol | 20−150 | Biodegradation | HPLC | 1,2-naphthalene-diol and 1,2-naphthoquinone | (Zang et al., 2010) |

Aromatic intermediates are further oxidized through the ring-rupturing reactions into the aliphatic compounds containing muconic acid, formic acid, acetic

acid, and acetaldehyde. Finally, the mineralization reaction to carbon dioxide may occur, since the stoichiometric formation of $CO_2$ was observed in the study (Qourzal et al., 2008). The formation of 1,2 naphthoquinone as the main intermediate product of the oxidation has been reported as well by Vellaisamy et al. (2011) during the study of kinetics and mechanistic transformation during the oxidation of 2-naphthol by nicotiniumdichromate. Gao et al. (2001) investigated 1-naphthol degradation in aqueous solution by using plasma and reported gradual transformation of 1-naphthol into the intermediate products and $CO_2$. During the reaction process, o-phthalic acid and dicarboxylic acids, such as oxalic, tartaric, and malic acid as well as formic and acetic acids, were detected. In addition, naphthalene-l,4-diol was found at the initiation of the discharge. As the electrolysis proceeded, the concentration of the o-phthalic acid initially increased until its maximum was reached, and then, it decreased. It was pointed out that the o-hydroxylbenzoic acid appeared as an intermediate product in the contact glow-discharge electrolysis as well (Gao et al., 2001). The complete degradation of the o-phthalic acid takes more time than that of 1-naphthol. Ortho-phthalic acid is first oxidized into o-hydroxylbenzoic acid and then into dicarboxylic acid by hydroxyl radical (Gao et al., 2001). Gradual production of some labile and accumulatable metabolites of 2-naphthol was observed as well by Zang et al. (2010), when exploring biodegradation of 2-naphthol and its metabolites. Under experimental conditions, the main metabolites of 2-naphthol were 1,2- naphthalene-diol and 1,2-naphthoquinone. Other metabolites were not identified because their concentrations were below the detection limits of the HPLC method.

From the experimental data presented above and the discussion of the literature data, the simplified sequence of 2-naphthol decomposition can be proposed, including the initial oxidation of the aromatic ring to yield various dione-like species that are followed by their decomposition, involving the opening of the ring to the yield phthalic compounds as well as complete ring opening resulting in heptane. Most importantly, it has been determined that the intermediary products such as 1,2-naphthalenedione, which were formed via ring opening reactions using plasma, are toxic; thus, DBD decomposition needs to be performed for at least 4–6 min to further decompose them into the corresponding less toxic intermediates. The proposed pathway is presented in **Figure 3.9**. Afterwards, a non-plasma based process should be used to fully mineralize these low concentration 2-naphthol decomposition products.
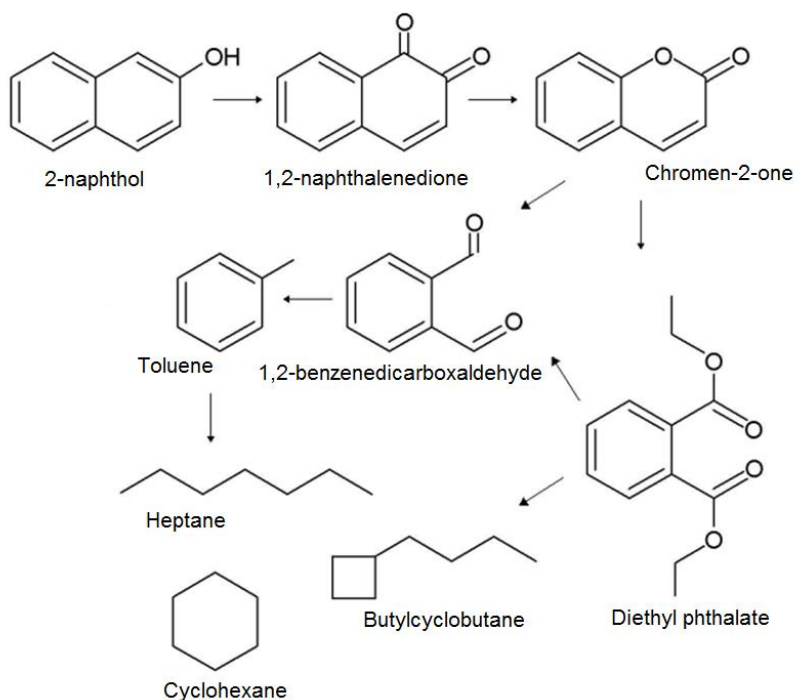
**Figure 3.9.** The proposed mechanistic pathway of 2- naphthol decomposition, using the DBD plasma.

## 3.3.   Removal of pharmaceuticals from water by using photocatalytic ozonation

This passage was quoted from the article entitled "Removal of diclofenac, ketoprofen, and carbamazepine from simulated drinking water by advanced oxidation in a model reactor" (10.1007/s11270-017-3517-z) with permission of Springer Nature.

### 3.3.1. Initial screening experiments

The experiments of diclofenac decomposition were performed to determine the key factors influencing the treatment process. First, thirty experiments were defined by the software, and laboratory experiments were further performed to obtain the decomposition efficiency of diclofenac, the ozone concentration in the air, and the amount of energy that is required for the ozone formation. These data are compiled in **Table 2.3**. The experiments performed according to the full-factorial design yielded diclofenac decomposition efficiency ranging from 11 up to 100%, ozone concentration in the air ranging from 0.41 to 4.49 mg/L, and energy consumption for ozone formation in a range between 127 and 390 kJ/g. These data were taken into account to obtain the final estimates of the regression model.

The dependence of ozone formation and diclofenac decomposition efficiency of various combinations of the experimental factors was modeled, as shown in **Figure 3.10**.

Ozone concentration in air, mg/L

Efficiency of Diclofenac decomposition, %
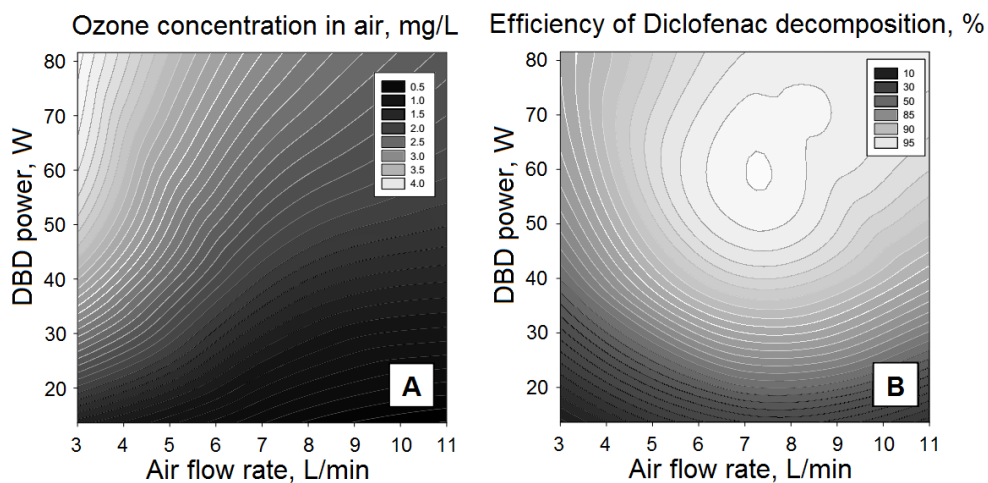


**Figure 3.10.** Effect of the process parameters on the ozone concentration in air (A) and efficiency of diclofenac decomposition (B).

In these surface plots, the effects of the simultaneous variation of two factors, namely the power of the DBD reactor and air flow rate, on ozone formation (**Figure 3.10A**) and diclofenac decomposition efficiency (**Figure 3.10B**) are presented. Initial concentration of diclofenac (10 mg/L) and working volume of the reactor (1.6 L) were kept constant. **Figure 3.10A** presents the variation of ozone concentration in air as a function of the DBD power and aeration intensity. Ozone concentration isolines are shown in the graph. The DBD power was the most significant factor affecting the ozone formation. The highest concentration (4.49 mg/L) of ozone in the air was achieved using 3 L/min flow rate and the highest DBD power of 81.6W. The lowest concentration (0.41 mg/L) of ozone in the air was achieved using 11 L/min flow rate and the lowest DBD power 13.6 W. Due to the dilution, the aeration intensity had a negative effect on the concentration of the ozone produced at the constant reactor power. This effect was higher at the lower DBD reactor power values. The average concentration of ozone (1.45 mg/L) at 13.6 W power was three times higher at the lower air flow rate compared to the concentration values (0.49 mg/L) that were obtained at the highest air flow rate. When it comes to the total amount of produced ozone, the effect of DBD power had a similar character, but the impact of aeration intensity was different. At the lowest reactor power value (13.6 W), the amount of produced ozone was roughly the same, varying in a range of 4–6 mg/min, despite the changes in the aeration intensity. Meanwhile, the increase in aeration intensity at higher reactor powers resulted in a more obvious increase in the amount of produced ozone. When the reactor power was 81.6 W, the observed increase in the amount of produced ozone at flow rates 3 and 11 L/min was double and on average ranged between 13 and 26 mg/min, accordingly. More intense aeration at constant DBD power enhances the efficiency of ozone generation. This is related to the improved cooling of the reactor by the increased air flow. It is known that the temperature has a

60

negative effect on the formation of ozone in the DBD based systems (Pekárek and Mikeš, 2014).

Similarly to the results that were obtained when analyzing the factors affecting ozone formation, the DBD power was the most significant factor influencing diclofenac decomposition efficiency but to a lower extent compared to the effect on the ozone formation. After 0.25 min of treatment, the average diclofenac decomposition efficiency, depending on the applied power, ranged from 21 to 82%. Additionally, aeration exhibited a significant effect on the diclofenac decomposition, especially at the low air flow rate (3 L/min). Higher aeration intensity (up to 7 L/min) resulted in the increase of decomposition efficiency at a constant power (**Figure 3.10B**). This can be explained by the enhanced efficiency of ozone generation and higher ozone mass transfer from the gas to liquid phase at the higher air flow. Further, the rising aeration intensity had negligible or even negative effect on the diclofenac decomposition, especially at lower power values. The highest decomposition efficiency was obtained using the highest DBD reactor power (**Figure 3.10B**) and air flow rate 7 L/min. Overall, the impact of DBD power and air flow rate on the efficiency of diclofenac decomposition was positive.

In the screening experiment, the minimum energy consumption for ozone generation, on average being 146 kJ/g, was obtained by employing DBD reactor power of 13.6 W and air flow ranging between 7 and 11 L/min and the reactor power of 39.2W at air flow in the system being 11 L/min. Meanwhile, the maximum energy consumption values, on average being 280 kJ/g, were obtained when DBD reactor power was 81.6 W and air flow ranged between 3 and 7 L/min and the reactor power was 39.2W at the air flow in the system being 3 L/min. It could be summarized that the higher DBD reactor power and lower air flow in the system have a positive impact on the ozone concentration in the air, but at the same time, it increases the energy consumption and treatment costs.

According to the results of the screening experiments, the optimal decomposition process parameters were selected for further comparative assessment of various advanced oxidation processes performed in the UV-photocatalysis reactor. Setting up the optimal process parameters for ozone formation, diclofenac decomposition and energy consumption factors were evaluated. The aeration intensity was set to 7 L/min, power of DBD reactor to 50 W, and time of pretreatment in DBD reactor to 2 min. This duration is enough to degrade 80–90% of initial pharmaceutical compound diclofenac.

### 3.3.2. Comparative assessment of various AOP's on the pharmaceuticals decomposition

The performance of tested AOPs was examined under the optimal process conditions in the DBD reactor as described in the previous chapter. The dependence of the initial compound decomposition efficiency on the oxidizing system that is applied for the treatment process is shown in **Figure 3.11A, B, C**.
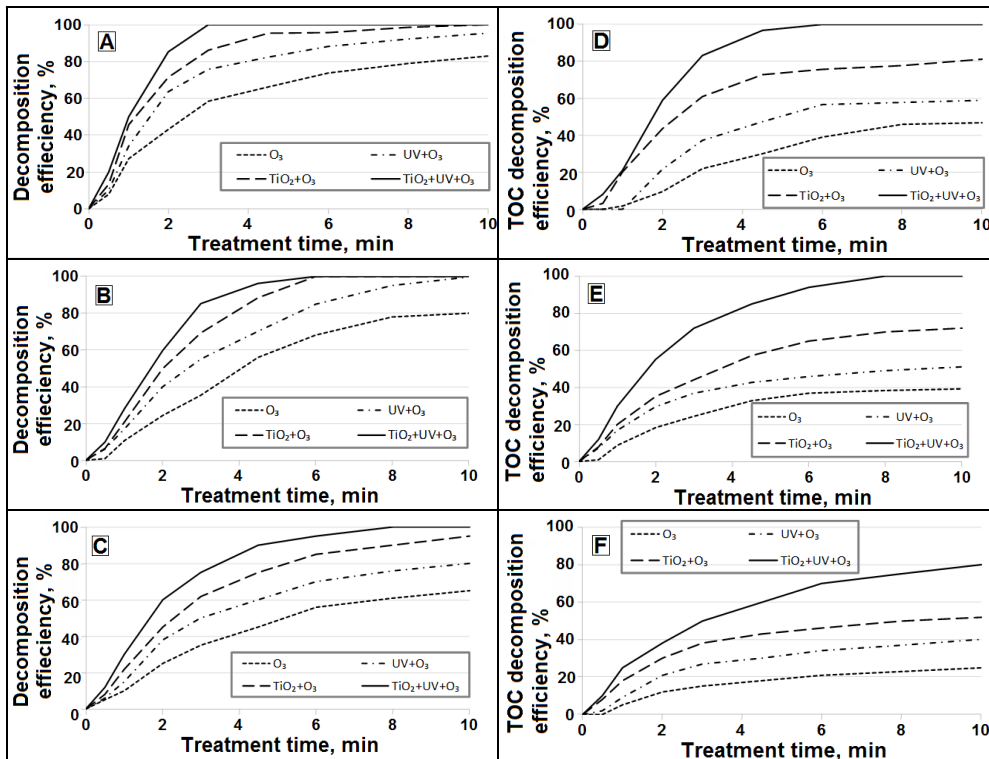
**Figure 3.11.** Decomposition efficiency and TOC removal of target pharmaceuticals for various oxidation processes: diclofenac (A, D), ketaprofen (B, E), and carbamazapine (C, F), under the following conditions: initial compound concentration - 10 mg/L, aeration intensity - 7 L/min, power of DBD reactor - 50 W, power of UVC lamp - 40 W, and time of pretreatment in the DBD reactor - 2 min.

For diclofenac, the greatest decomposition efficiency was achieved by using the oxidation system composed of catalyst, UV light source, and ozone ($TiO_2$+UV+$O_3$). One hundred percent decomposition efficiency was reached within 3 min of treatment process (**Figure 3.11A**). The combination of the catalyst with ozone ($TiO_2$+$O_3$) and UV light with ozone (UV+$O_3$) resulted in less intensive degradation of diclofenac. After 3 min of water treatment, decomposition efficiency reached 86 and 76%, respectively. In the case of ozone oxidation, decomposition efficiency was close to 60%. The complete decomposition of diclofenac was observed in two out of four oxidizing systems after 10 min of treatment. The major amount (about 90%) of diclofenac was decomposed within 3–4 min of treatment in all the oxidation systems, except for ozonation. Subsequently, the decomposition process slowed down. A similar tendency was observed during the process of ketoprofen decomposition. System $TiO_2$+UV+$O_3$ showed the highest decomposition efficiency (**Figure 3.11B**). Almost complete decomposition was reached within 6 min of the treatment process in two out of four tested systems. In the other two systems, UV+$O_3$ and $O_3$ decomposition efficiency at that time was 85 and 68%, respectively. The complete

decomposition of ketoprofen was achieved in three out of four tested systems. For the decomposition of ketoprofen, the increase in treatment efficiency was slower compared to that of the diclofenac. The degradation of carbamazepine showed a slightly different character (**Figure 3.11C**). The higher resistance of carbamazepine towards degradation has been noticed as well by the other researchers (Antoniou et al., 2013; Zhang et al., 2008). The complete decomposition of carbamazepine was observed only in one system ($TiO_2+UV+O_3$). Despite some differences between the pharmaceuticals, the treatment efficiency of applied oxidation processes increased in the following order:

$$O_3 < UV+O_3 < TiO_2+O_3 < TiO_2+UV+O_3.$$
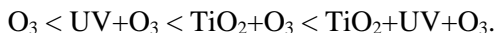
### 3.3.3. Evaluation of TOC removal

**Figure 3.11D, E, F** illustrate the TOC decay during the water treatment of each tested pharmaceutical compound applying different oxidative processes. Results show that the degree of mineralization achieved during the treatment process was significantly higher during the diclofenac decomposition compared to the other tested compounds. After 6 min of diclofenac treatment, 100% TOC removal was reached in the system $TiO_2+UV+O_3$ (**Figure 3.11D**). Meanwhile, the performance of the ozonation process was the least effective. After the same treatment duration, 40% TOC removal was achieved in the $O_3$ system. The performance of the other two systems, i.e., $TiO_2+O_3$ and $UV+O_3$, had a similar character with the combination of catalyst and ozone being more effective. The removal of TOC in these systems differed by almost 20%, and after 6 min of treatment, it was 76 and 57%, respectively. When analyzing the results of TOC removal during the degradation of ketoprofen and carbamazepine, it is obvious that there was no clear difference (**Figure 3.11E, F**).

In the case of ketoprofen, the degree of mineralization was slightly higher compared to that of carbamazepine. After 10 min of treatment depending on the oxidation system applied for the ketoprofen, it varied between 51 and 100%, while for carbamazepine, it ranged between 25 and 80%. When comparing various oxidation systems, it could be noticed that TOC removal demonstrated a similar tendency as it was observed during the target compound degradation described in the previous chapter. Advanced oxidation systems employing $TiO_2+UV+O_3$ and $TiO_2+O_3$ processes had the highest efficiency. In this study, complete mineralization was achieved for diclofenac and ketoprofen by applying the $TiO_2+O_3+UV$ system within a relatively short time (6–8 min). Whereas the mineralization of carbamazepine in this system was slower and less efficient, reaching 80% of TOC decomposition within 10 min. This suggests that the tested treatment system combining non-thermal plasma and UV photocatalysis is effective not only for the degradation of target compounds but as well for the mineralization of intermediate compounds.

### 3.3.4. Evaluation of energy efficiency

The AOPs may become applicable on the industrial scale when every effectiveness factor is optimized and different processes are combined to eliminate some of the drawbacks of the individual techniques for the final goal to achieve the

maximum efficiency with minimum energy input (Wang and Xu, 2012). In this study, apart from the decomposition efficiency, the energy consumption to decompose 1 g of TOC employing various oxidation processes was evaluated. Initial pharmaceutical compounds were mainly degraded by performing pretreatment in the DBD reactor and within the first few minutes of treatment in the UV-photocatalysis reactor. TOC removal mainly represents the decomposition of intermediate degradation products formed during the treatment process. Sometimes, these compounds might be more toxic and require more time and energy to be decomposed. The decomposition of pharmaceuticals that were tested in this study is followed by the formation of various intermediates (Salgado et al., 2013; Hübner et al., 2014). The energy requirements to decompose 1 g of TOC with ozonation and employing the combination of UV with ozonation (**Figure 3.12**) were higher than those for the other two oxidation systems, namely $TiO_2+O_3$ and $TiO_2+UV+O_3$. Depending on the target pharmaceutical compound, it varied between 5.4 and 9.8 MJ/g (TOC) and 7.5–10.6 MJ/g (TOC), respectively.
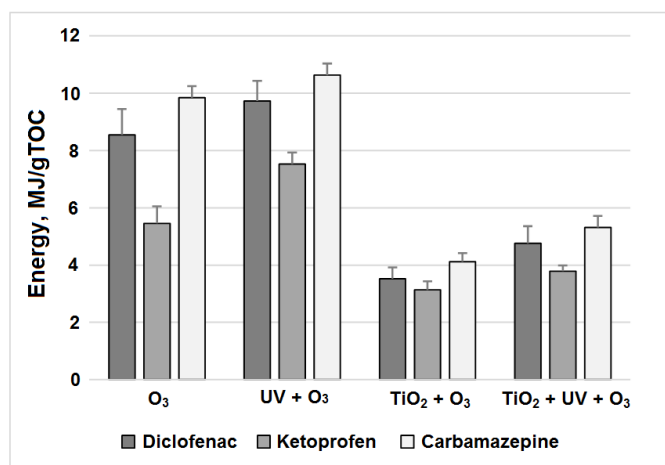


**Figure 3.12.** Energy consumption for the TOC removal by applying various oxidation processes for the water treatment.

Compared to the treatment of diclofenac and carbamazepine, the degradation of intermediate products that were formed during the ketoprofen decomposition was less energy intensive. The energy requirements for TOC removal in $O_3 + TiO_2$ and $O_3+TiO_2+UV$ systems were almost twice less compared to the former and on the average composed 3.6 and 4.6 MJ/g (TOC), respectively. These processes result in a more efficient decomposition of organic compounds. For these oxidation processes, the minimal energy consumption was found to be for the TOC removal during the treatment of model water containing ketoprofen. Depending on the AOPs, it was 3.1 and 3.8 MJ/g, accordingly. These energy consumption values are of similar order of magnitude or even lower compared with the other studies. After the evaluation of mineralization and energy consumption of humic acids by $H_2O_2/UV$ oxidation, Yen and Kang (2016) reported energy requirements for the dissolved organic carbon

removal in the range from 958 to 4850 kWh/kg DOC (3.4–17.6 MJ/g DOC). Based on the evaluation of energy efficiency, the preliminary evaluation of operational expenses was performed. For this, the decrease in TOC concentration and the amount of energy required for the mineralization process were considered.

### 3.3.5. Evaluation of toxicity

The toxicity tests were applied in order to evaluate the integrated rate of toxic impact that are occurring during the application of different oxidizing systems for the decomposition of selected pharmaceuticals in the UV-photocatalysis reactor. **Figure 3.13** shows the evaluation of toxicity of each target compound tested during this study.
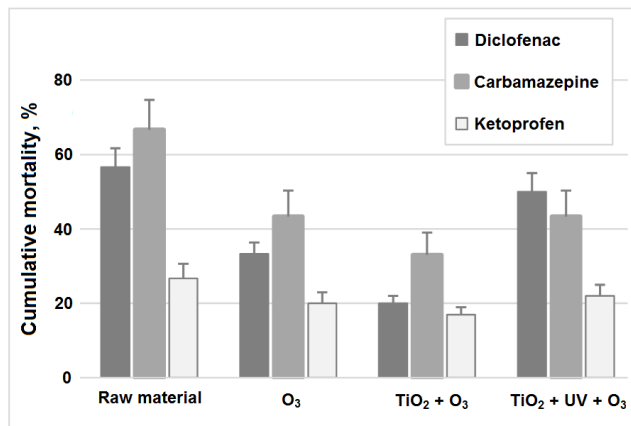


**Figure 3.13.** Toxicity of the initial solutions and solutions after the application of various oxidation processes for the water treatment.

As it was expected, samples of untreated initial solutions containing 10 mg/L of parent pharmaceutical compound demonstrated high mortality rate with cumulative mortality reaching up to 67%. The lowest toxicity on Chironomus sp. larvae, reaching 27% mortality rate, was exhibited by the initial sample of ketoprofen. The low toxicity of ketoprofen for higher organisms was as well observed by the other authors (Illés et al., 2014). Both initial samples of diclofenac and carbamazapine generated more than two times higher mortality rate, reaching 57 and 67%, respectively. Despite the fact that carbamazepine $LD_{50}$ (oral, rat) is up to 37 times higher than the same parameter of toxicity of the other examined substances (**Table 2.2**), low acute toxic effect on the test organisms in the tested concentration range of up to 10 mg/L is in line with literature data (Oetken et al., 2005). The oxidizing systems applied for the treatment process showed diverse removal efficiency of the tested pharmaceuticals. At the same time, their application resulted in the formation of various intermediate decomposition products. Toxicity testing is one of the supplementary methods to evaluate the overall effectiveness of treatment technologies. The treatment of solutions of the selected pharmaceuticals resulted in different toxicity effects described by the cumulative Chironomus sp. larvae mortality rate. For different solutions, it varied from 17 to 50%,

depending on the oxidizing process that was applied. The highest toxicity effect among the studied techniques was attained while using the system involving $O_3+TiO_2+UV$. Depending on the tested pharmaceutical, the observed mortality rate varied from 22 to 50% (**Figure 3.13**). The lowest toxicity, reaching from 17 to 33% mortality rate in 24 h exposure time, was observed for the oxidizing system $O_3+TiO_2$. The residual toxicity throughout the $O_3+TiO_2$ treatment may indicate the formation of intermediate compounds, in some cases generating higher toxicity than the parent compounds. The formation of toxic intermediates during the advanced oxidation processes have been observed by the other authors (Czech et al., 2014; Rizzo et al., 2009; Rozas et al., 2016). Toxicity variation, depending on the treatment time and method, is consistent with the results reported by L. Rizzo et al. (2009), where all samples resulted in toxicity and toxicity seemed to increase due to the higher initial diclofenac concentrations and $TiO_2$ loadings (Rizzo et al., 2009). The toxicity evaluation tests with Chironomus sp. larvae indicated that the reaction solutions, containing decomposition products of parent pharmaceuticals, result in the lowest toxicity when $O_3+TiO_2$ combination for oxidation is used when treatment time is no less than 5 min. The data obtained from the toxicity tests suggest that out of all the tested advanced oxidation processes, the combination of $O3+TiO_2$ could be proposed as the most promising. The observed variations in the toxicity response of each of the investigated pharmaceutical compounds may be attributed to their particular degradation pathway during the water treatment. It is important to notice that these toxicity results are limited and can only be used for comparative or presumptive reasons in this particular study. In order to make definite assumptions, further research on the intermediate oxidation products and their toxicity should be involved.

## 3.4. The treatment of water polluted with various organic compounds by using photocatalytic ozonation

This passage was quoted from the article entitled "Ozone-UV-catalysis based advanced oxidation process for wastewater treatment" (10.1007/s11356-017-9381-y) with permission of Springer Nature.

### 3.4.1. Characterization of the catalyst

The surface of the manufactured catalyst coating was relatively rough, as suggested by SEM imaging (**Figure 3.14A, B**) with a uniform distribution of the $TiO_2$ layer and various protrusions in the size range between 1 and 10 μm. In fresh catalyst (**Figure 3.14A**), some of these $TiO_2$ aggregates were as large as 5−10 μm, while they are not visible on a used catalyst surface (**Figure 3.14B**), where only small sized (1–5 μm) aggregates of $TiO_2$ occur. The larger $TiO_2$ aggregates possibly were "fluffy" and loosely attached and were washed away from the surface during the initial tests. Correspondingly, the degradation of 2-naphthol (which was run first) appeared as the most efficient. Such washout of the nanoparticle based catalyst is unwanted in the commercial applications due to the potentially adverse effects of nanoparticles released to the aqueous ecosystems. Newly made catalysts must be pretreated by

rinsing with distilled water before the installations in the operational environments for washing possibly poorly attached TiO₂ particles after the catalyst manufacturing process to avoid the release of these particles to the treated water.
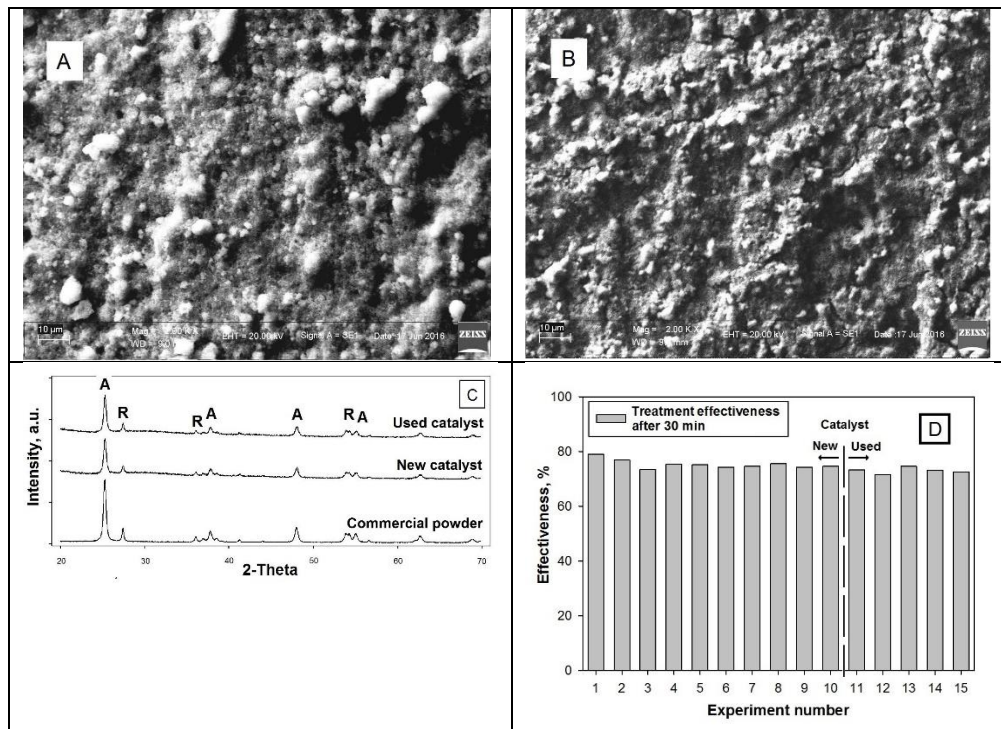


**Figure 3.14.** Catalyst characterization: A – SEM image of a newly made catalyst, B – SEM image of the used catalyst, C – XRD spectrum of catalyst samples (R – rutile phase, A – anatase phase), D - the change of decomposition efficiency vs catalyst aging. The first 10 experiments show the effectiveness of the photocatalytic ozonation using newly made catalyst; the last five show the same experiments with the used catalyst.

The crystalline structures of new and used catalysts were comparatively similar to each other and to the commercial powder (**Figure 3.14C**). The ratio between the anatase and rutile phases in the coating remained the same as in the commercial powder sample. Only slight reduction of all peaks was observed that is probably related to the agglomeration of nanopowder to the larger particles during the thermal processing.

After the first run, the activity of the catalyst decreased during the succeeding runs, but it remained stable (**Figure 3.14D**). The measured treatment efficiency was as well comparatively stable (75%) during all the series of durability testing experiments (1–10), except in the first two experiments where efficiencies were 78.9 and 76.9%. No significant loss of efficiency (72.9%) was observed after the secondary durability testing (experiments 11–15). A low difference (2.4%) between new and used catalyst can have attributed to the mechanical wearing when installing and

withdrawing catalyst constructions to the reactor between experiments, and it can be avoided in the industrial installations assuming the correct handling of the catalyst frames.

In general, the construction of the catalyst coated glass rods surrounding the UV source proved to be efficient in the upscaling to the bench scale, and potentially, to the industrial scale.

### 3.4.2. Degradation efficiency of pollutants by various combinations of AO components

The efficiency of degradation of the tested pollutants using various combinations of AO techniques are presented below, grouping to photolysis and photocatalysis, ozonation and catalytic ozonation as well as photolytic ozonation and photocatalytic ozonation. Such grouping was selected due to the comparable performance of these techniques in the degradation process.

**Photolysis and photocatalysis.** These two techniques performed the worst with a slight increase in efficiency after the introduction of the catalyst. The decrease in TOC concentration during the photolysis ranged from 0.4% in case of D-glucose to 99.7% in the case of oxalic acid. During the photocatalysis experiment, TOC decrease ranged from 10.2 to 99.7% using methylene blue and oxalic acid, respectively (**Figure 3.15A, B**). Such poor performance indicates that the production of oxidative species was inefficient, except for oxalic acid. This has been noticed in the earlier studies (Mano et al., 2015; Huang et al., 2016), suggesting the necessity of the introduction of ozone to initiate more rapid decomposition process. In both photolysis and photocatalysis experiments, a strong foaming of model wastewater was observed during the first 10 min of 2-naphthol decomposition. The foam was carried off to the foam dampers with the exhaust gas from the reactor. This led to a notable reduction of TOC, because the organic matter was removed without degradation. After the foaming stopped, no significant TOC reduction was observed. This indicates that special measures must be taken to observe the potential formation of foams in specific cases of industrial applications.

**Ozonation and catalytic ozonation.** Ozonation and catalytic ozonation were slightly more efficient experimental conditions, providing the decrease in the TOC values from 2.8% (oxalic acid) to 37.7% (phthalate) during the ozonation and from 3.1% (D-glucose) to 48.9% (phthalate) during the catalytic ozonation (**Figure 3.15C, D**). The other researchers, e.g., Orge et al. (2015), in case of oxalic acid, reported such small degradation efficiency. The obtained ranges of degradation are not suitable for the industrial applications, where more rapid and complete degradation of pollutants is expected. Strong foam formation was registered this time during the degradation of methylene blue. The mechanisms behind the formation of foam have not been identified, but possibly, they related to the primary decomposition by-products or initial compound, which can have foaming properties. It should be noted that the initial concentration of the pollutants was relatively high; thus, the foaming may be

68

not that pronounced in the industrial settings, although the presence of other matrix materials, such as surfactants, may be crucial for the operation of such technology. A slight increase of effectiveness during the catalytic ozonation against purely ozonation may be explained by the mechanism, where the adsorbed ozone reacts with the $TiO_2$ surface (without UV light) producing ozonide ions, which later can be transformed to the hydroxyl radicals (Hernández-Alonso et al., 2002).

  **Photolytic ozonation and photocatalytic ozonation.** Photolytic ozonation and photocatalytic ozonation processes yielded the best decomposition efficiencies, achieving decomposition efficiency as high as 99.9% for phenol after 1 h of photocatalytic ozonation treatment (**Figure 3.15E, F**). Similar results were found by Oh et al. (2006) (phthalate solution), where the photolytic ozonation showed much better results than only ozonation. Moreover, the foaming was comparatively less intense during these experiments. The above-mentioned data indicate that the photocatalytic ozonation ($O_3$+UV+Cat.) was the most efficient process that is capable of removing target compounds reaching 90–99% degradation after 1 h of treatment. While technically efficient, this combination should be further explored for its durability and robustness to be implemented in the industrial settings.
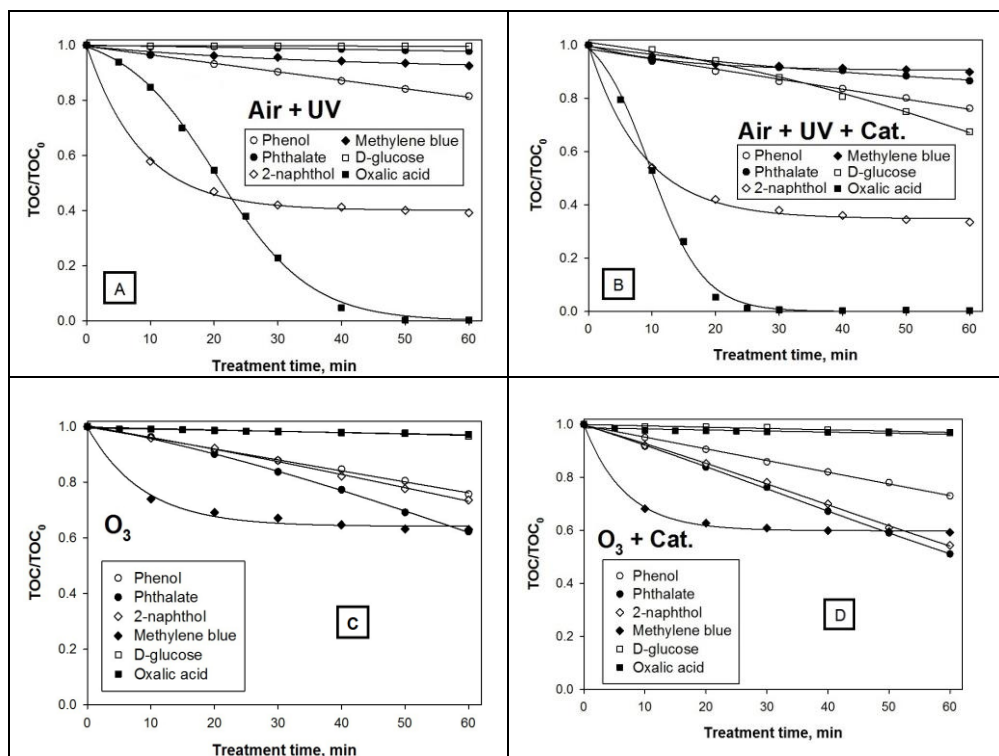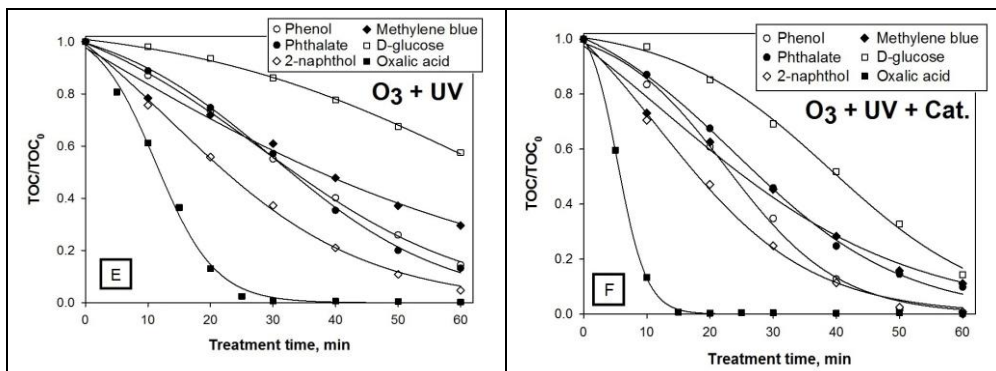
**Figure 3.15.** Decomposition kinetics and efficiency of the tested compounds. Photolysis (A), photocatalysis (B), ozonation (C), catalytic ozonation (D), photolytic ozonation (E), and photocatalytic ozonation (F). The data is given in relative units of measured TOC concentration. The linear and non-linear regression models are fitted at the graphs.

### 3.4.3. Degradation kinetics

The approximation of degradation kinetics by regression models allowed the estimation of time required for the 90% degradation efficiency and the energy consumption for each target pollutant at every experimental condition (**Table 3.4**).

The lowest energy requirement for the degradation was during photocatalytic ozonation and ranged between 0.16 and 2.16 MJ/g (oxalic acid and methylene blue, respectively). The photolytic ozonation was more energy demanding (0.34–3.58 MJ/g, oxalic acid and methylene blue, respectively). All other experimental conditions were found to be much more energy demanding. Three parameter exponential and sigmoidal decay functions were observed to be most suitable to approximate the degradation kinetics during the tested AO combinations. The exponential decay was appropriate to model the TOC concentration loss at the experiments where foaming was observed, such as in 2-naphthol photolysis and photocatalysis or methylene blue ozonation and catalytic ozonation. The foaming was rapid during the first minutes and then decreased with practically no degradation during the remaining treatment. The three-parameter sigmoidal models were found to be the most representative for the modeling of the degradation kinetics where the TOC value was chosen as the main parameter for the degradation measurements, as selected in this study. In cases where the kinetics is observed by the decrease of the concentration of the initial compound, the kinetics usually follows the exponential decay (Oh et al., 2006; Li et al., 2015; Moreira et al., 2016), while sigmoid kinetics is rare (De Witte et al., 2010). The kinetics represented by the degradation of TOC is more meaningful as it shows the process of full mineralization of organic compound, representing full degradation and the overall efficiency of the process. The mechanism of TOC concentration variation is a result of the initial degradation of the original compound to its by-products following step-by-step reactions (Marotta et al., 2011; Márquez et al., 2014; Dai et al.,

2015; Tay and Madehi, 2015; Krugly et al., 2015; Guo et al., 2016; Zhang et al., 2016). During the first minutes of degradation, the reduction of organic carbon and production of $CO_2$ is very low, as indicated by the upper asymptote of the sigmoid curve. Such low rate of conversion to $CO_2$ during the start of degradation was observed by Dobrin et al. (2013), where the corona discharge above water was used for the degradation of diclofenac. In the middle of the process, lower molecular mass compounds fully degrade to $CO_2$, thus increasing the mineralization rate, represented by the steepest slope of the S-curve and the inflection point. The mineralization rate decreases when the residual organic carbon approaches 30%, represented by the lower asymptote.

**Table 3.4.** Regression models and calculated data, including the DBD energy and total energy (including UV lamp energy consumption) requirements for the pollutant degradation and time required to reach 90% (3p. – 3 parametric).

| Model pollutant | Experimental conditions | Regression model | Degradation rate after 60 min. of treatment, % | Modeled time to decompose first 90% of TOC, min | Modeled energy to decompose first 90% of TOC, MJ | | Modeled energy to decompose 1g of TOC until 90% treatment efficiency, MJ | | Modeled energy to decompose 1g of pollutant until 90% treatment efficiency, MJ | |
|---|---|---|---|---|---|---|---|---|---|---|
| | | | | | DBD | DBD+UV | DBD | DBD+UV | DBD | DBD+UV |
| 2-naphthol | $O_3$ | Sigmoidal 3p. | 26.4 | 248.3 | 0.43 | 0.43 | 5.96 | 5.96 | 4.96 | 4.96 |
| | $O_3$+Cat. | Sigmoidal 3p. | 45.6 | 153.9 | 0.27 | 0.27 | 3.69 | 3.69 | 3.07 | 3.07 |
| | $O_3$+UV | Sigmoidal 3p. | 95.2 | 52.8 | 0.09 | 0.22 | 1.27 | 3.03 | 1.05 | 2.52 |
| | $O_3$+UV+Cat. | Sigmoidal 3p. | 99.2 | 41.7 | 0.07 | 0.17 | 1.00 | 2.39 | 0.83 | 1.99 |
| | Air+UV | Exponential 3p. | 66.5 | >1000 | 0.00 | >2.40 | 0.00 | >33.33 | 0.00 | >27.75 |
| | Air+UV+Cat. | Exponential 3p. | 60.8 | >1000 | 0.00 | >2.40 | 0.00 | >33.33 | 0.00 | >27.75 |
| Phenol | $O_3$ | Linear | 24.3 | 224.7 | 0.39 | 0.39 | 5.39 | 5.39 | 4.49 | 4.49 |
| | $O_3$+Cat. | Linear | 27.0 | 203.5 | 0.35 | 0.35 | 4.89 | 4.89 | 4.07 | 4.07 |
| | $O_3$+UV | Sigmoidal 3p. | 85.5 | 68.6 | 0.12 | 0.28 | 1.65 | 3.93 | 1.37 | 3.12 |
| | $O_3$+UV+Cat. | Sigmoidal 3p. | 99.9 | 42.9 | 0.07 | 0.18 | 1.03 | 2.46 | 0.86 | 1.95 |
| | Air+UV | Linear | 23.8 | 288.9 | 0.00 | 0.69 | 0.00 | 9.63 | 0.00 | 7.39 |
| | Air+UV+Cat. | Linear | 18.5 | 232.9 | 0.00 | 0.56 | 0.00 | 7.76 | 0.00 | 5.94 |
| Oxalic acid | $O_3$ | Linear | 2.8 | >1000 | >1.73 | >1.73 | >24.00 | >24.00 | >6.40 | >6.40 |
| | $O_3$+Cat. | Linear | 3.3 | >1000 | >1.73 | >1.73 | >24.00 | >24.00 | >6.40 | >6.40 |
| | $O_3$+UV | Sigmoidal 3p. | 99.7 | 22.0 | 0.04 | 0.09 | 0.53 | 1.26 | 0.14 | 0.34 |
| | $O_3$+UV+Cat. | Sigmoidal 3p. | 99.7 | 10.7 | 0.02 | 0.04 | 0.26 | 0.61 | 0.07 | 0.16 |
| | Air+UV | Sigmoidal 3p. | 99.7 | 37.0 | 0.00 | 0.09 | 0.00 | 1.23 | 0.00 | 0.33 |
| | Air+UV+Cat. | Sigmoidal 3p. | 99.7 | 19.3 | 0.00 | 0.05 | 0.00 | 0.64 | 0.00 | 0.17 |
| Phthalate | $O_3$ | Sigmoidal 3p. | 37.7 | 155.6 | 0.27 | 0.27 | 3.73 | 3.73 | 1.76 | 1.76 |
| | $O_3$+Cat. | Sigmoidal 3p. | 48.9 | 147.0 | 0.25 | 0.25 | 3.53 | 3.53 | 1.66 | 1.66 |
| | $O_3$+UV | Sigmoidal 3p. | 86.8 | 62.2 | 0.11 | 0.26 | 1.49 | 3.56 | 0.70 | 1.68 |
| | $O_3$+UV+Cat. | Sigmoidal 3p. | 90.2 | 55.4 | 0.10 | 0.23 | 1.33 | 3.18 | 0.62 | 1.49 |
| | Air+UV | Linear | 13.5 | >1000 | 0.00 | >2.40 | 0.00 | >33.33 | 0.00 | >15.67 |
| | Air+UV+Cat. | Exponential 3p. | 2.3 | >1000 | 0.00 | >2.40 | 0.00 | >33.33 | 0.00 | >15.67 |

**Table 3.4.** (Continued).

| Model pollutant | Experimental conditions | Apropriate type of decay function | Degradation rate after 60 min. of treatment, % | Modeled time to decompose first 90% of TOC, min | Modeled energy to decompose first 90% of TOC, MJ | | Modeled energy to decompose 1g of TOC until 90% treatment efficiency, MJ | | Modeled energy to decompose 1g of pollutant until 90% treatment efficiency, MJ | |
|---|---|---|---|---|---|---|---|---|---|---|
| | | | | | DBD | DBD+UV | DBD | DBD+UV | DBD | DBD+UV |
| Methylene blue | $O_3$ | Exponential 3p | 37.0 | >1000 | >1.73 | >1.73 | >24.00 | >24.00 | >14.41 | >14.41 |
| | $O_3$+Cat. | Exponential 3p | 40.7 | >1000 | >1.73 | >1.73 | >24.00 | >24.00 | >14.41 | >14.41 |
| | $O_3$+UV | Sigmoidal 3p. | 70.5 | 104.1 | 0.18 | 0.43 | 2.50 | 5.97 | 1.50 | 3.58 |
| | $O_3$+UV+Cat. | Sigmoidal 3p. | 88.8 | 62.8 | 0.11 | 0.26 | 1.51 | 3.60 | 0.91 | 2.16 |
| | Air+UV | Exponential 3p | 10.2 | >1000 | 0.00 | >2.40 | 0.00 | >33.33 | 0.00 | >20.01 |
| | Air+UV+Cat. | Exponential 3p | 7.5 | >1000 | 0.00 | >2.40 | 0.00 | >33.33 | 0.00 | >20.01 |
| D-glucose | $O_3$ | Linear | 3.5 | >1000 | >1.73 | >1.73 | >24.00 | >24.00 | >9.59 | >9.59 |
| | $O_3$+Cat. | Linear | 3.1 | >1000 | >1.73 | >1.73 | >24.00 | >24.00 | >9.59 | >9.59 |
| | $O_3$+UV | Sigmoidal 3p. | 42.5 | 116.5 | 0.20 | 0.48 | 2.80 | 6.68 | 1.12 | 2.67 |
| | $O_3$+UV+Cat. | Sigmoidal 3p. | 85.6 | 67.4 | 0.12 | 0.28 | 1.62 | 3.86 | 0.65 | 1.54 |
| | Air+UV | Linear | 32.6 | >1000 | 0.00 | >2.40 | 0.00 | >33.33 | 0.00 | >13.32 |
| | Air+UV+Cat. | Sigmoidal 3p. | 0.4 | 151.4 | 0.00 | 0.36 | 0.00 | 5.05 | 0.00 | 2.02 |
| Mixture | $O_3$ | Exponential 3p | 18.2 | >1000 | >1.73 | >1.73 | >24.00 | >24.00 | >11.33 | >11.33 |
| | $O_3$+Cat. | Exponential 3p | 18.0 | >1000 | >1.73 | >1.73 | >24.00 | >24.00 | >11.33 | >11.33 |
| | $O_3$+UV | Sigmoidal 3p. | 84.4 | 69.1 | 0.12 | 0.29 | 1.66 | 3.96 | 0.78 | 1.87 |
| | $O_3$+UV+Cat. | Sigmoidal 3p. | 97.8 | 42.2 | 0.07 | 0.17 | 1.01 | 2.42 | 0.48 | 1.14 |
| | Air+UV | Exponential 3p | 39.7 | >1000 | 0.00 | >2.40 | 0.00 | >33.33 | 0.00 | >15.74 |
| | Air+UV+Cat. | Exponential 3p | 25.9 | >1000 | 0.00 | >2.40 | 0.00 | >33.33 | 0.00 | >15.74 |

The linear regression model was found to be suitable for negligible degradation results, as phenol, D-glucose, or oxalic acid ozonation, where low or no degradation was achieved. In case of phenol degradation experiments, this model shows possible reduction of the phenol model wastewater TOC value due to the loss by possible phenol evaporation but not degradation.

### 3.4.4. Identification of decomposition by-products

Three samples of wastewater containing phthalate as the most persistent compound (excluding D-glucose as a nonhazardous substance) were analyzed, including the untreated sample with 100% initial TOC concentration, half-treated sample with 50% TOC concentration, and sample after 60 min of treatment. The time needed to treat the model wastewater to the remaining 50% TOC value (27 min) was calculated from the experiment on the catalyst activity testing. Various phthalate degradation products were found in the half-treated wastewater sample, including salicylic, 4 hydroxyphthalic, adipic acids, and salicylaldehyde. The proposed simplified pathway is presented in **Figure 3.16.** Possibly, the phthalate firstly degraded to salicylic acid and salicylaldehyde and then to adipic acid while losing the aromaticity. The formation of various acids, including aromatic ring containing and linear dicarboxylic acids, was observed by Q. Zhang et al. (2016), where Fenton oxidation was used for the phthalate degradation. The 4-hydroxyphthalic acid was formed from phthalate with accession of HO· radical directly to the aromatic ring. The direct accession of HO· radical to aromatic ring structure to form various hydroxybenzoates was as well confirmed by Yuan et al. (2008) and °Zhang et al. (2016). It should be noted that many more by-products are formed during the degradation of phthalate, but they are not detected due to the low concentrations. No significant peaks were observed in the mass spectrum after 60 min of degradation, suggesting that the residual carbon (as measured with TOC analyzer) consisted of a wide range of organic compounds of the high state of oxidation, such as simple organic acids. These compounds are comparatively less toxic and can be degraded completely to $CO_2$ and water with extended treatment time.
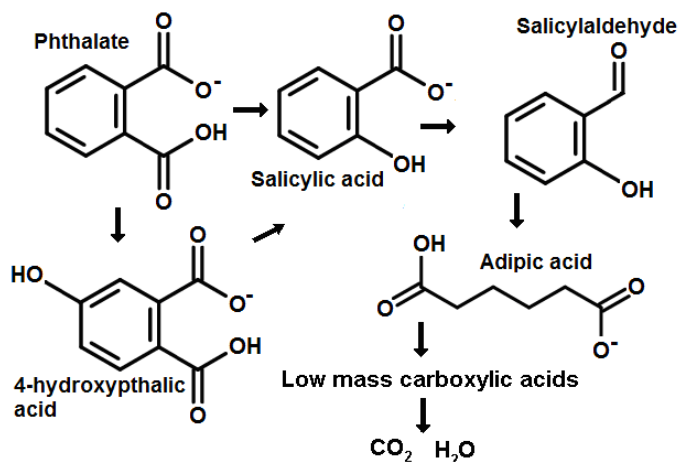
**Figure 3.16.** The formation of phthalate degradation by-products.

### 3.4.5. Toxicity of decomposition by-products

The toxicity of the model wastewater corresponds to the toxicity of the dissolved pollutant. The oxalic acid, methylene blue, 2-naphthol, and the mixture of all model pollutants were identified as very toxic (100% mortality) at the applied concentrations (**Figure 3.17**). The phenol solution was observed as the least toxic (~80% mortality). The phthalate and D-glucose at the selected concentrations were identified as non-toxic in all the cases and in all the treated wastewater samples. Phenol, methylene blue, and mixture solutions have lost their toxicity after the 50% TOC removal. The toxicity of the 2-naphthol solution was reduced by 20%, while oxalic acid remained as toxic as the initial solution. The obtained results suggest that the photocatalytic ozonation has a potential to reduce the toxicity of various toxic substances and their mixtures present in the industrial wastewater fully. The treatment to the residual TOC of 0–15% is sufficient to reduce the toxicity to almost zero.
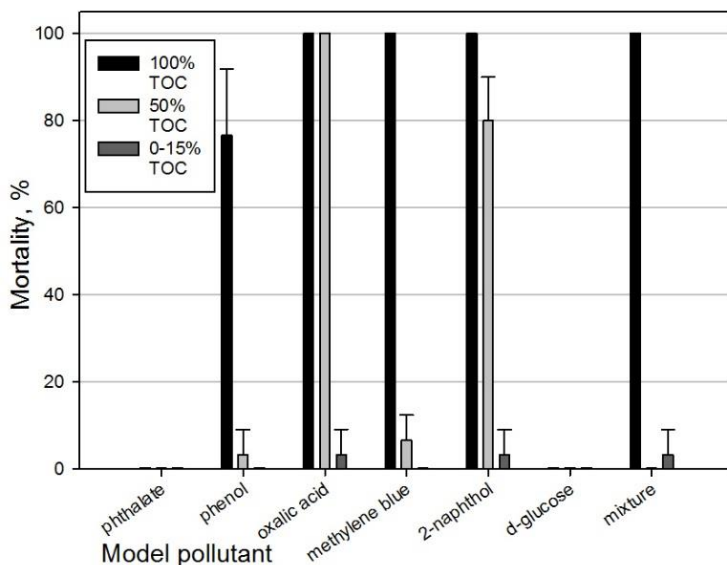
**Figure 3.17.** The mortality of Daphnia magna after 24 h, three samples of each model wastewater were examined: untreated, half treated (by TOC value), and after 1 h of treatment using photocatalytic ozonation.

### 3.4.6. System testing by using mixed pollutants wastewater and various pH values

The AO process has been shown to depend on the pH value of the wastewater (De Witte et al., 2010; Xiao et al., 2015), due to the changing reactions of ozone in water and production of the active radicals. The mixture model wastewater (No. 7 in **Table 2.4**), containing a composition of hardly and easily degradable pollutants, was tested against pH of the solution in the ozonation processes, measuring the effectiveness of the process as a portion of the remaining TOC concentration.
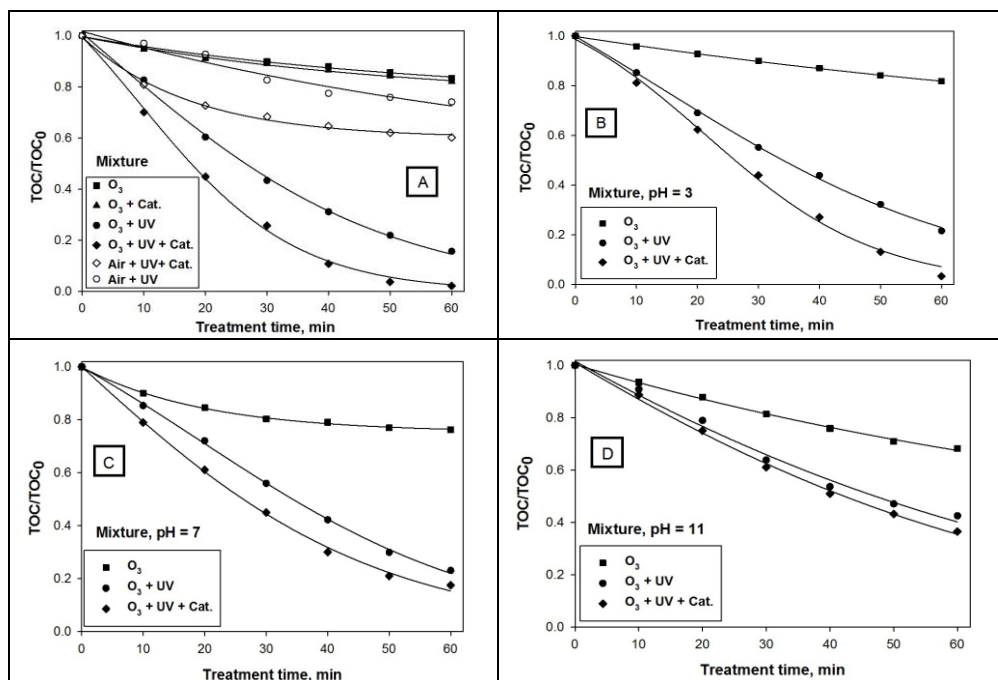
**Figure 3.18.** The effect of pH on the degradation efficiency of the mixture wastewater as represented by the TOC decrease: a - uncontrolled initial pH, b - artificially adjusted initial pH=3, c - pH=7, and d - pH=11.

In case of uncontrolled initial pH (equal to 3.38), the photocatalytic ozonation provided the best degradation efficiency (97.8%, **Figure 3.18A**). The photolytic ozonation reached 84.4%, while purely ozonation stayed at 18.2% after 60 min of treatment. Similar trends have been registered in the initial pH adjusted experiments, where the photocatalytic ozonation performed best, and ozonation performed worst (**Figure 3.18B, C, D**). However, the final efficiency varied broadly. The highest efficiency for the photocatalytic ozonation of 96.6% occurred at pH = 3, which is comparable to the unadjusted pH. Although the result was almost similar, the kinetics of the pH = 3.38 degradation was slightly faster in the initial phases, while in case of pH = 3, the kinetics followed more sigmoidal pattern. At the initial pH = 11, only 63.5% efficiency was measured using photocatalytic ozonation, 57.5%, for photolytic ozonation, and 31.8% for ozonation. This implies that single ozonation, although least efficient overall, is more efficient using elevated pH values. Similar findings were obtained during the ozonation of ciprofloxacin (De Witte et al., 2010), phenol (Contreras et al., 2011), and textile dyes (Gomes et al., 2012). At high pH, the formation of HO· radicals is facilitated by the reaction of $O_3$ with hydroxyl ions (Mehrjouei et al., 2015):

$$O_3 + OH^- \rightarrow O_2\bullet^- + HO_2\bullet; \qquad\qquad (29)$$

$$O_3 + HO_2\bullet \rightarrow 2O_2 + HO\bullet. \qquad\qquad (30)$$

However, the photocatalytic ozonation using TiO2 as catalyst is more efficient at low pH values (Sánchez et al., 1998; Gimeno et al., 2007). The formation of ozonide $(O_3\cdot^-)$ radical under photocatalytic ozonation conditions and subsequent reaction chain with $H^+$ ion to form $HO\cdot$ radicals has been suggested as the prevailing mechanism (Sánchez et al., 1998; Mehrjouei et al., 2015):

$$TiO_2 + h\nu \rightarrow e^- + h^+; \qquad\qquad (31)$$

$$O_3 + e^- \rightarrow O_3\bullet^-; \qquad\qquad (32)$$

$$O_3\bullet^- + H^+ \rightarrow HO_3\bullet; \qquad\qquad (33)$$

$$HO_3\bullet \rightarrow O_2 + HO\bullet. \qquad\qquad (34)$$
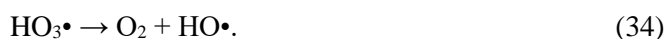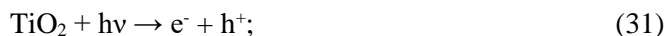
The UV effect on ozone utilization is explained as the radiation induced oxygen radical formation and further water decomposition to $HO\cdot$ radicals (Mehrjouei et al., 2015):

$$O_3 + h\nu \rightarrow O\bullet + O_2; \qquad\qquad (35)$$

$$O\bullet + H_2O \rightarrow HO\bullet. \qquad\qquad (36)$$

Thus, the selection of AO technology in the up-scaled systems may depend on the pH of the wastewater. In cases of high pH, it may be more profitable to use ozonation with longer treatment duration or adjust the pH before the treatment. The use of photocatalytic ozonation should be applied to the wastewaters of low pH. The reduction of the pH was registered in most cases (**Table 2.4**). This is associated with the fact that the formed degradation by-products often contain low-molecular weight organic acids (Marotta et al., 2011). The decrease of pH is as well associated with the efficiency of the degradation process. In case of full mineralization (95–100% TOC reduction), the pH has remained similar to the initial solution (when the initial compound was non-acidic) or increased (in case of oxalic acid). In less efficient processes with total TOC reduction of ~40–80%, the pH tends to decrease due to the increasing concentration of organic acids as by-products. In low efficiency processes with total TOC reduction of ~10–40%, the pH remained at similar levels to initial solution due to the minimal degradation of initial substance.

## 3.5. The treatment of industry wastewater by using photocatalytic ozonation

This passage was quoted from the article entitled "Advanced oxidation-based treatment of furniture industry wastewater" (10.1007/s11356-017-9381-y) with permission of Taylor & Francis Group.

### 3.5.1. Effects of various AO combinations on the treatment efficiency and kinetics

**Uncontrolled pH experiment.** The removal of TOC was not observed during the photolysis of the prepared industry wastewater sample, while ozonation and catalytic ozonation had a very low effect (efficiency of 9.5% and 10.5% after 180 min of treatment, respectively, **Figure 3.19A**). Photocatalysis was more effective, reaching 39.4% after 180 min of treatment. The most efficient combinations of AO components included the photolytic ozonation (96.6%) and photocatalytic ozonation (99.3%). Ninety percent effectiveness was reached after 100 min during the photocatalytic ozonation and 138 min at the photolytic ozonation. These findings indicate higher efficiency of photocatalytic ozonation against other tested AO combinations. Photocatalytic ozonation was confirmed as the most efficient by the other authors. Mano et al. (2015) investigated the activity of various transition metal oxides at different AO combinations, utilizing ozone, UV, and catalysts. In all the cases of Mano et al. (2015) experiments, the removal of TOC treating of oxalic acid solution was the highest when using the photocatalytic ozonation method. Mecha et al. (2016) evaluated the metal ion (Ag, Cu and Fe)-doped $TiO_2$ activity at the photocatalytic ozonation experiment and confirmed its highest efficiency against photocatalysis and ozonation by using phenol as the target compound in the municipal wastewater. The poor efficiency of single ozonation can as well be explained by the fact that low molecular weight carboxylic acids, recalcitrant to further ozone oxidation, are formed during the treatment (Martins and Quinta-Ferreira, 2014).

**Controlled initial pH experiment.** The three most effective AOPs (as determined at the uncontrolled pH experiments, including photocatalytic ozonation, photolytic ozonation, and photocatalysis) were tested using wastewater with adjusted initial pH. In case of the photocatalytic ozonation (**Figure 3.19B**), a comparatively high TOC reduction efficiency was achieved (>99.9% at the initial pH values of 3–5 and 90.3–96.2 at the initial pH of 9–11) after 180 min of treatment. The duration of 90% TOC reduction was 78 min at the initial pH = 3 and 84 min at pH = 5. The 90% reduction duration for pH values of 9–11 was higher (124–136 min) than non-adjusted initial pH (6.7). The obtained data show the relationship between wastewater pH and TOC reduction efficiency, where lower pH leads to a higher efficiency at the tested initial pH values. The variation of pH during photolytic ozonation (**Figure 3.19C**) yielded similar results to the photocatalytic ozonation. The two lowest pH values (3 and 5) had the most pronounced effect, where 90% TOC reduction efficiency was reached after 100 and 98 min of treatment, respectively. The duration for 90% TOC reduction at pH values of 9–11 was longer (134–148 min). Generally, both the photolytic ozonation and photocatalytic ozonation were proven as robust methods capable of tackling the change in pH of the wastewater. The increased efficiency of ozonation and photolytic ozonation at lower pH values is twofold and can be influenced by the enhanced formation of hydroxyl radicals at low pH and the behavior of carbonate ion as hydroxyl radical scavenger at high pH. In the first case, the possible cause of the pathway of hydroxyl radical formation influenced by $TiO_2$ and/or UV in the presence of $H^+$ ion in a liquid is discussed (Mecha et al., 2016; Mehrjouei

et al., 2015). The second one is related to the accumulation of carbonate ion in the liquid at high pH value. This $CO_3^{2-}$ ion acts as a hydroxyl radical scavenger and interferes with the degradation of organic pollutants (Quiñones et al., 2015). Photocatalysis process (**Figure 3.19D**) appeared to be the most dependent on the initial pH value. The highest treatment efficiency after 180 min was reached at pH = 5 (83.3%). This comparatively low efficiency indicates the necessity of the increase in the treatment duration and, subsequently, increased energy requirements.
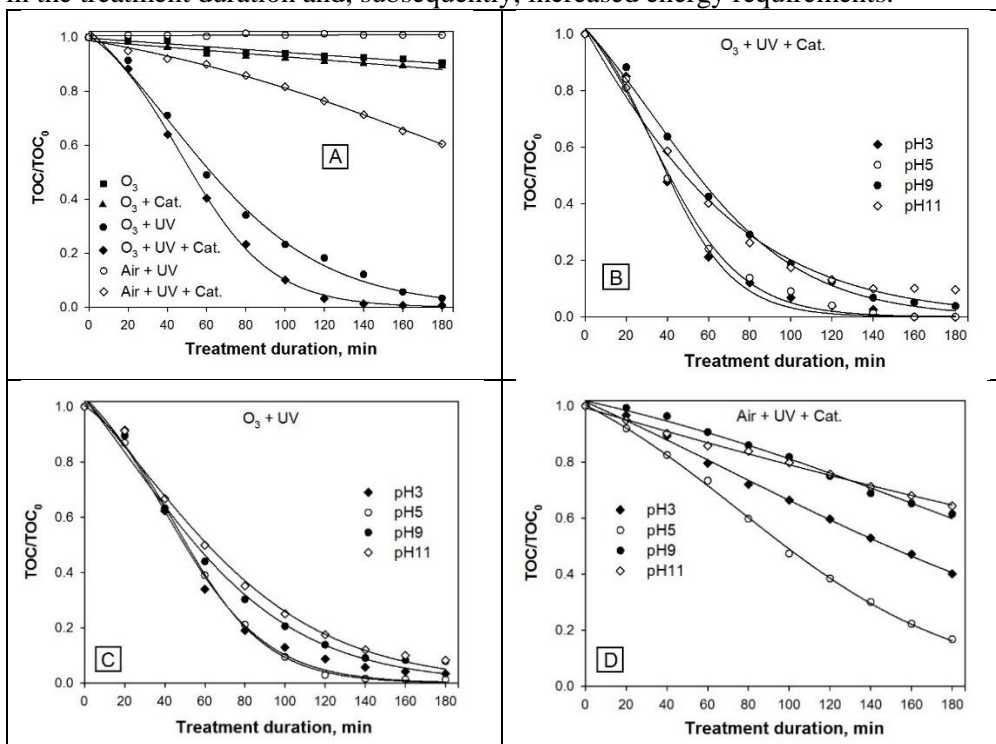


**Figure 3.19.** The degradation of wastewater under various AO combinations and pH values: A - the initial pH = 6.7 (non-adjusted), gas flow rate of 11 L/min, ozone concentration of 1.3 mg/L (if used), initial TOC= 50 mg/L; B - photocatalytic ozonation controlled initial pH experiment; C - photolytic ozonation controlled initial pH experiment; c – photocatalysis controlled initial pH experiment.

### 3.5.2. Energy requirements

Energy requirements were calculated using the data from the non-regulated pH experiments, where various AO combinations were tested. The calculated data are presented in **Table 3.5**.

**Table 3.5.** Calculated duration of treatment for the removal of 90% of TOC and energy requirements to reach this efficiency.

| Group of experiments | Regression model | Experimental conditions | Calculated time to reach 90% TOC removal efficiency, min | Energy consumed to 90% TOC reduction, MJ | Energy to 1 g of TOC decomposition until 90% efficiency, MJ |
|---|---|---|---|---|---|
| Uncontrolled initial pH value | Sigmoidal 3p. | $O_3$+UV+Cat. | 100 | 0.41 | 5.76 |
| | Sigmoidal 3p. | $O_3$+UV | 138 | 0.57 | 7.93 |
| | Sigmoidal 3p. | Air+UV+Cat. | 428 | 1.03 | 14.27 |
| | Linear | $O_3$+Cat. | 1503 | 2.60 | 36.06 |
| | Linear | $O_3$ | 1712 | 2.96 | 41.08 |
| | Linear | Air+UV | 33272 | 79.85 | 1109.07 |
| Controlled initial pH $O_3$+UV+Cat. | Sigmoidal 3p. | pH = 3 | 78 | 0.32 | 4.49 |
| | Sigmoidal 3p. | pH = 5 | 84 | 0.35 | 4.84 |
| | Sigmoidal 3p. | pH = 9 | 124 | 0.51 | 7.11 |
| | Sigmoidal 3p. | pH = 11 | 137 | 0.56 | 7.83 |
| Controlled initial pH $O_3$+UV | Sigmoidal 3p. | pH = 3 | 100 | 0.41 | 5.76 |
| | Sigmoidal 3p. | pH = 5 | 98 | 0.41 | 5.64 |
| | Sigmoidal 3p. | pH = 9 | 134 | 0.55 | 7.68 |
| | Sigmoidal 3p. | pH = 11 | 148 | 0.61 | 8.49 |
| Controlled initial pH Air+UV+Cat. | Sigmoidal 3p. | pH = 3 | 355 | 0.85 | 11.82 |
| | Sigmoidal 3p. | pH = 5 | 210 | 0.50 | 6.99 |
| | Sigmoidal 3p. | pH = 9 | 448 | 1.07 | 14.92 |
| | Sigmoidal 3p. | pH = 11 | 796 | 1.91 | 26.52 |

The energy requirements varied between 4.49 and 41.08 MJ/g TOC (except for the theoretically estimated extreme value of 1109 MJ/g TOC for the photolysis method, having low treatment efficiency), which are comparable to the results obtained by Yen and Kang (2016), where 3.44–17.46 MJ/g dissolved organic carbon energy consumption was achieved using the $H_2O_2$/UV system for the mineralization of the humic acid solution. The most energy-efficient AO combination in the case of uncontrolled initial pH (6.7) was photocatalytic ozonation (5.76 MJ/g TOC); this value may be reduced with a decreased pH value (4.49 MJ/g TOC at pH = 3). An opposite relationship between the decreasing pH and increasing energy efficiency may be explained by the availability of H+ ions for the formation of HO• radicals (Mehrjouei et al., 2015). Similar trends have been established with photolytic ozonation where the highest energy efficiency has been reached at low pH (5.76 MJ/g TOC at pH of 3, 5.64 MJ/g TOC at pH of 5, and 7.93 MJ/g TOC at the experiment with the uncontrolled initial pH of 6.7). Such a relationship between the pH and energy requirements was not observed during the photocatalysis, where the lowest energy (6.99 MJ/g TOC) has been reached at an initial pH of 5. This difference occurs due to the different formation mechanisms of oxidative radicals without the presence of ozone, thus indicating the necessity to control the pH of the wastewater close to neutral pH values. Generally, photocatalytic ozonation was the most energy efficient at all the initial pH values. Although the energy consumption of photocatalytic ozonation is not dramatically lower than that of photolytic ozonation (in the range of 7.4–27.4%), the installation of an immobilized catalyst into the photolytic ozonation is necessary to have the lowest costs of operation.

### 3.5.3. Toxicity of treated wastewater

The effect of wastewater on D. magna organisms was checked after 24, 48, and 72 h of incubation (**Figure 3.20**). The initial diluted wastewater was found to have comparatively low toxicity (13% after 72 h). Such low toxicity may be attributed to the fact that the wastewater was diluted before the treatment. The toxic effect increased (100–86%) during the treatment at 20–60 min, when the remaining TOC value was 88–40%. This finding confirms the hypothesis of high acute toxicity of the decomposition by-products even at low concentrations used in these experiments. The toxicity rapidly decreased after 80–100 min of treatment, relating to the decrease of the TOC concentration. The observed data show that the by-products of the AO based degradation of mixed organic materials in the industrial wastewater matrix can be more toxic than the initial substances. Similar findings of the increase in the toxicity at the beginning of ozonation were reported by Hamdi El Najjar et al. (2014), where paracetamol polluted water treatment was investigated; toxicity decreased only after the prolonged treatment, suggesting the highly toxic and persistent nature of degradation by-products.
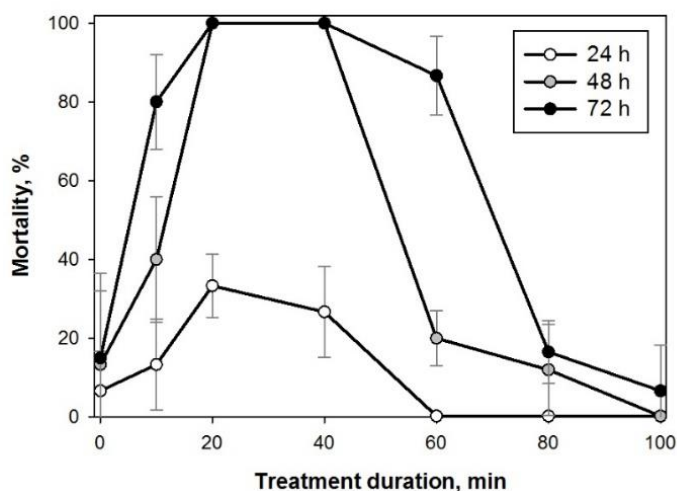


**Figure 3.20.** Variation in toxicity of wastewater during the treatment by photocatalytic ozonation. Daphnia mortality was checked after 24, 48, and 72 h. Note that wastewater samples were diluted two times before testing.

The formation of toxic degradation by-products was found by Kuang et al. (2013) where the increase in toxicity was registered after the trimethoprim ozonation experiment. However, many reports indicate the reduction of toxicity immediately after the beginning treatment, including the experiment by Zhao et al. (2016) with thiamethoxam ozonation and Kovacic et al. (2016) with diclofenac photolysis, but with a subsequent increase of toxicity at the next stage and the final decrease in toxicity after the full decomposition. Diverse results indicate that the treatment time must be carefully adjusted in each industrial setting in order to achieve close to zero toxicity values after the treatment with the AOPs. Additionally, the formation of by-

products having mutagenic and carcinogenic properties can occur during the chain reactions of the degradation of initial compounds. However, if the mineralization of 95–100% is reached, it is suggested that only "last stage" nontoxic by-products, such as low-mass organic acids, etc., are present in the treated water.

# 4. CONCLUSIONS

1. The capability of DBD plasma reactor to generate oxidizing species was confirmed as well as the applicability of this AOP based system for the water treatment. The power of the DBD plasma reactor and the initial concentration of pollutant in water were identified as the most important operational parameters: 2-naphthol was rapidly decomposed during the treatment process, and 90% decomposition efficiency was attained within 2 min. The formation of various reactive highly toxic intermediates was observed during the treatment process. They were further decomposed, resulting in the overall reduction of TOC in the next 10 minutes. This fact indicates the necessity of the appropriate treatment duration, leading to the loss of toxicity at the higher degree of mineralization.

2. The photocatalytic ozonation was confirmed to be the most efficient process, as opposed to the other ozone based treatment processes, such as ozonation and photolytic ozonation. The energy requirements of this process are low and depending on the pollutant that varied between 0.6 and 4 MJ/g of TOC reduction. The presented design of the photocatalytic ozonation reactor has a high potential to be up-scaled to the industrial AO system.

3. Among all the tested combinations in the industrial wastewater treatment, the photocatalytic ozonation was confirmed to be the most effective process. The final products of the degradation by photocatalytic ozonation as well were completely nontoxic, although the mid-process (at TOC values of 40–88% of the initial concentration) resulted in the formation of highly toxic by-products. It has been demonstrated that the photocatalytic ozonation is a viable advanced oxidation technology for the application of treatment of the industrial wastewaters, containing high concentration of organic hard-to-degrade compounds, if the operational parameters, such as dilution, pH, energy consumption, and treatment duration, are optimized.

# 5. RECOMMENDATIONS AND DISCUSSION FOR THE FUTURE RESEARCH

From the obtained study results, it can be stated that the ozone-photocatalysis based technology can be successfully applied for the treatment of hardly-degradable organic compounds polluted water. The recommendations regarding the further investigations and upscaling are presented below.

## 5.1. The basic designing issues of the industrial scale device

According to the literature review and the conducted experimental work, the designing of the easily up-scalable and energy efficient wastewater treatment reactor must be performed by evaluating the following key parameters:

- The use of three-element system: ozone, UV radiation, and catalyst system, is validated as most effective. The industrial scale device should be based on the conjunction of these three elements for the highest energy efficiency.
- Energy-efficient production of oxidative species. Nowadays, the dielectric barrier discharge (DBD) technique is the most efficient for the production of low temperature plasma, containing ozone and other oxidative species (Wei et al., 2016). This may be achieved by the application of high-voltage power converter that is working in the resonant mode with the reactor. Such principle is usually implemented by the industrial ozonizers.
- Energy efficient UV generation (Xiao et al., 2015). The most common source of UVC radiation is mercury luminescent lamps, which are comparatively energy efficient. The power of UV source must be calculated for the volume of treated water.
- Catalyst configuration, activity, and durability. The catalyst must have high catalytic activity as well as to be inert and highly resistant to aging to avoid wear and early replacement (Nawrocki, 2013; Martins and Quinta-Ferreira, 2014). While $TiO_2$ has been proved as chemically most suitable, the configuration of the introduction of the catalyst, including proper support and the layer quality, must be adequately solved in the up-scaled reactors.
- Optimal configuration of the running parameters (Tijani et al., 2014; Xiao et al., 2015). This technology is rather sensitive to the type of wastewater and the matrix that pollutants are dissolved in, including pH. This treatment method is applied for the specific industrial wastewater containing relatively low concentrations of highly persistent organic pollutants. The optimum configuration between plasma, UV, and catalyst operation must be achieved, in addition to the other engineering challenges for the prolongation of catalyst activity and highly efficient decomposition of pollutants.

## 5.2. Ozone generation

The DBD plasma based ozone generator was found to be suitable for the efficient ozone generation. The electrode materials (glass and quartz) were approved as highly durable under the working conditions. These electrode materials are inert to the impact of active radicals in the DBD plasma zone, air humidity, etc. The resonant mode high voltage power supply must be used to achieve the highest energy efficiency for the generation of plasma discharge, which is necessary for the ozone generation. The maximum ozone yield using the same plasma power can be obtained by selecting optimal working factors, such as feeding gas flow, DBD reactor geometry, and feeding gas parameters (humidity, gas composition). It should be noted that sufficient cooling of plasma zone must be ensured as well as the electrodes. It is recommended that the ozone generator should be installed as close to the water treatment reactor as possible. The ozone degrades over time; therefore, it is necessary to use it immediately after the generation. During the research, the side effects, such as the degradation of the silicone tubing near the DBD reactor, were observed during the experimental work; this observation suggests the explanation that the amount of the short-living active radicals can be higher closer to the ozone generator.

The feeding gas as an oxygen source is another issue related to the ozone generation. The ambient air has proved to be an appropriate oxygen source for the oxygen generation. In this case, the usage of pure oxygen is avoided, and correspondingly lower operational costs can be achieved.

## 5.3. Wastewater properties

The properties of wastewater have a direct influence on the efficiency of AOP based wastewater treatment processes. The treatment efficiency depends on the concentration and type of pollutant, pH value of the wastewater, the presence of inorganic substances and oxidative species, temperature, etc. Based on the results obtained in this study and reported by the other scientists, the concentration, chemical structure, and chemical properties as well as pH value have been found to be more important.

**Concentration.** As described before, the initial concentration of pollutants in water influences the treatment efficiency. In most of the cases, the increase in concentration had a negative effect on the treatment efficiency. The concentrations bellow few hundreds mg of TOC/L should not be exceeded. The treatment of wastewater with high concentrations of pollutants can take a lot of time and cause high-energy consumption. For this reason, the wastewaters should be pretreated using conventional treatment methods before using the AO processes or diluted.

**Chemical structure and chemical properties.** Evaluating the influence of chemical structure and chemical properties, it has been observed that these factors effect process performance as well. Comparing decomposition of 6 different pollutants (oxalic acid, phenol, 2-naphthol, glucose, phthalate, and methylene blue) under the same process conditions, the slight dependence of mineralization efficiency on the molecular weight of the compound was observed. The energy requirements for the TOC reduction revealed this dependence. For example, during the photocatalytic

ozonation, the energy requirements for the TOC reduction in case of oxalic acid (MW = 90.03) were the lowest and made up 0.61 MJ/g of TOC. This allows to assume that oxalic acid degraded easier compared to the other compounds. The phenol (MW = 94.11) and 2-naphthol (MW = 144.17) required more energy for TOC removal: 2.46 and 2.39 MJ/g of TOC, respectively. In case of phthalate (MW = 204.22) and methylene blue (MW = 319.85), the energy requirements were even higher: 3.18 and 3.60 MJ/g of TOC, accordingly. The number of decay reactions of the initial compound that are required to achieve full mineralization can explain these findings. In general, the higher is the molecular weight of the compound, the more decay reactions it takes to decompose it.

However, it has been observed that glucose had the highest energy requirements (3.86 MJ/g of TOC) even if the molecular weight (MW = 180.16) was lower, compared to some of the tested compounds. This indicates that the chemical structure of the initial compound has influence on the TOC reduction as well. The importance of chemical structure was noticed while evaluating the degradation of tested 6 compounds under the single ozonation. In this case, the compound having the lowest molecular mass, namely the oxalic acid, was completely resistant to the impact of ozone, while other compounds, having much higher molecular mass, had slightly higher degradability under the same process conditions.

**The pH value.** It has been confirmed that the pH value of wastewater has a strong influence on the degradation rates of pollutants during the AO based water treatment processes. This could be explained by the direct impact of pH on the mechanisms of formation of hydroxyl and oxygen radicals. Various AO processes, such as ozonation, photocatalytic ozonation, photocatalysis, differ in response to the changes in pH. Nevertheless, the most efficient of the tested processes — the photocatalytic ozonation — was found to be comparatively resistant to the pH changes. The pH values in range of 3−5 appeared to be suitable for the joint application of ozone-UV-catalysis based AO process, while higher pH values are more favorable for single ozonation based water treatment process.

The systemization of knowledge on the influence that various wastewater properties can have on the degradation pathways and treatment efficiency is needed. In most of the studies, the influence of these properties was studied separately. As simultaneous changes are likely, this could be one of the areas for the future research. Such knowledge would be useful for the design and operation of AO based wastewater treatment systems.

## 5.4. Potential problems, which must be solved at the industrial applications

**The problem of foaming.** Although the problem of foaming is not reported by other researchers, the phenomenon that occurred during some experiments of polluted water treatment can be called as negative for the technology application. In case of methylene blue, 2-naphthol, and real industrial wastewater (from furniture industry), a strong foaming at the first minutes of the treatment was observed. For this reason, some pollutants were removed from the water through the foam and were not degraded under the AO effect. According to this phenomenon, the special foam

dampers were designed and installed into the bench scale device, avoiding foam material to enter into the gas exhaust system. These solutions must be considered at the designing stage of the industrial scale device. The foam reduction system, which can reduce foam formation in the reactor by spraying the water on to the foam, can be considered a good solution.

**High concentration of pollutants.** As the AO technologies are more efficient at lower concentrations, it may be important to dilute the wastewater in some cases. The dilution can cause high consumption of dilution water. This consumption can be decreased by using the high operational volume reactor and comparatively low wastewater flow rate. The wastewater will be diluted with already treated wastewater in the reactor without consumption of additional fresh water.

**High operational costs.** It is known that AO method can decompose practically all organic contaminants in the water. However, it consumes the electrical energy, which comes at a cost. From this perspective, the conventional wastewater treatment methods as biological or chemical may look like more energy saving. For this reason, the AO technology should be used only for the treatment of wastewater polluted with hardly degradable or hazardous substances. The easy degradable pollutants can be removed from the water by biological methods, for example, active sludge systems. The AO technology may be applied in the second stage of the treatment for the final treatment of the wastewater to obtain ultra-pure water. This way of the wastewater treatment can be usual in industry for water recycle at the industrial processes. Primary pretreatment together with the secondary AO technology utilization may lead to the reduction of operational costs (energy consumption).

## 6. REFERENCES

Afzal, A., Drzewicz, P., Perez-Estrada, L.A., Chen, Y., Martin, J.W., Gamal El-Din, M. (2012). Effect of molecular structure on the relative reactivity of naphthenic acids in the UV/H2O2 advanced oxidation process. *Environmental Science and Technology*, 46, 10727−10734.

Antoniou, M.G., Hey, G., Rodríguez Vega, S., Spiliotopoulou, A., Fick, J., Tysklind, M., Jansen, J.L., Andersen, H.R. (2013). Required ozone doses for removing pharmaceuticals from wastewater effluents. *Science of the Total Environment*, 456–457, 42–49.

Bloh, J.Z., Dillert, R., Bahnemann, D.W. (2012). Transition metal-modified zinc oxides for UV and visible light photocatalysis. *Environmental Science and Pollution Research*, 19, 3688–3695.

Bubnov, A.G., Burova, E.Y., Grinevich, V.I., Rybkin, V.V., Kim, J.K., Choi, H.S. (2006). Plasma-catalytic decomposition of phenols in atmospheric pressure dielectric barrier discharge. *Plasma Chemistry and Plasma Processing*, 26, 19–30.

Byrne, J.A., Dunlop, P.S.M., Hamilton, J.W.J., Fernández- Ibáñez, P., Polo-López, I., Sharma, P.K., Vennard, A.S.M. (2015). A review of heterogeneous photocatalysis for water and surface disinfection. *Molecules*, 20, 5574−5615.

Cai, Y.X., Zhang, L.F., Wang, J., Ran, D.L., Wang, J. (2010). Measuring DBD main discharge parameters using Q-V Lissajous figures. *Asia-Pacific Power Energy Eng Conf,* APPEEC 1–4. doi: 10. 1109/APPEEC.2010.5449431

Chang, J., Chen, Z-L., Wang, Z., Kang, J., Chen, Q., Yuan, L., Shen, J-M. (2015). Oxidation of microcystin-LR in water by ozone combined with UV radiation: The removal and degradation pathway. *Chemical Engineering Journal*, 276, 97−105.

Chen, G., Zhou, M., Chen, S., Chen, W. (2009). The different effects of oxygen and air DBD plasma byproducts on the degradation of methyl violet 5BN. *Journal of Hazardous Materials*, 172, 786–791.

Chen, H.S., Lee, H.M., Chen, S.H., Chang, M.B. (2008). Review of packed-bed plasma reactor for ozone generation and air pollution control. *Industrial and Engineering Chemistry Research*, 47, 2122−2130.

Choi, Y.I., Jeon, K.H., Kim, H.S., Lee, J.H., Park, S.J., Roh, J.E., Khan, M.M., Sohn, Y. (2016). TiO2/BiOX(X = Cl, Br, I) hybrid microspheres for artificial waste

water and real sample treatment under visible light irradiation. *Separation and Purification Technology*, 160, 28–42.

Christensen, P.A., Yonar, T., Zakaria, K. (2013). The electrochemical generation of ozone: A review. *Ozone: Science and Engineering*, 35(3), 149–167.

Contreras, E.M., Bertola, N.C., Zaritzky, N.E. (2011). Monitoring the ozonation of phenol solutions at constant pH by different methods. *Industrial and Engineering Chemistry Research*, 50, 9799–9809.

Czech, B., Jośko, I., Oleszczuk, P. (2014). Ecotoxicological evaluation of selected pharmaceuticals to Vibrio fischeri and Daphnia magna before and after photooxidation process. *Ecotoxicology and Environmental Safety*, 104, 247–253.

Dai, Q., Chen, L., Chen, W., Chen, J. (2015). Degradation and kinetics of phenoxyacetic acid in aqueous solution by ozonation. *Separation and Purification Technology*, 142, 287–292.

Dai, Q., Wang, J., Yu, J., Chen, J., Chen, J. (2014). Catalytic ozonation for the degradation of acetylsalicylic acid in aqueous solution by magnetic $CeO_2$ nanometer catalyst particles. *Applied Catalysis B: Environmental*, 144, 686–693.

De Witte, B., Van Langenhove, H., Demeestere, K., Saerens, K., De Wispalaere, P., Dewulf, J. (2010). Ciprofloxacin ozonation in hospital wastewater treatment plant effluent: Effect of pH and $H_2O_2$. *Chemosphere*, 78, 1142–1147.

Dobrin, D., Bradu, C., Magureanu, M., Mandache, N.B., Parvulescu, V.I. (2013). Degradation of diclofenac in water using a pulsed corona discharge. *Chemical Engineering Journal*, 234, 389–396.

Fernández-Castro, P., Vallejo, M., San Román, M.F., Ortiz, I. (2015). Insight on the fundamentals of advanced oxidation processes: Role and review of the determination methods of reactive oxygen species. *Journal of Chemical Technology and Biotechnology*, 90, 796–820.

Gao, J.Z., Hu, Z.A., Wang, X.Y., Hou, J.G., Lu, X.Q., Kang, J.W. (2001). Degradation of anaphthol by plasma in aqueous solution. *Plasma Science and Technology*, 3, 641–651.

Gimeno, O., Rivas, F.J., Beltrán, F.J., Carbajo, M. (2007). Photocatalytic ozonation of winery wastewaters. *Journal of Agricultural and Food Chemistry*, 55, 9944–9950.

Gomes, A.C., Fernandes, L.R., Simões, R.M.S. (2012). Oxidation rates of two textile dyes by ozone: Effect of pH and competitive kinetics. *Chemical Engineering Journal*, 189–190, 175–181.

Guo, Y., Lin, Q., Xu, B., Qi, F. (2016). Degradation of benzophenone-3 by the ozonation in aqueous solution: Kinetics, intermediates and toxicity. *Environ Science and Pollution Research*, 23, 7962–7974.

Hamdi El Najjar, N., Touffet, A., Deborde, M., Journel, R., Karpel Vel Leitner, N. (2014). Kinetics of paracetamol oxidation by ozone and hydroxyl radicals, formation of transformation products and toxicity. *Separation and Purification Technology*, 136, 137–143.

Hansson, H., Kaczala, F., Amaro, A., Marques, M., Hogland, W. (2015). Advanced oxidation treatment of recalcitrant wastewater from a wood-based industry: A comparative study of $O_3$ and $O_3$/UV. *Water Air and Soil Pollution*, 226, 1–12.

Hashem, T.M., Zirlewagen, M., Braun, A.M. (1997). Simultaneous photochemical generation of ozone in the gas phase and photolysis of aqueous reaction systems using one VUV light source. *Water Science and Technology*, 35(4), 41–48.

Hernández-Alonso, M.D., Coronado, J.M., Maira, A.J., Soria, J., Loddo, V., Augugliaro, V. (2002). Ozone enhanced activity of aqueous titanium dioxide suspensions for photocatalytic oxidation of free cyanide ions. *Applied Catalysis B: Environmental*, 39, 257–267.

Homlok, R., Takács, E., Wojnárovits, L. (2013). Degradation of organic molecules in advanced oxidation processes: Relation between chemical structure and degradability. *Chemosphere*, 91, 383–389.

Huang, J., Wang, X., Pan, Z., Li, X., Ling, Y., Li, L. (2016). Efficient degradation of perfluorooctanoic acid (PFOA) by photocatalytic ozonation. *Chemical Engineering Journal*, 296, 329–334.

Hübner, U., Seiwert, B., Reemtsma, T., Jekel, M. (2014). Ozonation products of carbamazepine and their removal from secondary effluents by soil aquifer treatment—indications from column experiments. *Water Research*, 49, 34–43.

Illés, E., Szabó, E., Takács, E., Wojnárovits, L., Dombi, A., Gajda-Schrantz, K. (2014). Ketoprofen removal by $O_3$ and $O_3$/UV processes: Kinetics, transformation products and ecotoxicity. *Science of the Total Environment*, 472, 178–184.

Jiang, B., Zheng, J., Qiu, S., Wu, M., Zhang, Q., Yan, Z., Xue, Q. (2014). Review on electrical discharge plasma technology for wastewater remediation. *Chemical Engineering Journal*, 236, 348–368.

Kovacic, M., Perisic, D.J., Biosic, M., Kusic, H., Babic, S., Bozic, A.L. (2016). UV photolysis of diclofenac in water; kinetics, degradation pathway and environmental aspects. *Environmental Science and Pollutant Research*, 23, 14908–14917.

Krugly, E., Martuzevicius, D., Tichonovas, M., Jankunaite, D., Rumskaite, I., Sedlina, J., Racys, V., Baltrusaitis, J. (2015). Decomposition of 2-naphthol in water using a non-thermal plasma reactor. *Chemical Engineering Journal*, 260, 188–198.

Kuang, J., Huang, J., Wang, B., Cao, Q., Deng, S., Yu, G. (2013). Ozonation of trimethoprim in aqueous solution: Identification of reaction products and their toxicity. *Water Research*, 47, 2863–2872.

Li, D., Zhu, Q., Han, C., Yang, Y., Jiang, W., Zhang, Z. (2015). Photocatalytic degradation of recalcitrant organic pollutants in water using a novel cylindrical multi-column photoreactor packed with $TiO_2$-coated silica gel beads. *Journal of Hazardous Materials*, 285, 398–408.

Li, Y., Hsieh, W-P., Mahmudov, R., Wei, X., Huang, C.P. (2013). Combined ultrasound and fenton (US-fenton) process for the treatment of ammunition wastewater. *Journal of Hazardous Materials*, 244–245, 403–411.

Liu, Y., Mei, S., Iya-Sou, D., Cavadias, S., Ognier, S. (2012). Carbamazepine removal from water by dielectric barrier discharge: Comparison of ex situ and in situ discharge on water. *Chemical Engineering and Processing*, 56, 10–18.

Lu, N., Li, J., Wang, X., Wang, T., Wu, Y. (2012). Application of double-dielectric barrier discharge plasma for removal of pentachlorophenol from wastewater coupling with activated carbon adsorption and simultaneous regeneration. *Plasma Chemistry and Plasma Processing*, 32, 109–121.

Magureanu, M., Piroi, D., Mandache, N.B., David, V., Medvedovici, A., Parvulescu, V.I. (2010). Degradation of pharmaceutical compound pentoxifylline in water by non-thermal plasma treatment. *Water Research*, 44, 3445–3453.

Mano, T., Nishimoto, S., Kameshima, Y., Miyake, M. (2015). Water treatment efficacy of various metal oxide semiconductors for photocatalytic ozonation under UV and visible light irradiation. *Chemical Engineering Journal*, 264, 221–229.

Manoj Kumar Reddy, P., Rama Raju, B., Karuppiah, J., Linga Reddy, E., Subrahmanyam, C. (2013). Degradation and mineralization of methylene blue by dielectric barrier discharge non-thermal plasma reactor. *Chemical Engineering Journal*, 217, 41–47.

Marotta, E., Schiorlin, M., Ren, X., Rea, M., Paradisi, C. (2011). Advanced oxidation process for degradation of aqueous phenol in a dielectric barrier discharge reactor. *Plasma Processes and Polymers*, 8, 867–875.

Márquez, G., Rodríguez, E.M., Maldonado, M.I., Álvarez, P.M. (2014). Integration of ozone and solar $TiO_2$-photocatalytic oxidation for the degradation of selected pharmaceutical compounds in water and wastewater. *Separation and Purification Technology*, 136, 18–26.

Martins, R.C., Quinta-Ferreira, R.M. (2014). A review on the applications of ozonation for the treatment of real agro-industrial wastewaters. *Ozone: Science and Engineering*, 36, 3–35.

Mecha, A.C., Onyango, M.S., Ochieng, A., Fourie, C.J.S., Momba, M.N.B. (2016). Synergistic effect of UV-vis and solar photocatalytic ozonation on the degradation of phenol in municipal wastewater: A comparative study. *Journal of Catalysis*, 341, 116–125.

Mehrjouei, M., Müller, S., Möller, D. (2015). A review on photocatalytic ozonation used for the treatment of water and wastewater. *Chemical Engineering Journal*, 263, 209–219.

Mok, Y.S., Jo, J-O., Whitehead, J.C. (2008). Degradation of an azo dye Orange II using a gas phase dielectric barrier discharge reactor submerged in water. *Chemical Engineering Journal*, 142, 56–64.

Moon, J-D., Jung, J-S. (2007). Effective corona discharge and ozone generation from a wire-plate discharge system with a slit dielectric barrier. *Journal of Electrostatics*, 65, 660–666.

Moreira, F.C., Boaventura, R.A.R., Brillas, E., Vilar, V.J.P. (2017). Electrochemical advanced oxidation processes: A review on their application to synthetic and real wastewaters. *Applied Catalysis B: Environmental*, 202, 217–261.

Moreira, N.F.F., Sousa, J.M., Macedo, G., Ribeiro, A.R., Barreiros, L., Pedrosa, M., Faria, J.L., Pereira, M.F.R., Castro-Silva, S., Segundo, M.A., Manaia, C.M., Nunes, O.C., Silva, A.M.T. (2016). Photocatalytic ozonation of urban wastewater and surface water using immobilized $TiO_2$ with LEDs: Micropollutants, antibiotic resistance genes and estrogenic activity. *Water Research*, 94, 10–22.

Morrow, J.B., Almeida, J.L., Fitzgerald, L.A., Cole, K.D. (2008). Association and decontamination of Bacillus spores in a simulated drinking water system. *Water Research*, 42, 5011–5021.

Nawrocki, J. (2013). Catalytic ozonation in water: Controversies and questions. Discussion paper. *Applied Catalysis B: Environmental*, 142–143, 465–471.

Neyens, E., Baeyens, J. (2003). A review of classic Fenton's peroxidation as an advanced oxidation technique. *Journal of Hazardous Materials*, B98, 33–50.

Oetken, M., Nentwig, G., Löffler, D., Ternes, T., Oehlmann, J. (2005). Effects of pharmaceuticals on aquatic invertebrates. Part I. The antiepileptic drug carbamazepine. *Archives of Environmental Contamination and Toxicology*, 49(3), 353–361.

Oh, B.S., Jung, Y.J., Oh, Y.J., Yoo, Y.S., Kang, J-W. (2006). Application of ozone, UV and ozone/UV processes to reduce diethyl phthalate and its estrogenic activity. *Science of the Total Environment*, 367, 681–693.

Orge, C.A., Pereira, M.F.R., Faria, J.L. (2015). Photocatalytic ozonation of model aqueous solutions of oxalic and oxamic acids. *Applied Catalysis B: Environmental*, 174–175, 113–119.

Panizza, M., Cerisola, G. (2003). Electrochemical oxidation of 2-naphthol with in situ electrogenerated active chlorine. *Electrochimica Acta*, 48, 1515–1519.

Panizza, M., Cerisola, G. (2004). Influence of anode material on the electrochemical oxidation of 2-naphthol: Part 2. Bulk electrolysis experiments. *Electrochimical Acta*, 49, 3221–3226.

Panizza, M., Michaud, P.A., Cerisola, G., Comninellis, C. (2001). Anodic oxidation of 2-naphthol at boron-doped diamond electrodes. *Journal of Electroanalytical Chemistry*, 507, 206–214.

Pavia, D., Lampman, G., Kriz, G. (2000). *Introduction to Spectroscopy* (3rd ed.). Saunders College.

Pekarek, S. (2013). Asymmetric properties and ozone production of surface dielectric barrier discharge with different electrode configurations. *The European Physical Journal D*, 67, 94.

Pekárek, S., Mikeš, J. (2014). Temperature-and airflow-related effects of ozone production by surface dielectric barrier discharge in air. *The European Physical Journal D*, 68, 310.

Qourzal, S., Barka, N., Tamimi, M., Assabbane, A., Ait-Ichou, Y. (2008). Photodegradation of 2-naphthol in water by artificial light illumination using $TiO_2$ photocatalyst: Identification of intermediates and the reaction pathway. *Applied Catalysis A-General*, 334, 386–393.

Quiñones, D.H., Álvarez, P.M., Rey, A., Beltrán, F.J. (2015). Removal of emerging contaminants from municipal WWTP secondary effluents by solar photocatalytic ozonation. A pilot-scale study. *Separation and Purification Technology*, 149, 132–139.

Rizzo, L., Meric, S., Kassinos, D., Guida, M., Russo, F., Belgiorno, V. (2009). Degradation of diclofenac by $TiO_2$ photocatalysis: UV absorbance kinetics and process evaluation through a set of toxicity bioassays. *Water Research*, 43(4), 979–988.

Rozas, O., Vidal, C., Baeza, C., Jardim, W.F., Rossner, A., Mansilla, H.D. (2016). Organic micropollutants (OMPs) in natural waters: Oxidation by $UV/H_2O_2$ treatment and toxicity assessment. *Water Research*, 98, 109–118.

Salgado, R., Pereira, V.J., Carvalho, G., Soeiro, R., Gaffney, V., Almeida, C., Cardoso, V.V., Ferreira, E., Benoliel, M.J., Ternes, T.A., Oehmen, A., Reis, M.A.M., Noronha, J.P. (2013). Photodegradation kinetics and transformation products of ketoprofen, diclofenac and atenolol in pure water and treated wastewater. *Journal of Hazardous Materials*, 244–245, 516–527.

Sánchez, L., Peral, J., Domènech, X. (1998). Aniline degradation by combined photocatalysis and ozonation. *Applied Catalysis B: Environmental*, 19, 59–65.

Solís, R.R., Rivas, F.J., Martínez-Piernas, A., Agüera, A. (2016). Ozonation, photocatalysis and photocatalytic ozonation of diuron: Intermediates identification. *Chemical Engineering Journal*, 292, 72–81.

Stuart, B., Ando, D.J. (1996). *Modern Infrared Spectroscopy: Analytical Chemistry by Open Learning*. Wiley.

Tay, K.S., Madehi, N. (2015). Ozonation of ofloxacin in water: By-products, degradation pathway and ecotoxicity assessment. *Science of the Total Environment*, 520, 23–31.

Tichonovas, M., Krugly, E., Racys, V., Hippler, R., Kauneliene, V., Stasiulaitiene, I., Martuzevicius, D. (2013). Degradation of various textile dyes as wastewater pollutants under dielectric barrier discharge plasma treatment. *Chemical Engineering Journal*, 229, 9–19.

Tijani, J.O., Fatoba, O.O., Madzivire, G., Petrik, L.F. (2014). A review of combined advanced oxidation technologies for the removal of organic pollutants from water. *Water Air and Soil Pollution*, 225, 2102.

Vellaisamy, M., Suryakala, K., Ravishankar, M. (2011). Kinetics and mechanism of oxidation of 2-naphthol by nicotinium dichromate. *Journal of Chemical Pharmaceutical Research*, 3, 678–681.

Wang, J.L., Xu, L.J. (2012). Advanced oxidation processes for wastewater treatment: Formation of hydroxyl radical and application. *Critical Reviews in Environmental Science and Technology*, 42(3), 251–325.

Wang, N., Zheng, T., Zhang, G., Wang, P. (2016). A review on Fenton-like processes for wastewater treatment. *Journal of Environmental Chemical Engineering*, 4, 762–787.

Wei, C., Zhang, F., Hu, Y., Feng, C., Wu, H. (2016). Ozonation in water treatment: The generation, basic properties of ozone and its practical application. *Reviews in Chemical Engineering*, 33, 49–89.

Wei, Z.S., Li, H.Q., He, J.C., Ye, Q.H., Huang, Q.R., Luo, Y.W. (2013). Removal of dimethyl sulfide by the combination of non-thermal plasma and biological process. *Bioresource Technology*, 146, 451–456.

Weltje, L., Rufli, H., Heimbach, F., Wheeler, J., Vervliet- Scheebaum, M., Hamer, M. (2007). The chironomid acute toxicity test: Development of a new test system. *Integrated Environmental Assessment and Management*, doi:10.1897/IEAM_2009-069.1

Wen, G., Wang, S.J., Ma, J., Huang, T.L., Liu, Z.Q., Zhao, L., Su, J.F. (2014). Enhanced ozonation degradation of di-n-butyl phthalate by zero-valent zinc in aqueous solution: Performance and mechanism. *Journal of Hazardous Materials*, 265, 69–78.

Xiao, J., Xie, Y., Cao, H. (2015). Organic pollutants removal in wastewater by heterogeneous photocatalytic ozonation. *Chemosphere*, 121, 1–17.

Yen, H.Y., Kang, S.F. (2016). Effect of organic molecular weight on mineralization and energy consumption of humic acid by $H_2O_2$/UV oxidation. *Environmental Technology*, 37(17), 2199–2205.

Yuan, B-L., Li, X., Graham, N. (2008). Reaction pathways of dimethyl phthalate degradation in $TiO_2$-UV-$O_2$ and $TiO_2$-UV-Fe(VI) systems. *Chemosphere*, 72, 197–204.

Zang, S., Lian, B., Wang, J., Yang, Y. (2010). Biodegradation of 2-naphthol and its metabolites by coupling Aspergillus niger with Bacillus subtilis. *Journal of Environmental Sciences*, 22, 669–674.

Zhang, Q., Wang, C., Lei, Y. (2016). Fenton's oxidation kinetics, pathway, and toxicity evaluation of diethyl phthalate in aqueous solution. *Journal of Advanced Oxidation Technologies*, 19, 125–133.

Zhang, Y.J., Geißen, S.U., Gal, C. (2008). Carbamazepine and diclofenac: Removal in wastewater treatment plants and occurrence in water bodies. *Chemosphere*, 73(8), 1151–1161.

Zhao, Q., Ge, Y., Zuo, P., Shi, D., Jia, S. (2016). Degradation of thiamethoxam in aqueous solution by ozonation: Influencing factors, intermediates, degradation mechanism and toxicity assessment. *Chemosphere*, 146, 105–112.

Zhu, S.N., Hui, K.N., Hong, X., Hui, K.S. (2014). Catalytic ozonation of basic yellow 87 with a reusable catalyst chip. *Chemical Engineering Journal*, 242, 180–186.

# LIST OF PUBLICATION ON THE TOPIC OF THE DISSERTATION

Publications corresponding to the list of the CA "Web of Science", directly related to the dissertation:

1. Krugly, Edvinas; Martuzevičius, Dainius; **Tichonovas, Martynas**; Jankūnaitė, Dalia; Rumskaitė, Inga; Sedlina, Jolanta; Račys, Viktoras; Baltrušaitis, Jonas. Decomposition of 2-naphthol in water using a non-thermal plasma reactor // Chemical Engineering Journal. Lausanne : Elsevier. ISSN 1385-8947. 2015, vol. 260, p. 188-198. DOI: 10.1016/j.cej.2014.08.098.

2. **Tichonovas, Martynas**; Krugly, Edvinas; Jankūnaitė, Dalia; Račys, Viktoras; Martuzevičius, Dainius. Ozone-UV-catalysis based advanced oxidation process for wastewater treatment // Environmental Science and Pollution Research. Berlin : Springer. ISSN 0944-1344. eISSN 1614-7499. 2017, vol. 24, iss. 21, p. 17584-17597. DOI: 10.1007/s11356-017-9381-y.

3. **Tichonovas, Martynas**; Krugly, Edvinas; Grybauskas, Arturas; Jankūnaitė, Dalia; Račys, Viktoras; Martuzevičius, Dainius. Advanced oxidation-based treatment of furniture industry wastewater // Environmental Technology. Oxon : Taylor & Francis. ISSN 0959-3330. eISSN 1479-487X. 2017, vol. 00, iss. 00, p. 1-8. DOI: 10.1080/09593330.2017.1352037.

4. Jankūnaitė, Dalia; **Tichonovas, Martynas**; Buivydienė, Dalia; Radžiūnienė, Inga; Račys, Viktoras; Krugly, Edvinas. Removal of diclofenac, ketoprofen, and carbamazepine from simulated drinking water by advanced oxidation in a model reactor // Water, Air and Soil Pollution. Dordrecht : Springer. ISSN 0049-6979. eISSN 1573-2932. 2017, vol. 228, iss. 9, article 353, p. 1-15. DOI: 10.1007/s11270-017-3517-z.

List of the presentations in the international conferences:

1. **Tichonovas, Martynas;** Kudirkaitė, Aistė; Jankauskas, Jonas; Krugly, Edvinas; Račys, Viktoras. Influence of pH on dielectrical barrier discharge plasma process for wastewater treatment // *Chemistry and chemical technology: Proceedings of the international conference*, 25 April, 2014/Kaunas University of Technology. Kaunas: Technologija. ISSN 2351-5643. 2014, pp. 42–45.

2. **Tichonovas, Martynas;** Krugly, Edvinas; Kudirkaitė, Aistė; Jankauskas, Jonas; Račys, Viktoras. A pilot scale Dielectrical Barrier Discharge plasma system for wastewater treatment // *7th European Meeting on Chemical Industry and Environment 2015*.

3. **Tichonovas, Martynas;** Krugly, Edvinas; Grybauskas, Arturas; Račys, Viktoras. Ozone based advanced oxidation for water treatment // *Chemistry and*

*chemical technology 2017: Proceedings of the international conference*, 28 April, 2017, Kaunas. Kaunas University of Technology. ISSN 2538-7359. 2017, p. 100.

**LIST OF PUBLICATION NOT RELATED TO THE DISSERTATION**

Publications corresponding to the list of the CA "Web of Science":

1.  **Tichonovas, Martynas**; Krugly, Edvinas; Račys, Viktoras; Hippler, Rainer; Kaunelienė, Violeta; Stasiulaitienė, Inga; Martuzevičius, Dainius. Degradation of various textile dyes as wastewater pollutants under dielectric barrier discharge plasma treatment // Chemical engineering journal. Lausanne : Elsevier Science. ISSN 1385-8947. 2013, vol. 229, p. 9-19.

2.  Matulevičius, Jonas; Kliučininkas, Linas; Martuzevičius, Dainius; Krugly, Edvinas; **Tichonovas, Martynas**; Baltrušaitis, Jonas. Design and characterization of electrospun polyamide nanofiber media for air filtration applications // Journal of nanomaterials. New York : Hindawi. ISSN 1687-4110. 2014, vol. 2014, article No. 859656, p. [1-13]. DOI: 10.1155/2014/859656.

3.  Stasiulaitienė, Inga; Martuzevičius, Dainius; Abromaitis, Vytautas; **Tichonovas, Martynas**; Baltrušaitis, Jonas; Brandenburg, Ronny; Pawelec, Andrzej; Schwock, Alexander. Comparative life cycle assessment of plasma-based and traditional exhaust gas treatment technologies // Journal of cleaner production. Oxford : Elsevier. ISSN 0959-6526. eISSN 1879-1786. 2016, vol. 112, pt. 2, p. 1804-1812. DOI: 10.1016/j.jclepro.2015.01.062.